

# Geochemistry, Geophysics, Geosystems®

## RESEARCH ARTICLE

10.1029/2022GC010606

### Key Points:

- Multi-variate statistical data analysis (t-distributed stochastic neighbor embedding) identifies global Sr-Nd-Hf-Pb isotopic affinities of oceanic basalts
- There is no “common mantle component;” rather, global mid ocean ridge-ocean island basalts sample stochastically distributed small-scale isotopic heterogeneities
- Globally distributed regional domains of isotopically alike oceanic lavas define a new basis for relating isotopic variations to geodynamics

### Supporting Information:

Supporting Information may be found in the online version of this article.

### Correspondence to:

A. Stracke,  
[astr...@uni-muenster.de](mailto:astra_01@uni-muenster.de)

### Citation:

Stracke, A., Willig, M., Genske, F., Béguelin, P., & Todd, E. (2022). Chemical geodynamics insights from a machine learning approach. *Geochemistry, Geophysics, Geosystems*, 23, e2022GC010606. <https://doi.org/10.1029/2022GC010606>

Received 7 JUL 2022

Accepted 21 SEP 2022

### Author Contributions:

**Conceptualization:** A. Stracke  
**Data curation:** F. Genske  
**Formal analysis:** A. Stracke, M. Willig  
**Investigation:** A. Stracke  
**Methodology:** A. Stracke, M. Willig, P. Béguelin  
**Project Administration:** A. Stracke  
**Validation:** F. Genske, P. Béguelin  
**Visualization:** A. Stracke, M. Willig  
**Writing – original draft:** A. Stracke  
**Writing – review & editing:** M. Willig, F. Genske, P. Béguelin

© 2022 The Authors.

This is an open access article under the terms of the Creative Commons Attribution-NonCommercial License, which permits use, distribution and reproduction in any medium, provided the original work is properly cited and is not used for commercial purposes.

## Chemical Geodynamics Insights From a Machine Learning Approach

A. Stracke<sup>1</sup> , M. Willig<sup>1,2</sup>, F. Genske<sup>1</sup> , P. Béguelin<sup>1</sup>, and E. Todd<sup>3</sup>

<sup>1</sup>Institut für Mineralogie, Westfälische Wilhelms-Universität Münster, Münster, Germany, <sup>2</sup>GS1 Netherlands, Amstelveen, The Netherlands, <sup>3</sup>USGS, Alaska Science Center, Anchorage, AK, USA

**Abstract** The radiogenic isotope heterogeneity of oceanic basalts is often assessed using 2D isotope ratio diagrams. But because the underlying data are at least six dimensional ( $^{87}\text{Sr}/^{86}\text{Sr}$ ,  $^{143}\text{Nd}/^{144}\text{Nd}$ ,  $^{176}\text{Hf}/^{177}\text{Hf}$ , and  $^{208}\text{Pb}/^{206}\text{Pb}$ ,  $^{207}\text{Pb}/^{206}\text{Pb}$ ), it is important to examine isotopic affinities in multi-dimensional data space. Here, we apply t-distributed stochastic neighbor embedding (t-SNE), a multi-variate statistical data analysis technique, to a recent compilation of radiogenic isotope data of mid ocean ridge (MORB) and ocean island basalts (OIB). The t-SNE results show that the apparent overlap of MORB-OIB data trends in 2-3D isotope ratios diagrams does not exist in multi-dimensional isotope data space, revealing that there is no discrete “component” that is common to most MORB-OIB mantle sources on a global scale. Rather, MORB-OIB sample stochastically distributed small-scale isotopic heterogeneities. Yet, oceanic basalts with the same isotopic affinity, as identified by t-SNE, delineate several globally distributed regional domains. In the regional geodynamic context, the isotopic affinity of MORB and OIB is caused by capturing of actively upwelling mantle by adjacent ridges, and thus melting of mantle with similar origin in on, near, and off-ridge settings. Moreover, within a given isotopic domain, subsidiary upwellings rising from a common deep mantle root often feed OIB volcanism over large surface areas. Overall, the t-SNE results define a fundamentally new basis for relating isotopic variations in oceanic basalts to mantle geodynamics, and may launch a 21st century era of “chemical geodynamics.”

**Plain Language Summary** The isotopic heterogeneity of basalts erupted at mid ocean ridges (MORB) and ocean islands (OIB) reflects the chemical evolution of Earth's mantle. The visual inspection of various 2D isotope ratio diagrams has fueled a four decade-long discussion whether basalt heterogeneity reflects melting of only a small number of mantle components, and in particular, whether the apparent overlap of local data trends in global 2D isotope ratio diagrams indicates that melting of a common mantle component contributes to most MORB-OIB. Here, we use multi-variate statistical data analysis to show that the apparent overlap of MORB-OIB data trends in 2D isotope ratio diagrams does not exist in multi-dimensional isotope data space. Our finding invalidates any inference made for mantle compositional evolution based on the previously proposed existence of a common mantle component, its potential nature or distribution within the mantle. Rather, global MORB-OIB sample small-scale isotopic heterogeneities that are distributed stochastically in the Earth's mantle. Yet, MORB-OIB with the same isotopic affinity, as identified by our multi-variate data analysis, delineate several globally distributed regional domains. Within the regional geodynamic context, this discovery forms a fundamentally new basis for relating isotopic variations in MORB-OIB to mantle geodynamics.

## 1. Introduction

The isotopic heterogeneity of oceanic basalts is the surface expression of mantle heterogeneity (e.g., Allègre, 1982; Gast et al., 1964; Hart et al., 1973; Hofmann, 1997; Stracke, 2012, 2018, 2021a, 2021b; Stracke et al., 2005; Tatsumoto, 1966; Tatsumoto et al., 1965; White, 1985; White and Schilling, 1978; Zindler and Hart, 1986). Thousands of oceanic basalts have been analyzed in the last six decades, building up a large database of Sr, Nd, Hf, and Pb isotope ratios. A characteristic feature of these data is that they are not randomly distributed. In 2D and 3D isotope ratio diagrams, the isotopic variation of oceanic basalts on a local scale, that is, for basalts from one ocean island or ridge segment, is often in form of approximately linear data trends. Combining the local data into a large global data set does not have a randomizing effect. Rather, despite considerable overlap, higher-order structures, that is, reproducible trends or clusters composed of groups of local data, appear in 2-3D isotopic space. These higher-order trends or clusters of the global data set have often been described as linear combinations



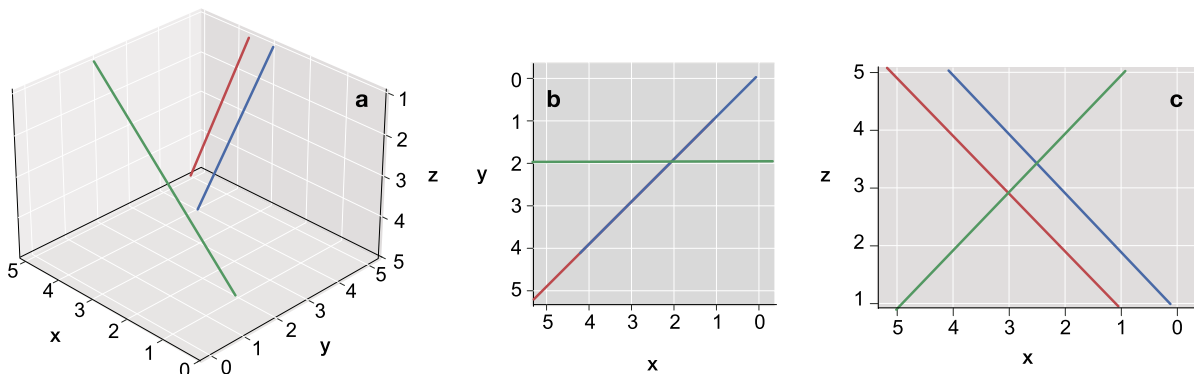


**Figure 1.** Diagram showing (a) three lines that do not intersect in three dimensions ( $x$ ,  $y$ ,  $z$ ). Two lines, the red and blue one, overlap in the 2D plot of  $x$  versus  $y$  (panel b), and both intersect the green line. In a 2D plot of  $x$  versus  $z$ , the red and blue line are parallel (panel c), and both intersect the green line. But comparing the 3D plot (a) with the 2D plots (b and c) shows that the apparent overlap in the 2D plots is an artifact caused by losing the respective third dimension.

formed by mixing between a limited number of discrete isotopic “end-members” (e.g., White, 1985; Zindler and Hart, 1986; Zindler et al., 1982).

But the interpretation of these higher-order structures in 2-3D isotopic space is subjective, fueling the discussion over the last four decades as to how many different isotopic “end-members” are needed to describe the distribution of global mid ocean ridge and ocean island basalt data (MORB-OIB) in 2-3D isotopic space. Particularly controversial is whether substantial overlap requires a “component” internal to the observed 2-3D isotopic data trends (Farley et al., 1992; Hanan and Graham, 1996; Hart et al., 1992; Stracke, 2012; Stracke et al., 2005; Zindler and Hart, 1986; Zindler et al., 1982). We use the term “end-member” or “component” in the original sense of Zindler et al. (1982), that is, to define basalt “phenotypes” at the end of, or within the spectrum of isotope ratios of oceanic basalts which relate to an unidentified number of mantle materials with unknown isotope composition (see also Section 4.1.1). It is important however, to “examine isotopic variations in multi-dimensional space to investigate systematics which may be obscured in 2D variation diagrams” (Zindler et al., 1982). In this context, note that the coherent global data trends in some 2D isotope spaces (e.g., Sr-Nd, Hf-Nd), but divergent trends in others (Pb-Nd, Pb-Sr), may be an effect of inspecting 5-6D data in various combinations of 2D isotope ratio diagrams, thereby losing 3–4 degrees of freedom (e.g., McKenzie and O’Nions, 1998). For an illustration of this effect, see Figure 1 for losing just one degree of freedom from 3D to 2D isotope ratio diagrams, and compare to Figures 2 and 3.

With increasing number of MORB-OIB radiogenic isotope data, and increasing number of elements analyzed (Sr, Nd, Pb, and Hf), the structure of the global data set has become increasingly complex. Visually inspecting multi-dimensional data in low dimensional data space (2-3D isotope ratio diagrams) may therefore either obscure the genuine or suggest spurious systematics, and thus lead to misinterpretations. This is a problem that many scientific fields (e.g., biology, astronomy, and social sciences) have faced with the availability of increasingly larger, and multi-variate data sets. Hence applying quantitative data analysis strategies, such as summary statistics or dimensional reduction techniques, has become increasingly important for accurate analysis of large, multi-dimensional data sets.

Dimensionality reduction techniques have also been explored for interpreting the spectrum of global radiogenic isotope ratios of MORB and OIB, including factor analysis (FA), and principal or independent component analysis (PCA, ICA, e.g., Albarède, 1995; Allègre et al., 1987; Hart et al., 1992; Iwamori and Albarède, 2008; Iwamori et al., 2017; Stracke, 2012; Zindler and Hart 1986; Zindler et al., 1982; White and Duncan, 1996). These methods may identify higher-order structures in the investigated data sets, for example, by finding directions along which variance is maximum, as for PCA. But they often do not preserve, or may ignore the inherent lower-order data trends or clusters of the data. However, the low-order structures of the global MORB-OIB isotopic database, the data trends or clusters formed by the local data sets, contain the principal information about the isotopic composition of the underlying mantle source. That is, they represent melts whose isotopic composition is variably dispersed around a weighted average of the isotopically different mantle source ingredients (e.g., Stracke, 2021b and references therein). When using dimensionality reduction algorithms such as PCA

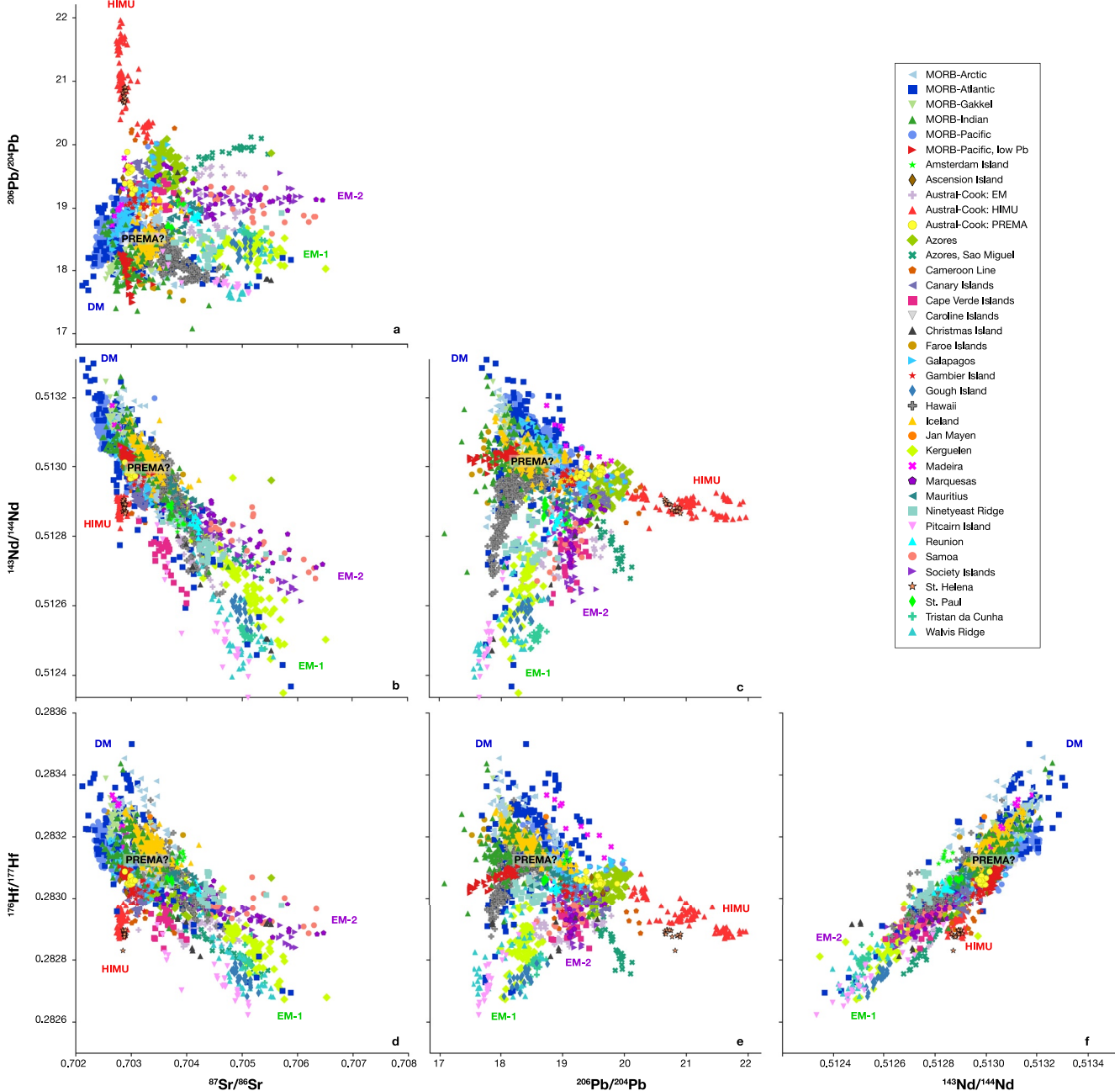


**Figure 2.** Radiogenic isotope data of mid ocean ridge and ocean island basalts compiled for this study, which have combined Sr-Nd-Hf-Pb isotope ratios ( $n = 2,744$ , Table S1), plotted in 2D diagrams using different combinations of  $^{87}\text{Sr}/^{86}\text{Sr}$ ,  $^{143}\text{Nd}/^{144}\text{Nd}$ ,  $^{176}\text{Hf}/^{177}\text{Hf}$ , and  $^{206}\text{Pb}/^{204}\text{Pb}$ . The plots also show the prevailing categorization into 4–5 basalt “phenotypes” according to Zindler and Hart (1986): Depleted Mantle, DM, PREMANTLE, PREMA, high  $\mu$ , HIMU, Enriched Mantle, EM 1 and 2.

that ignore these small-scale structures, it must therefore be demonstrated that the higher-order structures in the overall data set reflect natural processes, rather than being a fortuitous result of combining the local data (e.g., Albarède, 1995; Stracke, 2021b).

Here, we apply t-distributed stochastic neighbor embedding (t-SNE) on a recent compilation of radiogenic isotope data of MORB and OIB. T-SNE is a multi-variate statistical data analysis technique that performs dimensionality reduction while preserving the local pairwise similarities (van der Maaten, 2014; van der Maaten and Hinton, 2008), which depend on locally scaled distances up to a certain number of nearest neighbors. This means that t-SNE aims to preserve the local relative sample distances in a given multi-parameter data space

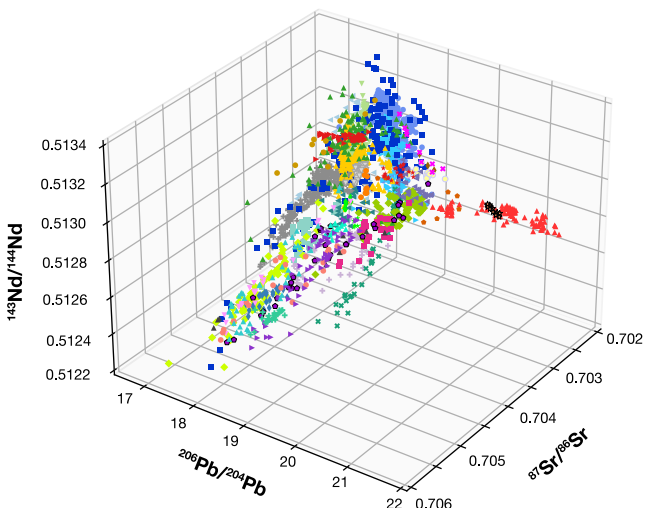


**Figure 3.** Radiogenic isotope data of mid ocean ridge and ocean island basalts complied for this study shown in a 3D plot of  $^{87}\text{Sr}/^{86}\text{Sr}$ ,  $^{143}\text{Nd}/^{144}\text{Nd}$ , and  $^{206}\text{Pb}/^{204}\text{Pb}$ . Symbols are the same as in Figure 2.

(e.g., the radiogenic isotope ratios in oceanic basalts) with the aim to group data with similar characteristics together and visualize them in plots of two variables (2D data space). It has become a routine data analysis tool in the biological or computational sciences, but has rarely been applied in geochemistry, for example, in geochemical exploration (e.g., Balamurali and Melkumyan, 2016; Cevik et al., 2021; Horrocks et al., 2019). We show that t-SNE is a powerful and robust machine learning technique for identifying global-scale similarities between the individual, local data sets that contribute to the global MORB-OIB radiogenic isotope database.

Our results confirm that analyzing multi-dimensional isotope data qualitatively in 2-3D isotope ratio space can be misleading, that is, the dimensions that are ignored in 2D diagrams are important for defining similarities or differences between the samples in multi-dimensional space. The apparent overlap of MORB-OIB data trends in 2-3D isotope ratios diagrams, for example, is non-existent in multi-dimensional isotope data space, showing that there is no discrete “component” common to most MORB-OIB mantle sources. Rather, groups of isotopically similar MORB-OIB identified with t-SNE delineate several globally distributed latitudinal domains. The implications of this observation will be discussed within the regional geodynamic context, which will outline several key questions to address further, both regionally and globally.

## 2. Materials and Methods

### 2.1. Data Set

The underlying isotope data set contains literature data for MORB ( $n = 2,298$ ) and OIB from 29 ocean islands or volcanic chains ( $n = 4,508$ ), with a complete set of Sr-Nd-Pb isotope ratios (Table S1). This database includes new Sr-Pb isotope data for rocks from the Cook-Austral islands (Nd-Hf data have been reported in Salters et al., 2011), and new Pb isotope data for rocks from St. Helena, Tristan da Cunha and Gough Island for which Sr-Nd-Hf data have been reported in previous publications (Willbold and Stracke, 2010; Salters et al., 2011; for major and trace element data see Willbold and Stracke, 2006; Table S2). If available, major and trace element concentrations are also included (Tables S1 and S2).

For the t-SNE analysis, however, we use only samples for which Hf isotope ratios are also available, resulting in a six-dimensional (6D) data set (i.e.,  $^{87}\text{Sr}/^{86}\text{Sr}$ ,  $^{143}\text{Nd}/^{144}\text{Nd}$ ,  $^{176}\text{Hf}/^{177}\text{Hf}$ ,  $^{206}\text{Pb}/^{204}\text{Pb}$ ,  $^{207}\text{Pb}/^{204}\text{Pb}$ ,  $^{208}\text{Pb}/^{204}\text{Pb}$ ) with a total of  $n = 2,744$  samples. We have only included localities with  $n > 5$  samples with combined Sr-Nd-Hf-Pb isotope ratios, and have not included continental basalts due to ubiquitous crustal contamination. Although restricting the number of data by only including samples with combined Sr-Nd-Hf-Pb isotope ratios, it adds an extra dimension compared to the 5D data set (i.e.,  $^{87}\text{Sr}/^{86}\text{Sr}$ ,  $^{143}\text{Nd}/^{144}\text{Nd}$ ,  $^{206}\text{Pb}/^{204}\text{Pb}$ ,  $^{207}\text{Pb}/^{204}\text{Pb}$ , and  $^{208}\text{Pb}/^{204}\text{Pb}$ ), which is important for capturing the full diversity of the global MORB-OIB radiogenic isotope ratios. For further discussion see Section 2.2, and Supporting Information S2, where we present the results of a t-SNE analysis for the 5D data set, consisting of  $n = 6,273$  samples for which combined Sr-Nd-Pb isotope ratios are available (Table S1 and Figures S3–S8 in Supporting Information S2).

Different combinations of 2D Sr-Nd-Hf-Pb isotope ratio plots in Figure 2 show that the investigated data set covers the entire known radiogenic isotope diversity of oceanic basalts (compare to Figure S3 in Supporting Information S2). Figure 2 also highlights the non-random data distribution and the prevailing categorization into 4–5 different basalt “phenotypes” (e.g., Hofmann, 1997; Stracke, 2012, 2018, 2021a, 2021b; Stracke et al., 2005; Zindler and Hart, 1986; Zindler et al., 1982; White, 1985). In short, there are some reproducible clusters and higher-order trends in different 2D isotope ratio plots. Samples categorized as “HIMU,” for example, form a reproducible cluster in different combinations of 2D isotope ratio plots. In contrast, samples categorized as “EM (1 or 2)” form trends that either extend (Sr-Nd, Hf-Nd) or diverge from (e.g., Sr-Pb, Nd-Pb, and Hf-Pb) the direction of the higher-order trend formed by the global MORB data. The latter is an indication that loss of additional dimensions affects the data representation in 2D isotope ratio diagrams (compare Figures 1–3).

## 2.2. Methods: t-SNE

T-distributed stochastic neighbor embedding (t-SNE) is performed using the scikit-learn tools implemented in Python (Pedregosa et al., 2011; for detailed documentation: <https://scikit-learn.org/stable/modules/generated/sklearn.manifold.TSNE.html>). Prior to the t-SNE analysis the isotope ratios are standardized by calculating the deviation from the mean value for each isotope ratio of the analyzed data set ( $n = 2,744$ ) and dividing it by the total range. This standardization of the isotope data is done to assure that differences in absolute values of the different isotope systems (e.g.,  $^{176}\text{Hf}/^{177}\text{Hf} \sim 0.00\text{xx}$  vs.  $^{206}\text{Pb}/^{204}\text{Pb} \sim 0.\text{xx}$ ) do not bias the statistical results.

Similar to PCA and related multi-variate data analysis techniques (FA, ICA), t-SNE performs dimensionality reduction of an n-dimensional matrix, and produces a corresponding matrix of low dimensional points (typically 2D; van der Maaten and Hinton, 2008). This allows visualization of high dimensional data in 2D space represented by two variables, simply termed t-SNE variable 1 and 2 (Figure 4). Unlike PCA, ICA and FA, however, t-SNE aims to preserve the relative local point-to-point distances, and essentially produces a 2 or 3D “map” which groups data points together that are similar (i.e., lie close to each other) in multi-dimensional space (Figure 4).

On basis of several artificial data sets with different inherent structure, Figure 4 shows how t-SNE represents these multi-dimensional data in 2D “maps.” Each of the five generic data sets used for the examples illustrated in Figure 4 is composed of 1,000 randomly generated points, and described by six parameters (i.e., six dimensions), similar to the MORB-OIB radiogenic isotope data set that includes six isotope ratios. Hence, by analogy to the 6D global MORB-OIB data set, Figure 4 also shows what to expect from analyzing the oceanic basalt data with respect to resolving similar groups of data and, especially, the identification of “components” that are common to several or most groups of data (i.e., putative “internal components”).

In the left panels of Figure 4, the different data distributions are shown as 2D scatterplots using the first two of the six dimensions (t-SNE parameter 1 vs. t-SNE parameter 2). The right panels in Figure 4 show the corresponding 2D t-SNE “maps” of the 6D data reduced to two dimensions. For randomly distributed data points (samples) in Figure 4a, the corresponding t-SNE map in Figure 4b also shows a random pattern. A similar pattern is observed using a random Gaussian data distribution (Figures 4c and 4d).

How t-SNE may help identify distinct groups of data (clusters) that are obscured when inspecting the 6D data in 2D is shown in Figures 4e and 4f. The underlying 6D data are arranged in seven groups (clusters), but two of them overlap with one of the other in the 2D space chosen for Figure 4e, hence resolving only five apparent clusters. T-SNE recognizes and resolves all seven clusters and depicts them as seven discrete clusters in the 2D t-SNE map (Figure 4f). This example shows that resolving distinct clusters in multi-dimensional data, that is, groups of similar samples in 6D data space, by visual inspection in 2D may suggest similarities that actually do not exist. T-SNE may thus help resolving crucial information about the multi-dimensional data that would otherwise have been obscured in 2D.

Figures 4g and 4h show data distributed along an overall linear trend (vector) from [0,0,0,0,0,0] to [5,5,5,5,5,5] composed of five sub-trends perpendicular to the overall trend (along [-1,1,-1,1,-1,1]). Note that this data distribution is similar to the so-called local and global trends of the  $\text{Na}_8\text{-Fe}_8$  variability in global MORB (Klein and Langmuir, 1989). The t-SNE diagram in Figure 4h resolves the five sub-trends much more clearly than the 2D plot of the actual data (Figure 4g), but does not depict the higher-order trend of the data. Hence t-SNE, in this case, is appropriate for resolving low-order groups or clusters, but does not preserve the higher-order pattern of the multi-dimensional data.

The underlying data in Figures 4i and 4k form four trends emerging from a central point in 6D, but two of these trends overlap in the dimensions plotted in Figure 4i. This example is selected to illustrate how t-SNE resolves data trends that may be mixtures between one common and various other end-members (in this case 4). The t-SNE map shows four elongated trends or curves that converge in a common cluster, producing a pattern reminiscent of an octopus. As in Figure 4h, t-SNE resolves the four groups, and it also resolves the common end-member as a separate cluster, but it does not preserve the higher-order linear structure of the actual data trends (see the Supporting Information S2 for further discussion and Figures S1 and S2 in Supporting Information S2 for more examples). The examples shown in Figure 4 confirm, however, that the algorithm is a powerful tool for identifying low-order groups or clusters of data that are similar in multi-dimensional space.

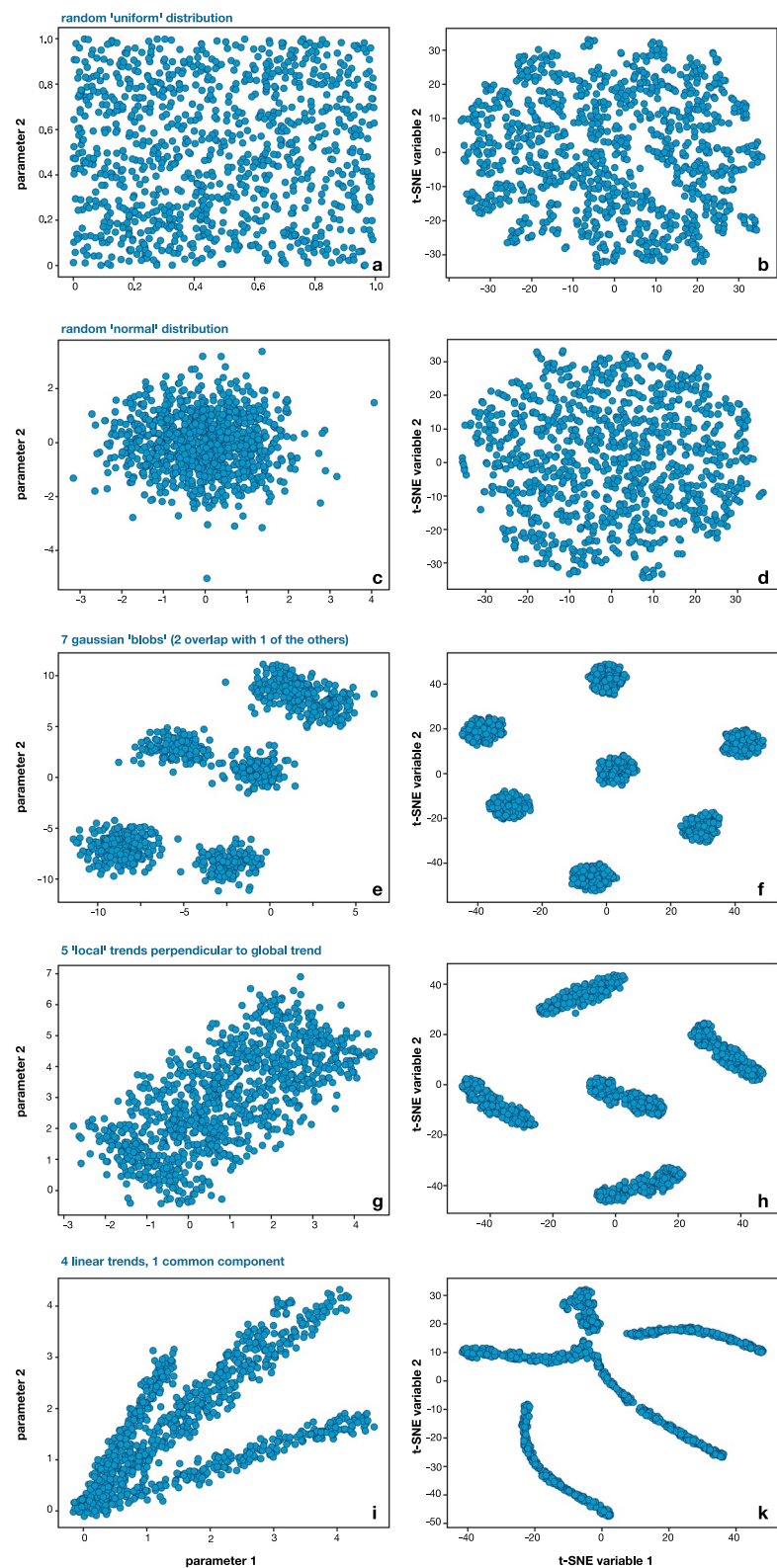


Figure 4.

For more explanations and instructive examples how t-SNE represents various data distributions see Wattenberg et al. (2016, <https://distill.pub/2016/misread-tsne>). It should be noted that the stochastic nature of t-SNE means that multiple runs will not always produce the exact same pattern. But for well-chosen input parameters, the resulting patterns are reproducible, so t-SNE gives robust results (Belkina et al., 2019; Linderman and Steinerberger, 2019; van der Maaten and Hinton, 2008). The t-SNE algorithm has several input parameters, so-called hyper-parameters in machine learning, which are parameters whose value is set before the learning begins, and thus have an important control on the output. The most important one is the so-called perplexity (Kobak and Berens, 2019; van der Maaten, 2014; van der Maaten and Hinton, 2008; Wattenberg et al., 2016), which is effectively the number of nearest neighbors t-SNE considers for converting the pairwise similarities (affinities) of data points to probabilities (i.e., the 2D output variables, t-SNE variable 1 and t-SNE variable 2). For high-enough values of perplexity, typically  $n/100$  (where  $n$  is the number of samples, Kobak and Berens, 2019), the performance of t-SNE is robust (e.g., for the default value of 30 set in the scikit-learn tools in python, and used in this study with  $n = 2,744$ , van der Maaten and Hinton, 2008; Wattenberg et al., 2016). However, as any dimensionality reduction technique distorts original distances between data points, neither the relative sizes of clusters, the distances between clusters, nor the arrangement of trends or curves is generally preserved, which is a typical feature of t-SNE (Figures 4g, 4h, 4i, and 4k; Figures S1 and S2 in Supporting Information S2; see also Wattenberg et al., 2016). This also means that the data density of the actual data trends or clusters is not preserved in the t-SNE map, meaning that “dense” and “sparse” clusters in the full 6D space may have similar visual densities in the t-SNE map. But although the geometry of the resulting patterns of the t-SNE output therefore does not reflect the actual geometry of the data in multi-dimensional space, the number of clusters and the grouping of samples into discrete clusters are robust outputs for high-enough values of perplexity (Figures 4e–4k, Figures S1 and S2 in Supporting Information S2; Kobak and Berens, 2019; van der Maaten and Hinton, 2008; Wattenberg et al., 2016).

Hence, applied to the radiogenic isotope data set of global MORB-OIB (Table S1), t-SNE should be able to identify groups of samples that are similar (i.e., close to each other) in 6D space, and thus reveal whether there are only 4–5 isotopic “end-members”. In particular, a cluster formed by the intersection of various elongated curvilinear trends (an “octopus” as in Figure 4k and Figure S1 in Supporting Information S2) should appear, if there is indeed a common component that is sampled in many locations (e.g., “PREMA” by Zindler and Hart (1986) or “FOZO” by Hart et al. (1992)).

### 3. Results

#### 3.1. The “t-SNE Map” of the MORB-OIB Isotope Data Set

The 2D t-SNE “map” of the MORB-OIB data set shown in Figure 5a confirms that the radiogenic isotope data of global MORB-OIB are not randomly distributed, but instead form several distinct groups or clusters. Subjectively, there are at least 10–12 disconnected clusters. Most clusters are well defined (e.g., that of the Hawaiian data in Figure 5a), but identifying unique clusters is more ambiguous in other cases. How many clusters, for example, should be defined for the group of samples from several different localities in the central or lower part of Figure 5a?

To more objectively distinguish between different clusters of the t-SNE map, we therefore performed single linkage agglomerative clustering using the scikit-learn tools implemented in Python (Pedregosa et al., 2011; <https://scikit-learn.org/stable/modules/clustering.html>). Starting by assigning each data point to its own initial cluster, agglomerative clustering progressively links each data point to its closest neighboring data point, and successively merges or re-assigns data points to clusters until a pre-defined number of clusters is formed (Figure 5b). “Single linkage” agglomerative clustering means that in each step the minimum Euclidian point-to-point distance between every data point of one cluster and every data point of any other cluster is found. Compared to other linkage methods, therefore, the “single linkage” method appears most suitable for objectively grouping the t-SNE

**Figure 4.** Diagrams showing how t-distributed stochastic neighbor embedding (t-SNE) represents different data distributions. The panels on the left (a, c, e, g, and i) show several artificial datasets with different inherent structure, each composed of 1,000 randomly generated points, and described by six parameters (i.e., six dimensions). The different data distributions are shown as 2D scatterplots using the first two of the six dimensions (parameter 1 vs. parameter 2). The panels on the right (b, d, f, h, and k) show how t-SNE represents the 6D data in corresponding 2D t-SNE “maps,” showing that t-SNE is particularly useful for identifying low-order groups or clusters of data that are similar in multi-dimensional space. For further description and explanations see Section 2.2, and Figures S1 and S2 in Supporting Information S2. The t-SNE analysis is done with the scikit-learn tools implemented in Python (<https://scikit-learn.org/stable/modules/generated/sklearn.manifold.TSNE.html>).

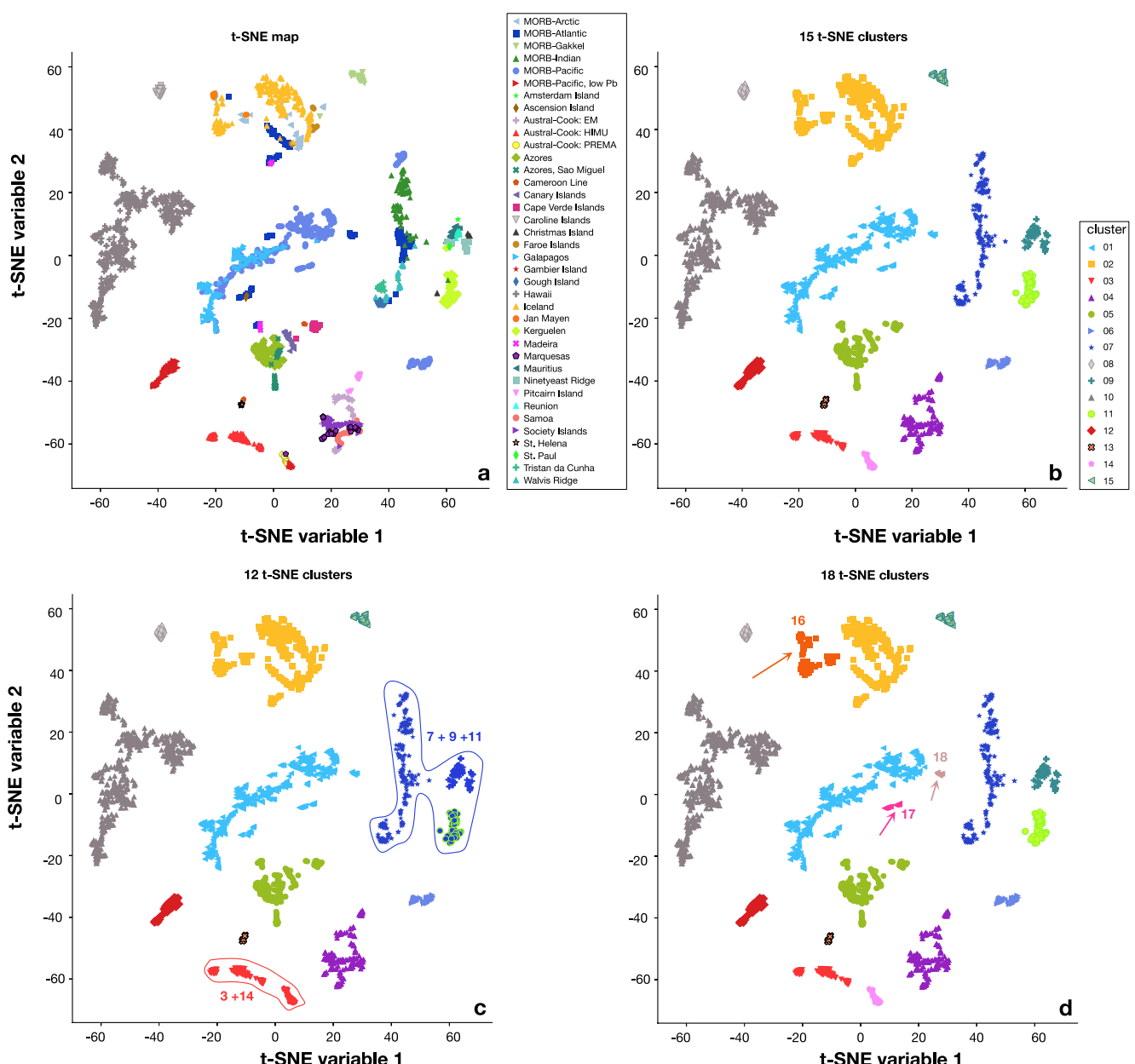


**Figure 5.** The diagrams show the t-distributed stochastic neighbor embedding (t-SNE) “map” of the MORB and OIB isotope data compiled for this study (Figures 2 and 3, Table S1). Panel (a) shows the t-SNE “map” using the same symbols as in Figures 2 and 3. Panel (b) compartmentalizes the data in 15 clusters using single linkage agglomerative clustering, panel (c) in 12 and (d) in 18 clusters. The combined t-SNE and agglomerative clustering analysis are done with the scikit-learn tools implemented in Python (<https://scikit-learn.org/stable/modules/generated/sklearn.manifold.TSNE.html>, <https://scikit-learn.org/stable/modules/clustering.html>). For further details see Section 3.1, and the Supporting Information S2 for the results of a t-SNE analysis of the larger 5D data set with  $n = 6,723$  samples with combined Sr-Nd-Pb isotope data (Figure S4 in Supporting Information S2).

output into different clusters (see instructive examples in the scikit-learn documentation: [https://scikit-learn.org/stable/auto\\_examples/cluster/plot\\_linkage\\_comparison](https://scikit-learn.org/stable/auto_examples/cluster/plot_linkage_comparison)). In each step, the two clusters with the smallest “single linkage distance” are merged, resulting in a hierarchical set of nested clusters (e.g., Igual and Segui, 2017; Maimon and Rokach, 2006; Nielsen, 2016).

While agglomerative clustering is a quantitative means for grouping the t-SNE map into clusters, the algorithm works with a user-defined, and thus subjective number of clusters. The results for choosing 12, 15, and 18 clusters are shown in Figures 5b–5d, which shows that the grouping of samples into different clusters depends to some extent on the chosen number of clusters. But for  $n > 15$  clusters, dissection of the larger clusters into smaller

ones leads to more and more incremental, and thus perhaps artificial differences in isotopic affinity between the samples in the resulting clusters (Figure 5d). For  $n \leq 12$ , isotopically distinct data points will be forced into progressively larger clusters, perhaps blurring meaningful isotopic differences (Figure 5c). Hence, selecting 15 clusters is probably a good compromise between defining more and more incremental clusters (Figure 5d) and forcing distinct data points into unjustifiably large clusters (Figure 5c). The following data analysis is therefore based on grouping the t-SNE map into 15 clusters by agglomerative clustering (Figure 5b).

The robustness of the combined output of the t-SNE and cluster analysis was assured by repeated runs of t-SNE with different values for the perplexity input parameter followed by agglomerative clustering for 15 clusters. The reproducibility of the resulting “t-SNE clusters,” the 15 clusters produced by agglomerative clustering analysis of the t-SNE map, was evaluated with the “adjusted rand score” (as implemented by the scikit-learn tools in Python, Pedregosa et al., 2011, [https://scikit-learn.org/stable/modules/generated/sklearn.metrics.adjusted\\_rand\\_score.html](https://scikit-learn.org/stable/modules/generated/sklearn.metrics.adjusted_rand_score.html)). The latter is a quantitative measure for how similar the resulting clusters for two runs are. An adjusted rand score of 1 means the combined t-SNE plus agglomerative clustering analysis results in identical clusters, that is, the same points always define the same cluster. An adjusted rand score of 0 is expected for non-reproducible clusters, that is, random assignment of points to different clusters. We also used a range of values for the perplexity, and compared the results for all possible combinations of perplexity between 25 and 45. Table S3 shows that the adjusted rand score is 0.9 for most combinations of perplexity values within this range, and confirms that the default value of 30 results in reproducible t-SNE maps (as shown in Figure 5a).

### 3.2. Similarities of the “t-SNE Clusters” to the Prevailing MORB-OIB Categorization

Figure 5 clearly identifies more than the 4–5 groups or “end-members” frequently used to describe the pattern of radiogenic isotope data in various 2D diagrams (Figures 2 and 3). Nevertheless, the t-SNE analysis conforms with some aspects of this prevailing categorization, although in detail, there are important differences.

Samples from Tristan da Cunha, Gough Island, and the Walvis Ridge, for example, which were heretofore often classified as “EM-1,” also form a distinct t-SNE cluster (cluster 7 in Figure 5b). However, MORB, mostly from the southern Atlantic and Indian ocean, are also included in this t-SNE cluster. Similarly, samples categorized as “EM-2” (Figures 2 and 3) from the Samoan, Society and Marquesas Island chains fall into a single t-SNE cluster (cluster 4 in Figure 5b). But this cluster also includes samples from the Austral-Cook Islands with “EM” affinity, and perhaps surprisingly, samples from Pitcairn Island, which were traditionally often classified as “EM-1” (e.g., Eisele et al., 2002; Garapic et al., 2015; Zindler and Hart, 1986).

In contrast, samples from St. Helena and from some of Cook-Austral Islands, which were generally categorized into a single “HIMU” group based on visual analysis of the 2D isotope ratios diagrams (Figures 2 and 3), are resolved as two distinct t-SNE clusters (cluster 3 and 13 in Figure 5b). In this case, the t-SNE analysis reveals differences between samples that are not apparent in the 2-3D isotope ratios diagrams. When choosing 12 clusters, however, which appears as a reasonable minimum number of clusters (Figure 5c), the Cook-Austral HIMU samples merge with samples from Gambier Island and samples from the Austral-Cook Islands with “PREMA” affinity into a common group (clusters 3 + 14 in Figure 5c). A similar effect is observed for clusters 7, 9, and 11 when reducing the number of clusters from 15 to 12, that is, these clusters combine and form a common cluster of MORB and OIB from the South Atlantic and Indian Ocean (Figure 5c).

### 3.3. Differences of the “t-SNE Clusters” to the Prevailing MORB-OIB Categorization

Several clusters reproduce, and identify samples with similar isotopic affinity, independent of how many clusters within the range of 12–18 are chosen (Figures 5b–5d). The calculated contribution of samples from each location to each of the 15 t-SNE clusters is shown in Figure 6. A value of 1 means that all samples from one location fall into a single t-SNE cluster. This is the case for Hawaii (cluster 10 in Figures 5b, e.g., White, 1985), but also for the HIMU-type OIB from some of the Austral-Cook islands, basalts from the Caroline Islands, and the Kerguelen Plateau (clusters 3, 8, and 11 in Figures 5b and 6). Similarly, MORB from Gakkel Ridge, and a peculiar group of Pacific MORB with unusually low Pb isotope ratios, labeled “Pacific MORB, low-Pb” (Mougel et al., 2014), define t-SNE clusters made up of samples only from these specific ridge segments (clusters 15 and 12 in Figures 5b and 6).

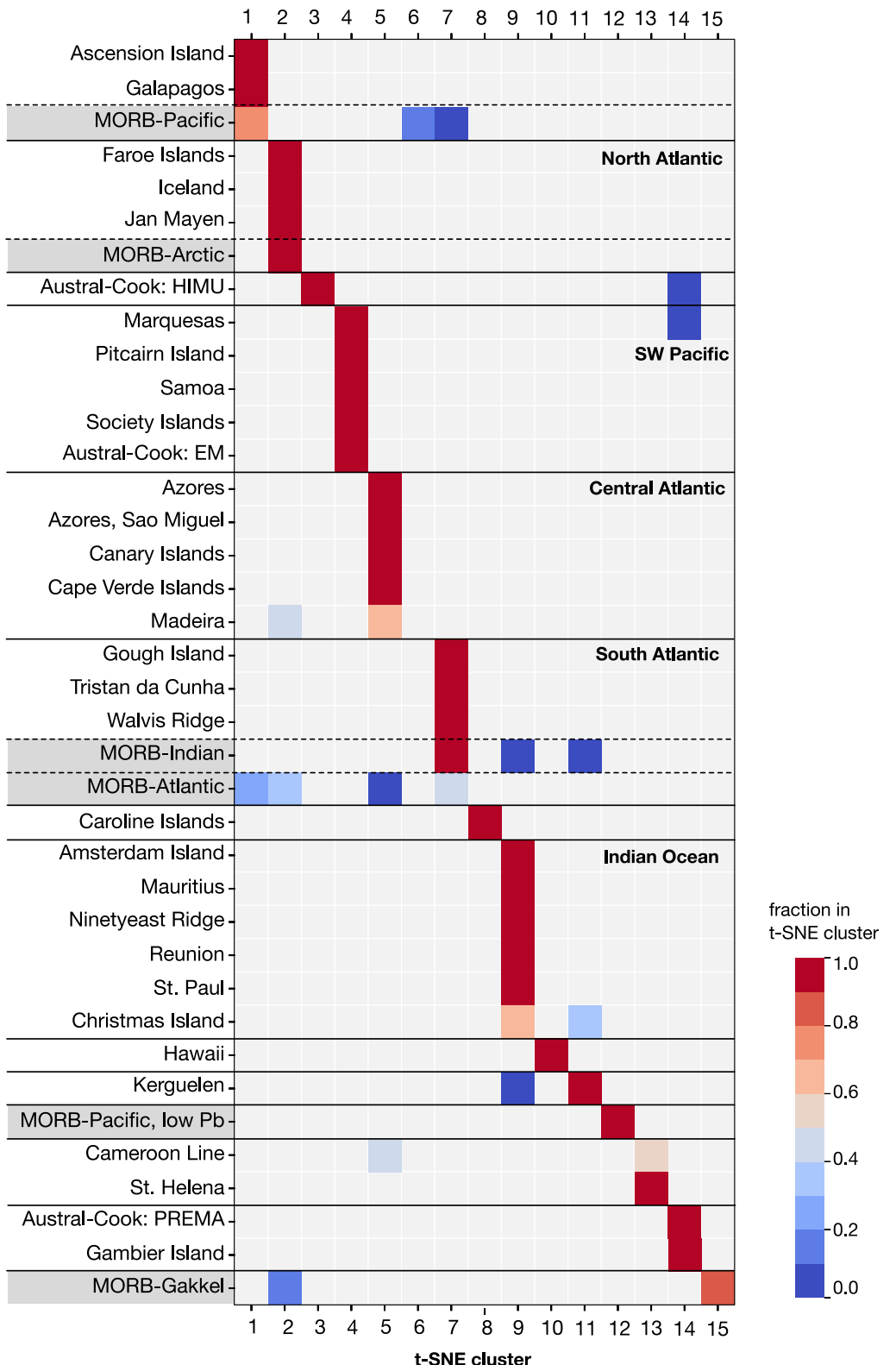


**Figure 6.** Plot showing what fraction of samples from one locality falls into each of the 15 t-distributed stochastic neighbor embedding (t-SNE) clusters defined in Figure 5b. A value of 1 means that all samples from one location fall into a single t-SNE cluster. For most ocean islands and island groups, but also some ridge segments, the majority of the samples fall into a single t-SNE cluster. Isotopic affinities are therefore clearly defined.

Most OIB from one location, but also MORB from several ridge segments, fall into a single t-SNE cluster, and thus isotopic affinities are clearly defined. But several t-SNE clusters encompass OIB from different localities, such as the clusters formed by samples with “EM” affinity discussed above (clusters 4 and 7 in Figure 5b). Similarly, cluster 2 in Figure 5b consists mostly of samples from Iceland, but also from Jan Mayen, the Faroe Islands, and MORB from the Atlantic Ridge immediately north and south of Iceland (“MORB-Arctic,” Figures 5a and 5b). Another t-SNE cluster is formed by samples from the Azores (including peculiar samples from São Miguel), the Canary and Cape Verde Islands, as well as Madeira, including several samples from the adjacent central Mid-Atlantic Ridge and scattered samples from the Cameroon line (cluster 5; Figures 5b and 6). Remarkably, these “composite t-SNE clusters” are formed by samples from restricted geographic regions, that is, the North, Central and South Atlantic (clusters 2, 5, and 7), the SW Pacific (cluster 4), and the Indian Ocean (cluster 9; Figures 5b and 6); an aspect we will discuss further below.

It is also apparent that, except for the SW Pacific OIB (cluster 4; Figures 5b and 6), these composite t-SNE clusters include not only OIB but also MORB from adjacent ridges, thus revealing an isotopic affinity of oceanic basalts from ridge and intra-plate tectonic settings. This result may be surprising, considering the conventional notion that MORB and OIB are isotopically distinct (e.g., White, 2010 and references therein). But considering that MORB cover about 92% of the global range for  $^{143}\text{Nd}/^{144}\text{Nd}$  of OIB and MORB combined, and approximately two-thirds of the range for  $^{206}\text{Pb}/^{204}\text{Pb}$  (Table S1), the subjective impression gleaned from visual inspection of 2-3D isotopic ratio diagrams that MORB and OIB are isotopically distinct has long been contradictory to such quantitative measures of MORB-OIB isotopic similarity.

## 4. Discussion

### 4.1. Beyond the Prevailing MORB-OIB Categorization

#### 4.1.1. Canonical “End-Members”

The t-SNE map (Figure 5a) clearly shows that the 4–5 canonical “end-members” (e.g., Zindler and Hart, 1986) do not adequately describe the isotopic diversity of oceanic basalts. Importantly, the affinity between different samples given in the t-SNE map is a robust output, although choosing different numbers of clusters for agglomerative clustering compartmentalizes the t-SNE output somewhat differently (Figures 5b–5d).

We have chosen 15 clusters for agglomerative clustering as a reasonable choice for describing the t-SNE map (Figure 5b), but these should not be rationalized in terms of a finite number of basalt “phenotypes” or “end-members”, let alone mantle compositions, that describe the global MORB-OIB radiogenic isotope data. Note that Zindler et al. (1982) cautioned against equating the 4–5 distinct basalt “end-members” or “components” directly with mantle source composition: “The term “component” is used so as not to imply [...] that a physical entity with these compositions actually exists in the mantle. We also do not mean to imply that only [4–5] isotopically distinct materials exist within the mantle: a brief look at the crust should dispel any such notion.” Similarly, White (1985) pointed out that “the five groups [...] should not be regarded as a final enumeration of possible mantle reservoirs.”

Hence the emphasis in this study is not on defining a finite number of clusters with the intention to best describe the full extent of mantle isotopic heterogeneity. This would be a futile exercise, because the isotopic compositions of MORB-OIB samples themselves only reflect a weighted isotopic average of their mantle source ingredients. Thus any inferred finite number of basalt groups with similar isotopic affinity also depends on the scale of observation, and does not reflect the actual isotopic composition of an unidentified number of mantle materials with unknown isotopic composition (see quote from Zindler et al. (1982) above and, e.g., Stracke (2021b)). Moreover, how many clusters best describe the radiogenic isotope data is also subject to change with the ever-growing number of samples and eventually including other radiogenic isotope ratios (e.g., Ce, Os) in the MORB-OIB database (compare to the results of the t-SNE analysis of the 5D data set discussed in Supporting Information S2). The focus of the analysis of the current Sr-Nd-Hf-Pb isotope database will therefore be on assessing the isotopic affinity of samples from different locations and tectonic settings in multi-dimensional data space quantitatively, as given by the t-SNE clusters.

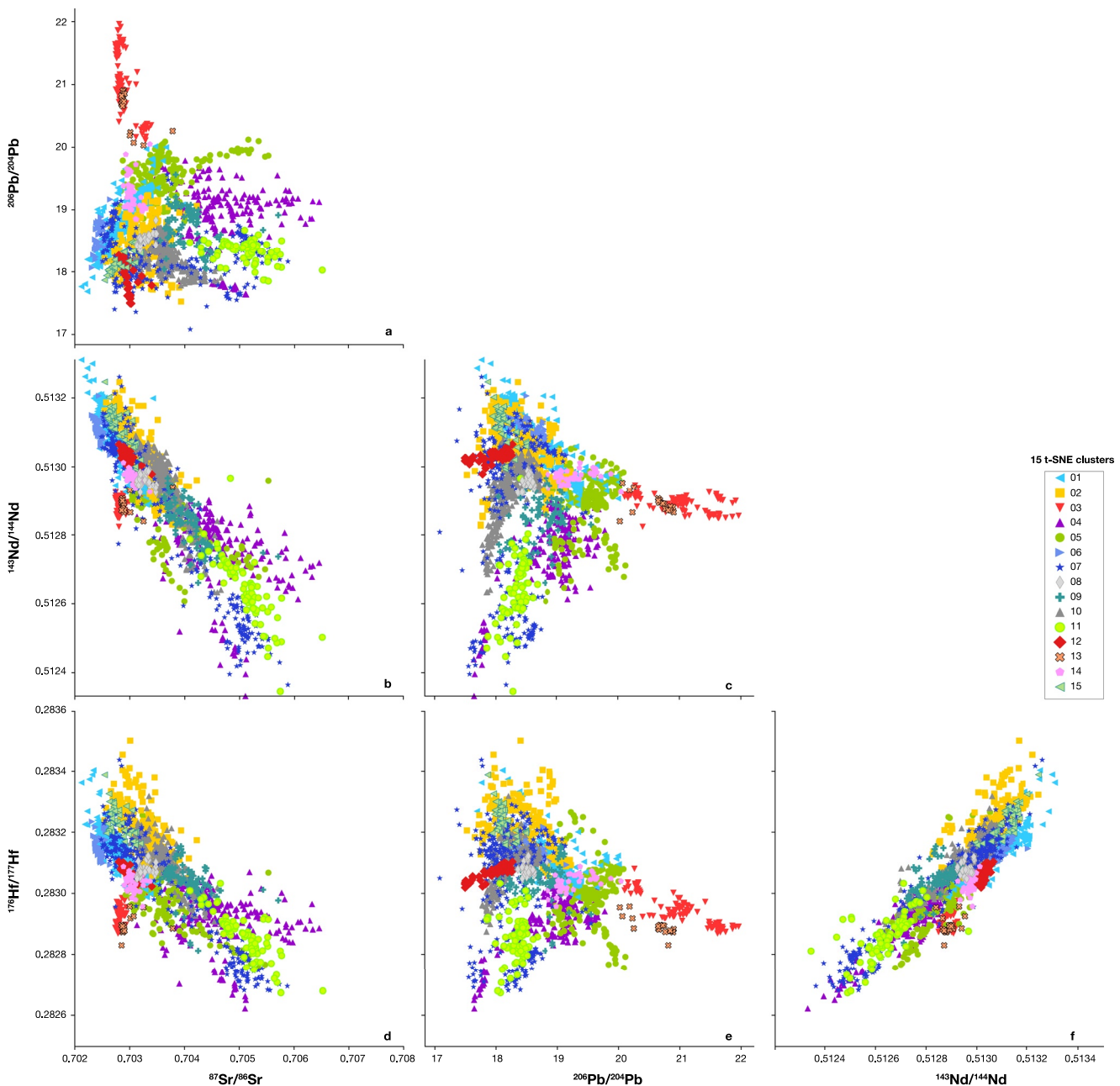


**Figure 7.** 2D plots of the Sr-Nd-Hf-Pb isotope data (Figures 2 and 3, Table S1), labeled by their assignment to the 15 t-distributed stochastic neighbor embedding (t-SNE) clusters defined in Figure 5b. The Sr-Nd-Hf-Pb isotope ratios of basalts from a given locality within each t-SNE cluster have variable ranges and overlap to different extents with one another, and with basalts in other clusters. This observation shows that the 2D plots are insufficient for identifying groupings in multi-isotopic space. It also suggests that oceanic basalts sample small-scale, stochastically distributed isotopic heterogeneities rather than a small number of discrete, isotopically homogeneous components (e.g., equivalent to the number of t-SNE clusters).

#### 4.1.2. “Common Component”

Figure 7 shows that many of the samples that constitute the different t-SNE clusters overlap in the 2D plots of the actual data. Yet, suites that overlap in one or more panels in Figure 7, do not overlap in Figure 5, so crucial information is lost when inspecting multi-dimensional data in 2D diagrams, which cannot be fully compensated for by considering multiple combinations of 2D diagrams (e.g., Zindler et al., 1982, compare Figure 1 with Figures 2 and 3). The 2D isotope ratio diagrams are therefore useful for comparing ranges of the parameters plotted, but not

for evaluating isotopic similarities or differences between samples from a multivariate isotopic data set (compare Figure 1 and Figures 2 and 3).

The latter is critical for assessing whether a common component might contribute to the isotopic variability of oceanic basalts, as often inferred from the large degree of overlap of the MORB-OIB data trends in 2-3D isotope ratios diagrams (e.g., Farley et al., 1992; Hanan and Graham, 1996; Hart et al., 1992; Zindler and Hart, 1986; Zindler et al., 1982). If such a “common component” were involved, a t-SNE cluster formed by the intersection (overlap) of various curvilinear trends would be expected, that is, an octopus-shaped pattern similar to Figure 4k (see also Figure S1 in Supporting Information S2). All t-SNE clusters in Figure 5 are clearly disconnected, however, and hence there is no indication that a common component contributes to the isotopic diversity of MORB-OIB on a global scale.

The apparent overlap of the MORB-OIB isotope data trends from different locations in 2-3D isotope ratios diagrams (Figures 2 and 7) is therefore an artifact caused by losing 3–4 degrees of freedom when inspecting 5-6D data in 2-3D (Zindler et al., 1982). This invalidates any inference made for mantle compositional evolution based on the existence of such a discrete “common component,” its potential nature or distribution within the mantle.

#### 4.2. Isotopic Similarities Between Oceanic Basalts

To investigate the isotopic similarities between oceanic basalts from different ocean islands or ridge segments quantitatively, the fraction of samples from a given location in one of the 15 t-SNE clusters,  $f_{\text{t-SNE } i\text{-location}_j}$ , is shown in Figure 8 (see caption for further details). The higher the value for  $f_{\text{t-SNE } i\text{-location}_j}$  the greater the contribution of samples from location  $j$  to a single t-SNE $_i$  group. A value  $f_{\text{t-SNE } 10\text{-Hawaii}} = 1$ , for example, indicates not only that all samples from Hawaii fall into t-SNE cluster 10, but also that no samples from other locations contribute to this t-SNE cluster (Figures 5 and 8). Values for  $f_{\text{t-SNE } i\text{-location}_j} < 1$  indicate that either all samples from location  $j$  fall into t-SNE cluster  $i$ , yet there are samples from other locations that also contribute to the same t-SNE cluster, or, that some samples from location  $j$  fall into t-SNE cluster  $i$ , but others from the same location are in at least one other cluster (hence the differences between Figures 6 and 8).

The calculated values for  $f_{\text{t-SNE } i\text{-location}_j}$  define a unique color pattern for each group of samples in Figure 8; similar patterns reflect similar relative contributions to the same t-SNE clusters, and thus a high degree of isotopic similarity between samples from the different groups. Calculating a correlation coefficient between the arrays of  $f_{\text{t-SNE } i\text{-location}_j}$  values for each sample group (rows in Figure 8) allows assessing their similarity quantitatively and results in a matrix of correlation coefficients between each sample group, shown in Figure 9. Because many OIB samples from distinct sample groups, and also some ridge segments, fall into a single t-SNE cluster, the t-SNE clusters straightforwardly define different “genera” of isotopically similar samples (Figures 5, 6, 8, and 9, Section 3.3). In addition, Figure 9 shows that several t-SNE clusters are formed by samples from a single locality, for example, OIB from Hawaii or MORB from Gakkel Ridge (clusters, 10 and 15, Figures 5b and 9). The composite t-SNE clusters (North, Central, and South Atlantic, the Indian Ocean, SW Pacific, clusters 2, 5, 7, 9, and 4 in Figures 5–9), show some expected similarities, such as those between the neighboring ocean islands Gough, Tristan da Cunha, and Walvis Ridge in the South Atlantic, the Canary and Cape Verde Islands in the Central Atlantic, or the similarity between basalts from St. Helena and the Cameroon Line. Other apparent isotopic affinities are perhaps more surprising, such as those between samples from Pitcairn and Society Islands in the SW Pacific, or the close similarity between OIB from the Galapagos Islands in the Pacific and those from Ascension Island in the equatorial Atlantic. Overall, Figures 6, 8, and 9 reveal a striking provinciality of samples that constitute the composite t-SNE clusters, which will be discussed in more detail in the following.

#### 4.3. The Isotopic “Provinciality” of Oceanic Basalts

Plotting the location of samples in each t-SNE cluster on a geographic map (Figure 10) shows that the distinct “provinciality” revealed by Figures 6, 8, and 9 is manifest as latitudinal (i.e., E-W oriented) domains of isotopically similar basalts (i.e., those in the different t-SNE clusters).

In the polar regions, these are the t-SNE clusters of the MORB from Gakkel Ridge in the North (cluster 15, Figure 10), and the Pacific Antarctic Ridge and southern East Pacific Rise in the South (cluster 6, Figure 10). MORB from the East Pacific and Mid-Atlantic Ridges approximately between 20°S and 20°N, and OIB from

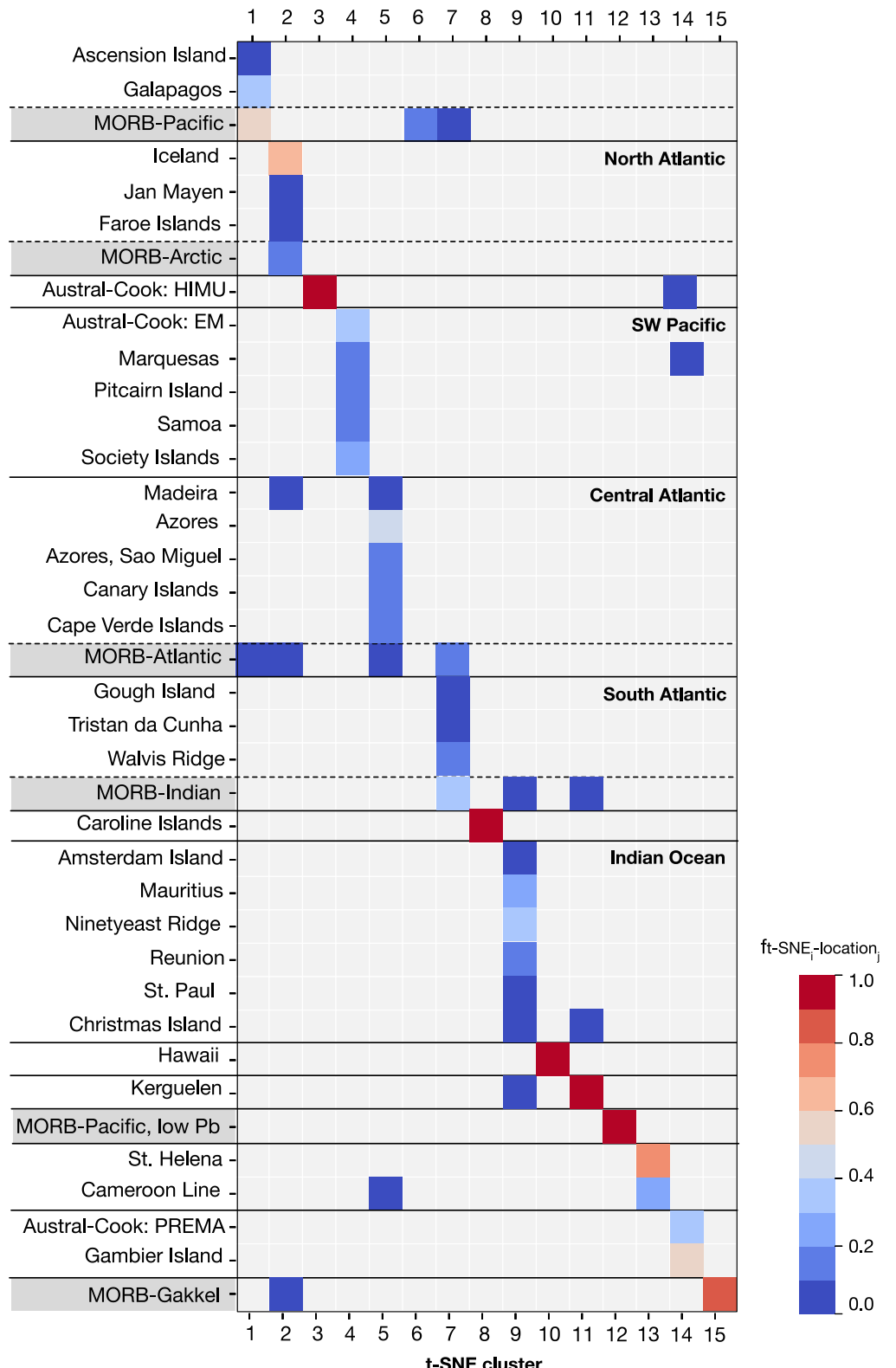


**Figure 8.** Plot showing the fraction of samples from a given location in one of the 15 t-distributed stochastic neighbor embedding (t-SNE) clusters defined in Figure 5b, calculated as  $f_{t\text{-SNE}_i\text{-location}_j} = (n_{t\text{-SNE}_i\text{-location}_j}) / (n_{\text{location}_j} + n_{t\text{-SNE}_i} - n_{t\text{-SNE}_i\text{-location}_j})$  meaning if there are 50 samples in location  $j$  ( $n_{\text{location}_j} = 50$ ) and 50 samples in t-SNE group  $i$  ( $n_{t\text{-SNE}_i} = 50$ ), and all 50 samples in t-SNE group  $i$  come from location  $j$  ( $n_{t\text{-SNE}_i\text{-location}_j} = 50$ ), then  $f_{t\text{-SNE}_i\text{-location}_j} = 50/(50 + 50 - 50) = 1$ . For further explanations see main text.

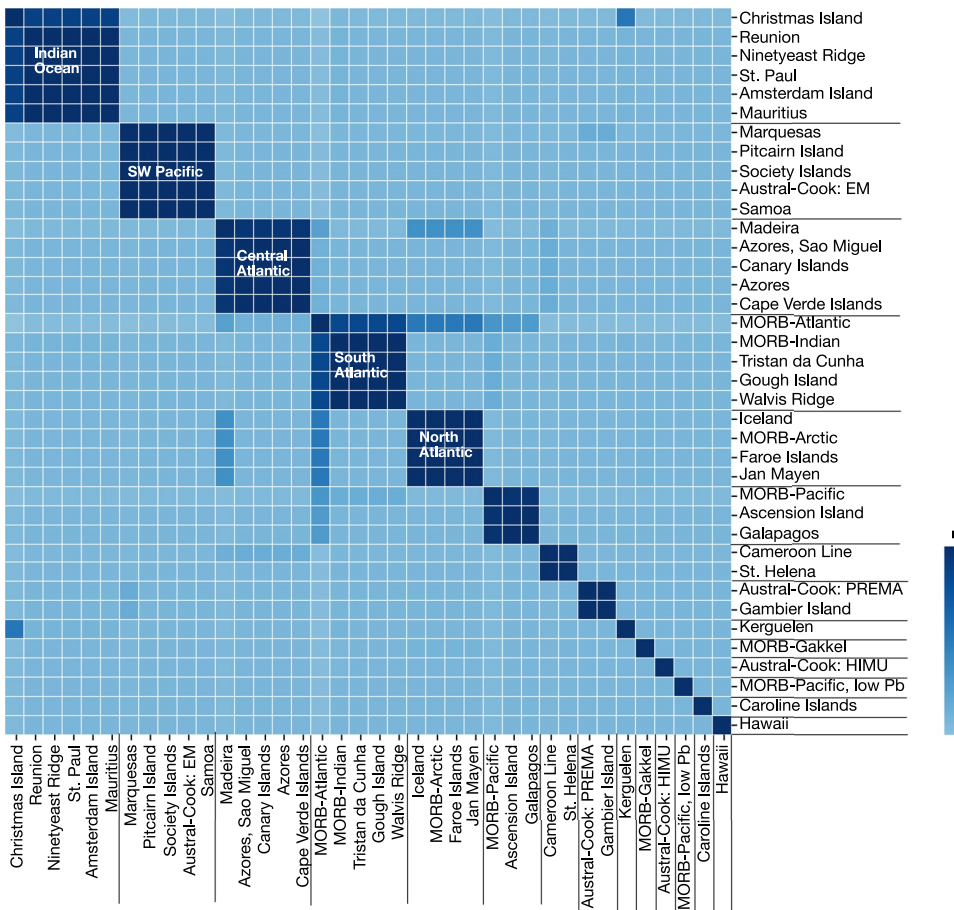


**Figure 9.** “Heatmap” based on a correlation matrix that is calculated from the data plotted in Figure 8 as follows: For each sample we assign which location it belongs to and in which t-distributed stochastic neighbor embedding cluster it is. This approach results in a matrix with true (1) or false (0) entries for each sample and each cluster and location. This allows calculating the total number of samples from each sample location (as defined in Figure 2) in any given t-SNE cluster. The fraction of samples from each location in each t-SNE cluster is then calculated with the formula given in the caption of Figure 8. This results in a (t-SNE cluster) versus (location) matrix where each cell contains the fraction of samples from each location in each t-SNE cluster. The location correlation matrix (location vs. location) is the basis for the “heatmap” plotted above. A correlation coefficient of 1 indicates that the same fraction of samples from a given location fall in the same t-SNE cluster. Table S4 explains the approach step-by-step.

Galapagos and Ascension Island define an equatorial domain that extends across different ocean basins and the South American continent (cluster 1, Figure 10). The OIB and MORB from adjacent ridges in the North (Iceland, Jan Mayen, Faroe Islands, cluster 2, Figure 10) and Central Atlantic (Azores, Canary and Cape Verde Islands; cluster 5, Figure 10) also form discrete domains, despite some geographic overlap of MORB in these two t-SNE clusters. The domains with the largest geographical extent are those of the OIB and MORB from the Southern Atlantic and Indian Ocean clusters (clusters 7 and 9, Figure 10). A distinct cluster is also formed by samples from several of the ocean island chains in the SW Pacific (cluster 4, Figure 10). Some of these global isotopic domains are reminiscent of large-scale “isotopic anomalies” postulated previously, namely the so-called “DUPAL anomaly” (Dupré and Allègre, 1983; Hart, 1984) or the “South Pacific Isotopic and Thermal Anomaly” (SOPITA; Staudigel et al., 1991), but do not reveal systematic ocean basin-scale differences between MORB from the Atlantic, Pacific, and Indian Ocean.

There are also a few point sources, especially the t-SNE clusters formed by the large-volume intra-plate basalts of Hawaii or the Caroline Islands (clusters 10 and 8, Figure 10), but in general, basalts from large latitudinal domains share the same isotopic affinity, that is, belong to the same composite t-SNE clusters.

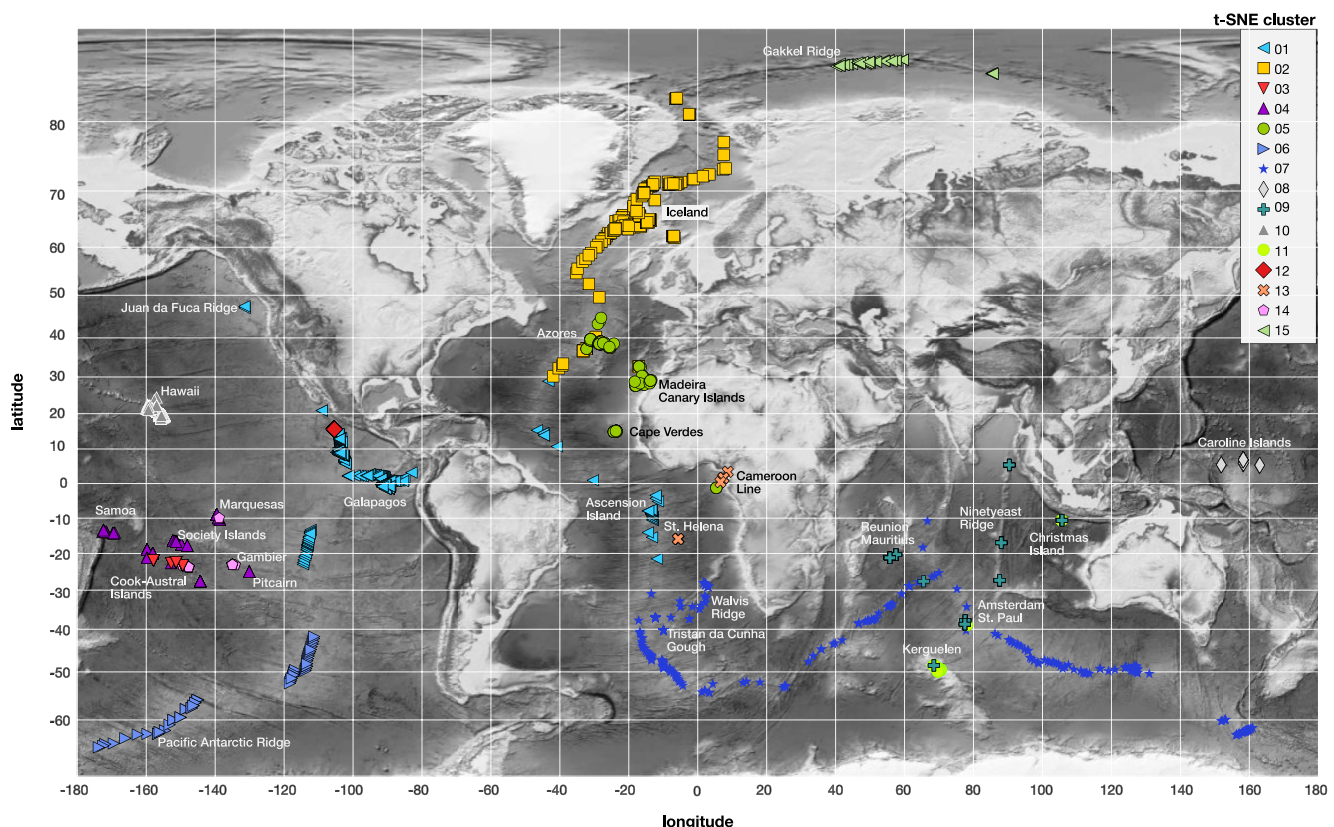


**Figure 10.** World-map showing the geographical distribution of samples in each of the 15 t-distributed stochastic neighbor embedding (t-SNE) clusters defined in Figure 5b. Groups of isotopically similar oceanic basalts, that is, those that fall in the same t-SNE cluster, delineate several globally distributed latitudinal domains. For further discussion see Sections 4.3 and 4.4.

#### 4.4. The Chemical Geodynamics of the Global Isotopic “Provinces”

The evident provinciality of samples that constitute the t-SNE clusters suggests that the weighted average of the mantle ingredients reflected by these basalts differs between different regions, or isotopic “domains” on a global scale. The latitudinal (E-W) arrangement of these isotopic domains suggests that similar mantle is dispersed laterally, consistent with global mantle flow patterns. That is, owing to the dominant influence of plate motions, asthenospheric mantle moves laterally away from zones of passively and/or actively upwelling mantle and towards areas of downwelling (subduction zones), and thus distributes mantle foremost laterally in the uppermost 200–300 km of Earth’s mantle (e.g., Bull et al., 2010; Hager and O’Connell, 1979, 1981; Steinberger, 2000; Steinberger and O’Connell, 1998).

##### 4.4.1. The North Atlantic

An instructive example for the lateral dispersal of upwelling mantle is the region around Iceland. According to the high-resolution reconstruction of seismic mantle velocities in the North Atlantic, Celli et al. (2021) conclude that: “[mantle] material rises upwards and eastwards from under Greenland and then follows the Mid-Atlantic Ridge southwards in the shallow upper mantle to under the Reykjanes Ridge. This indicates that once the flow of the hot material reaches the shallow asthenosphere, it is captured by the ridge and, instead of proceeding further east, flows southwards along the ridge axis, channeled within the thinner lithosphere beneath it” (see also Ito et al., 1999; Morgan, 1978; Schilling, 1973; Schilling et al., 1983; Sleep, 1997; Steinberger et al., 2019; Vogt, 1974; Whittaker et al., 2015). In other words, mantle from the same upwelling structure melts directly underneath Iceland, but also replaces the pre-existing asthenospheric mantle at or near the Mid-Atlantic Ridge north and south of Iceland. The latter is a simple and self-consistent explanation for the distribution and rate of volcanism in the North Atlantic region over the last ca. 60 Ma (e.g., Celli et al., 2021; Steinberger et al., 2019),

but also for the isotopic similarity between ridge and off-ridge basalts in the area, which define a common t-SNE cluster (cluster 2, Figures 6 and 8–10).

Within this framework, the isotopic similarity of ridge and off-ridge basalts in the North Atlantic region results from large-scale lateral dispersal of mantle from a more or less focused mantle upwelling (“plume”) in the shallow mantle (aka “plume-ridge interaction”). Consequently, melting of compositionally identical, albeit inherently heterogeneous mantle occurs in on-, near-, or off-ridge settings. Similar scenarios may also explain the latitudinally confined isotopic domains, and the striking isotopic similarity between MORB and OIB basalts in several other regions defined by composite t-SNE clusters (Figure 10).

#### 4.4.2. The Central Atlantic

In the Central Atlantic, on- and off-ridge volcanism at the Azores plateau and intra-plate volcanism at the Canary and Cape Verdes Islands is probably fed by several focused mantle upwellings (“plumes”) rising from a larger, deep-mantle upwelling (e.g., Civieiro et al., 2021; Davaille et al., 2005; French and Romanowicz, 2015; Montelli et al., 2004; O’Neill and Sigloch, 2018; Saki et al., 2015; Steinberger, 2000; Yang et al., 2006). Hence the smaller, upper mantle upwellings that branch off from a common, deep-mantle root probably have a common origin, and thus produce isotopically similar basalts, even at islands located 100–1,000 km apart.

The different locations of these upper mantle upwellings within the Central Atlantic relative to the Mid-Atlantic Ridge is responsible for the different style of volcanism. Far from the Mid-Atlantic Ridge, ocean island volcanism at the Canary and Cape Verdes Islands occurs over focused mantle upwellings in intra-plate settings, but closer to the Mid-Atlantic Ridge, the upwelling mantle flows laterally towards the elevated lithosphere–asthenosphere boundary and replaces pre-existing asthenospheric mantle over some distance along the adjacent ridge axis. Owing to the changing plate movement at the Azores triple junction (migrating ridge axis) relative to the deeper mantle upwelling, a stable region of high melt production forms, and creates unusually thick oceanic crust, the Azores plateau (e.g., Adam et al., 2013; Gente et al., 2003; Jellinek et al., 2003; Morgan, 1978; O’Neill and Sigloch, 2018; Ribe, 1996; Sleep, 1997; Steinberger, 2000; Vogt and Jung, 2018; Whittaker et al., 2015; Yang et al., 2006). The latter is a reasonable framework for generating the Azores plateau and for explaining why OIB from the Azores Islands and MORB from nearby ridges have the same isotopic affinity, that is, fall into the same t-SNE cluster (cluster 5, Figures 5–10; e.g., Bourdon et al., 1996; Davies et al., 1989; Dupré and Allègre, 1980; Goslin and Party, 1999; Schilling et al., 1983; White and Schilling, 1978).

Note that the t-SNE analysis of the larger 5D data set (Sr-Nd-Pb isotope ratios,  $n = 6,723$ ) presented in Supporting Information S2 includes more data from the Cape Verdes Islands with a greater isotopic range compared those in the 6D data set (compare Figure 2 and Figure S3 in Supporting Information S2). The 5D t-SNE results group the Cape Verde Islands into a distinct t-SNE cluster (Figures S3–S8 in Supporting Information S2), and thus including the Hf isotope data for these samples will be crucial for confirming whether the Cape Verdes form a unique t-SNE cluster, that is, are a group of ocean islands with isotopic affinity distinct from that of the other Central Atlantic OIB (Azores, Madeira, Canary Islands). This will also be key for assessing whether the upwelling mantle beneath the Cape Verdes is ultimately sourced from a different mantle root zone than the other Central Atlantic OIB, and thus for assessing the geodynamic evolution in this region in more detail.

#### 4.4.3. The South Atlantic

Arguably, the geodynamic setting in the South Atlantic is more complex than in the North and Central Atlantic, with a much larger aerial extent reaching into the Indian Ocean and a large bathymetric swell over several “hot-spots” (Discovery, Shona, and Bouvet). Nevertheless, recent geodynamic models provide a self-consistent framework for the distribution of volcanism by the interplay between deep-sourced mantle upwellings and the motion and lithospheric structure of the African Plate (e.g., Celli et al., 2020; Colli et al., 2018; Gassmöller et al., 2016; Morgan et al., 2020; O’Connor et al., 2018; Sleep, 2002). Capturing of a single mantle upwelling (the Tristan “plume”) into the South Atlantic Ridge leads to a broad region of volcanic activity, and the development of the Walvis Ridge (Gassmöller et al., 2016; O’Connor et al., 2018). Notably, the age-progressive volcanism from Tristan-Gough along the Walvis Ridge, but also the parallel off-axis plateaus or seamount chains further south of this bathymetric swell (at the Discovery, Shona, and Bouvet area), probably originate by interaction between the South Atlantic Ridge and mantle upwellings sourced from a common, stable or slowly moving deeper-mantle upwelling (Davaille and Romanowicz, 2020; Gassmöller et al., 2016; O’Connor and Jokat, 2015; O’Connor et al., 2012, 2018). Generally consistent with recent seismic tomography (Celli et al., 2020; Davaille

and Romanowicz, 2020), lateral dispersal of upper mantle upwellings towards lithospheric lows in the developing South Atlantic ocean basin thus leads to decompression melting of compositionally similar, albeit heterogeneous mantle in a large area, and local tectonic settings, and is responsible for the isotopic resemblance of on- and near-ridge basalts, and OIB and in this region (e.g., Class and le Roex, 2011; Douglass et al., 1999; Hanan et al., 1986; Hoernle et al., 2015, 2016; Rohde et al., 2013; Schilling, 1985, 1991; Schwendrofska et al., 2016).

#### 4.4.4. The Indian Ocean

Present volcanism at Réunion and Mauritius is sourced by a deep-mantle upwelling, the Réunion “plume” (French and Romanowicz, 2015; Montelli et al., 2004, 2006), whose “interaction with the Central Indian Ridge has shaped volcanism in the Indian Ocean over the last ca. 65 Ma (e.g., Bredow et al., 2017 and references therein). The intermittent replacement of pre-existing asthenosphere with upwelling mantle when the Central Indian Ridge traversed the Réunion upwelling also explains the occurrence of geochemically anomalous MORB at approx. 20°S (e.g., Füri et al., 2011; Mahoney et al., 1989; Nauret et al., 2006; Schilling, 1991). There are only a handful of combined Sr-Nd-Hf-Pb isotope data from the Central Indian Ridge in our database, but these fall in the South Atlantic-Indian Ocean t-SNE cluster (cluster 7 in Figures 6 and 8–10), together with MORB from the Southwest and Southeast Indian Ridges, Atlantic MORB south of 30°S, and basalts from the Walvis Ridge, Tristan da Cunha and Gough Island. This grouping is confirmed by the t-SNE analysis of the 5D data set (Supporting Information S2), which contains a larger amount of data from the Central Indian Ridge (compare Figure 10 and Figure S8 in Supporting Information S2, but note that MORB from the Southeast Indian Ridge form a distinct t-SNE cluster in the 5D t-SNE analysis; see Supporting Information S2 for further discussion). Nonetheless, additional Hf isotope data for basalts from the Central Indian Ridge with available Sr-Nd-Pb isotope data, would allow a more detailed consistency test.

Since ca. 120 Ma, a deep-seated mantle upwelling, which is now located underneath Kerguelen island (the Kerguelen “plume”), and repeated, prolonged inflow of the upwelling material into the ridge system in the evolving Indian Ocean created the Kerguelen Plateau (e.g., Bredow and Steinberger, 2018; Jiang et al., 2020; Whittaker et al., 2013, 2015). Basalts from the Kerguelen Plateau form its own t-SNE cluster (cluster 11, Figures 5, 6, 8, and 10), consistent with derivation from a compositionally distinct, long-lived mantle upwelling. Several other massive volcanic features in the Indian Ocean, such as the Broken Ridge, Ninetyeast Ridge, and the Amsterdam-St. Paul Plateau are also attributed to capturing of the Kerguelen plume into the evolving ridge system in the Indian Ocean.

The Ninetyeast Ridge, for example, probably formed by capturing of the Kerguelen upwelling into the ridge between the Indian and Australian plate from ca. 90–80 to ~40 Ma (Bredow and Steinberger, 2018), consistent with the age-progressive volcanism along the ridge (e.g., Coffin et al., 2002; Duncan, 1991; Mahoney et al., 1983). At ca. 40 Ma, the onset of seafloor spreading at the Southeast Indian Ridge separated the Ninetyeast and Broken Ridge from the Kerguelen Plateau (e.g., Mutter and Cande, 1983; Müller et al., 2016). Since ca. 20 Ma, the “Chain of Dead Poets” seamount chain and the Amsterdam-St. Paul Plateau may also have formed by inflow of the Kerguelen plume into the Southeast Indian Ridge (e.g., Bredow and Steinberger, 2018; Morgan, 1978; Yale and Morgan, 1998), although most previous isotopic studies relate the formation of the Amsterdam-St. Paul Plateau to a separate mantle upwelling (e.g., Doucet et al., 2004; Graham et al., 1999; Janin et al., 2011; Johnson et al., 2000; Maia et al., 2011; Nicolaysen et al., 2007; Nobre Silva et al., 2013; Scheirer et al., 2000).

Strikingly, the basalts from the Ninetyeast Ridge and most basalts from the Amsterdam-St. Paul Plateau group into t-SNE cluster 9 (Réunion, Mauritius, etc.) rather than 11 (Kerguelen Plateau, Figures 5, 6, 8, and 10). Previous isotopic studies already noted that the Ninetyeast Ridge basalts are isotopically intermediate between those from the Kerguelen and the Amsterdam-St. Paul Plateau; thus, an explicit isotopic similarity to basalts from the Kerguelen Plateau could not be established (e.g., Frey and Weis, 1995, 1996; Nobre Silva et al., 2013; Saunders et al., 1991; Weis and Frey, 1991; Weis et al., 1992). Owing to the marginal, or lack of overlap of basalts from the Amsterdam-St. Paul Islands with those from the Kerguelen Plateau in various 2D Sr-Nd-Nd-Hf isotope ratios diagrams (e.g., Doucet et al., 2004; Graham et al., 1999; Johnson et al., 2000; Nicolaysen et al., 2007; Nobre Silva et al., 2013, Figure 2), their isotopic relation to the Kerguelen plume has also remained ambiguous. In part, this observation has motivated postulating a distinct Amsterdam-St. Paul “plume”. There is considerable overlap in 2D Sr-Nd-Hf-Pb isotope ratios, however, between basalts from the Amsterdam and St. Paul Islands and those from Réunion and Mauritius (Figure 2), and the t-SNE map (Figure 5a) also groups the Amsterdam-St. Paul basalts together with those from Réunion and Mauritius (cluster 9, Figures 5, 6, 8, and 10). An actual geodynamic

relation to the Réunion plume, however, appears implausible based on recent geodynamic models and the general tectonic evolution of the Indian Ocean (e.g., Bredow et al., 2017; Bredow and Steinberger, 2018; Whittaker et al., 2013, 2015). Similarly, formation of the Ninetyeast Ridge started at ca. 90–80 Ma (e.g., Coffin et al., 2002; Duncan, 1991; Mahoney et al., 1983), that is, before the appearance of the Réunion plume at ca. 65 Ma (e.g., Courtillot et al., 1986; Hofmann et al., 2000; Schoene et al., 2015), making it impossible to connect the formation of the Ninetyeast Ridge to the Réunion plume. Hence, although basalts from the Ninetyeast Ridge and Amsterdam-St. Paul Plateau group within the same t-SNE cluster as basalts from Réunion-Mauritius, there is an obvious discrepancy between geodynamic models (e.g., Bredow et al., 2017; Bredow and Steinberger, 2018) and isotopic affinity (Figures 5, 6, 8, and 10), which is an issue that is also not resolved by the t-SNE analysis of the larger 5D data set (Figures S3–S8 in Supporting Information S2). Better matching the geodynamic evolution of the Indian Ocean with the isotopic affinity of the on-, near-ridge and intra-plate basalts in this ocean basin may therefore be an intriguing target for refining chemical geodynamic models.

Interestingly, if 12 clusters are used to categorize the t-SNE map (Figure 5c), the clusters defined by the basalts from Kerguelen, Réunion (plus Amsterdam-St. Paul, Ninetyeast Ridge), but also the South Atlantic (including Tristan da Cunha, Gough and Walvis Ridge) merge together and assemble basalts from an enormous area across the South Atlantic and Indian Ocean in a common t-SNE cluster, reminiscent of the so-called “DUPAL anomaly” (Dupré and Allègre, 1983; Hart, 1984). One possible explanation for this large-scale isotopic similarity of basalts in the Indo-Atlantic is that the upper mantle upwellings beneath Kerguelen, Réunion, and the South Atlantic originate from a common deep-mantle root beneath South Africa (e.g., Bredow et al., 2017; Civieiro et al., 2021; Colli et al., 2018; Davaille et al., 2005; Davaille and Romanowicz, 2020; French and Romanowicz, 2015; Gassmöller et al., 2016; Montelli et al., 2004, 2006; O’Connor et al., 2018; Tsekhnistrenko et al., 2021; Wamba et al., 2021). Aggregation and dispersion of such deep-mantle material over several 100 Ma (e.g., Davaille et al., 2005; Davaille and Romanowicz, 2020; Flament et al., 2022) could therefore feed mantle of similar origin and thus composition into divergent upper mantle upwellings that surface over a prolonged time period (10–100 Ma), and enormous geographic area. Such “episodic destabilization of a hot, chemically heterogeneous thermal boundary layer at the bottom of the mantle” (Davaille et al., 2005) may be one possible scenario for explaining the occurrence of several widely spaced mantle upwellings with common deep-mantle origin, and thus the isotopic resemblance of basalts from the Indian and South Atlantic Ocean (Doucet et al., 2020; Tsekhnistrenko et al., 2021), but also in the SW Pacific, as discussed in the following.

#### 4.4.5. The SW Pacific

Basalts from the Societies, Samoa, and Pitcairn Island together with most samples from the Marquesas Islands and some from the Cook-Austral Islands (“Cook-Austral: EM,” Figure 5b) form t-SNE cluster 4 (Figures 5b, 6, 8, and 10). In contrast, highly diverse isotopic signatures are observed for the lavas from the Cook-Austral Islands, which fall into three different t-SNE clusters (cluster 3, 4, and 14, Figures 5b, 6, 8, and 10). Some of the “Cook-Austral: EM” samples are in cluster 4, but samples from Gambier Island and the “Cook-Austral: PREMA” samples form t-SNE cluster 14, and the “Cook-Austral: HIMU” samples, the ones with the highest Pb isotope ratios (Figure 2), form cluster 3.

Overall, there is no simple relation between the isotopic affinity, inferred mantle upwelling structures from seismology, geodynamic models, or geographic age patterns of volcanism in the SW Pacific. The SW Pacific is a bathymetric high, the so-called “Pacific Superswell” (Adam et al., 2014; McNutt and Fisher, 1987) that overlies a large area of low seismic velocities in the lower mantle (e.g., Grand, 2002; Maggi et al., 2006; Masters et al., 2000; Mégnin and Romanowicz, 2000; Montelli et al., 2006; Ritsema et al., 2011; Zhao, 2004), which may represent a broad mantle upwelling or a cluster of smaller upwellings that are seismically difficult to resolve as separate structures (e.g., Bull et al., 2009; Davaille and Romanowicz, 2020; Kelly and Bercovici, 1997; Schubert et al., 2004). Low seismic velocities are also identified in the upper mantle beneath most island chains (Society, Pitcairn, and Rarotonga Island and Arago and Macdonald Seamount of the Cook-Austral chain), with the exception of the Marquesas Islands (e.g., Obayashi et al., 2016; Suetsugu et al., 2009; Tanaka et al., 2009). The geometry of these low seismic anomalies is complex, however, and a connection between upper and lower mantle seismic structure is only identified beneath Rarotonga (Obayashi et al., 2016). Moreover, volcanism conforms to age-progressive volcanism over a single focussed mantle upwelling for Samoa (e.g., Duncan, 1985; Hart et al., 2004; Jackson et al., 2010; Koppers et al., 2008) and the Societies (e.g., Blais et al., 2002; Cordier et al., 2016; Guillou et al., 2005; Uto et al., 2007; White and Duncan, 1996), but does not for the Cook-Austral

and Marquesas Islands (e.g., Bonneville et al., 2006; Chauvel et al., 1997, 2012; Konter et al., 2008; Legendre et al., 2005; McNutt et al., 1997). Rather, near-synchronous volcanic eruptions occur on several different, and widely spaced islands within the Austral-Cook chain (>1,000 km; Ballmer et al., 2009; Bonneville et al., 2006; Chauvel et al., 1997; Turner and Jarrard, 1982) and the Marquesas Archipelago (several 100 km, Chauvel et al., 2012; Legendre et al., 2005).

Volcanism in the SW Pacific region has therefore often been related to several small upper mantle upwellings rising from a deep, broad mantle root zone (Cadio et al., 2011; Chauvel et al., 2012; Davaille, 1999; Davaille et al., 2005; Konter et al., 2008; Koppers et al., 2003; McNamara and Zhong, 2004; Suetsugu and Hanyu, 2013). In this scenario, short, systematic age progressions along the same vector as plate motion would be expected (Ballmer et al., 2009, 2010), but are not always observed (see above). Moreover, the complex spatial and temporal patterns of volcanism at the Cook-Austral chain would require that several closely-spaced, short-lived upper mantle upwellings coexist(ed) (e.g., Ballmer et al., 2010; Bonneville et al., 2006; Clouard and Bonneville, 2005; Clouard and Gerbault, 2008; McNutt et al., 1997). The local, or regional lithospheric structure may therefore also have an important control on volcanic activity (e.g., Adam et al., 2010, 2014; Jordahl et al., 2004; Koppers et al., 2003; McNutt and Bonneville, 2000; McNutt et al., 1997; Suetsugu and Hanyu, 2013), for example, by inducing mantle melting due to “small scale sublithospheric convection” (Ballmer et al., 2009, 2010), or “shear-driven upwelling” (Bianco et al., 2011; Conrad et al., 2010, 2011). These mechanisms may enhance melting and spread volcanism over localized, and perhaps transient, upper mantle upwellings (e.g., Davaille and Vatteville, 2005; Koppers et al., 2003), but may also be alternative mechanisms to produce linear chains of volcanoes by passive mantle upwellings on larger scales (Ballmer et al., 2009, 2010; Bianco et al., 2011; Conrad et al., 2010, 2011). Hence there is no common recipe, or cause of volcanism for the SW Pacific Islands. Rather, a specific combination of factors is required to produce the observed volcanism at each archipelago, or island chain in the SW Pacific through time, and these factors may also differ during different phases of volcanism (e.g., Konter and Jackson, 2012).

Despite the complexity of volcanism in the SW Pacific, it is remarkable that most OIB in this region fall in a single t-SNE cluster (cluster 4, Figures 5b, 6, 8, and 10) which is also confirmed by the t-SNE analysis of the larger 5D data set (Figures S3–S8 in Supporting Information S2). That is, on a global scale they form an isotopically distinct group (Figure 10), reminiscent of the “South Pacific Isotopic and Thermal Anomaly” (SOPITA, Staudigel et al., 1991). Staudigel et al. (1991) related the origin of the “SOPITA” to a large lower mantle upwelling that acquired its isotopic characteristics by accumulating an assemblage of recycled materials distinct from those sampled in other ocean basins. The isotopic variability in OIB on a local or regional scale would then be explained by feeding a slightly different combination of materials from a common lower mantle root into the more localized upper mantle upwellings under a given island or chain of islands (e.g., Castillo, 1988; Davaille and Romanowicz, 2020; Doucet et al., 2020; Konter et al., 2008; Jackson et al., 2018; Nebel et al., 2013). Notably, this scenario is similar to that discussed above for the large-scale isotopic domain in the South Atlantic and Indian Ocean (Section 4.4.4).

Nevertheless, the large isotopic diversity of the lavas from the Cook-Austral Islands is unique (e.g., Bonneville et al., 2006; Chauvel et al., 1997; Hanyu et al., 2011, 2013; Hauri and Hart, 1993; Hémond et al., 1994; Kogiso et al., 1997; Lassiter et al., 2003; Nakamura and Tatsumoto, 1988; Palacz and Saunders, 1986; Schiano et al., 2001; Woodhead, 1996), and shows that their mantle sources contain isotopically different components, which are small (<< size of melting region in shallow mantle), and heterogeneously distributed in space and time. The latter is also the case for other island groups in the SW Pacific (Samoa, Societies and Marquesas, e.g., Cordier et al., 2016; Chauvel et al., 2012; Duncan et al., 1986; Dupuy et al., 1987; Farley et al., 1992; Guillou et al., 2014; Jackson et al., 2007, 2015; Le Dez et al., 1996; Vidal et al., 1984; White and Duncan, 1996; Wright and White, 1987). Moreover, fast plate motions in the SW Pacific lead to fast lateral transport of mantle away from melting regions, which may lead to remelting of previously melted material, perhaps by lithosphere-controlled processes (see Section 4 above). If it indeed occurs, such renewed melting may tap different source components owing to prior preferential melting of more fusible source components and/or melting under different conditions (e.g., Ito and Mahoney, 2005), and may, in some cases, contribute to the observed spatial and temporal isotopic variability. Overall, the complex interplay between actively or passively upwelling mantle, lithospheric structure, plate movement, and melting highly heterogeneous mantle under different conditions, perhaps even repeatedly, makes the SW Pacific a puzzling, yet fascinating area for improving our understanding of the chemical geodynamics of Earth's mantle.

#### 4.4.6. The Equatorial Pacific and Atlantic

Capturing of a deep mantle upwelling in a nearby ridge feeds volcanism at the Galapagos Archipelago and the Galapagos Spreading Center (Hooft et al., 2003; Ito and Bianco, 2015; Morgan, 1978; Schilling et al., 1982; Villagomez et al., 2007), and readily accounts for the isotopic similarity of the associated basalts (e.g., Blichert-Toft and White, 2001; Christie et al., 2005; Detrick et al., 2002; Geist et al., 1988; Harpp and White, 2001; Harpp et al., 2002; Mittelstaedt et al., 2012; Schilling et al., 2003; White et al., 1993), which group into t-SNE cluster 1 (Figures 5b, 6, 8, and 10).

Although there is no apparent geodynamic relation, basalts from Ascension Island in the equatorial Atlantic and MORB from the Atlantic and East Pacific Ridges between  $\sim 30^{\circ}\text{N}$  and  $\sim 30^{\circ}\text{S}$ , also fall into t-SNE cluster 1 (Figures 5b, 6, 8, and 10). The denser data coverage of the larger 5D data set shows, however, that grouping the Atlantic MORB between ca.  $30^{\circ}\text{N}$  and  $30^{\circ}\text{S}$  together with those from the equatorial East Pacific Rise, the Galapagos Spreading Center, and OIB from the Galapagos Archipelago is an artifact resulting from the sparse data coverage of Atlantic MORB between ca.  $30^{\circ}\text{N}$  and  $30^{\circ}\text{S}$  (Figures S3–S8 in Supporting Information S2). Complementary Hf isotope analysis on previously analyzed samples of Atlantic MORB between ca.  $30^{\circ}\text{N}$  and  $30^{\circ}\text{S}$  (e.g., Gale et al., 2013) will thus be crucial for defining regional isotopic boundaries and affinities between MORB and OIB in the Central and South Atlantic north of ca.  $30^{\circ}\text{S}$  (compare Figures 10 and Figure S8 in Supporting Information S2), including the basalts from St. Helena and the Cameroon volcanic line discussed in the following.

#### 4.4.7. St. Helena—Cameroon Volcanic Line

Isotopically similar basalts from St. Helena and the Cameroon Volcanic Line form t-SNE cluster 13 (Figures 5b, 6, 8, and 10). The origin of volcanism on St. Helena Island (e.g., Chaffey et al., 1989; Hanyu et al., 2014; Kawabata et al., 2011) is generally related to a focused upper mantle upwelling, inferred from global seismic data (French and Romanowicz, 2015; Montelli et al., 2006). A recent tomography model shows that St. Helena Island is located over a seismically slow zone in the mantle's upper 200 km that extends towards to the Mid-Atlantic Ridge (Celli et al., 2020). Celli et al. (2020) interpret this structure as an upper mantle upwelling that is funneled westwards from St. Helena to the Mid-Atlantic Ridge, consistent with the observed age-progression along the overlying seamounts of the St. Helena Rise (e.g., Maher et al., 2015; O'Connor and Le Roex, 1992; O'Connor et al., 1999). The upper mantle seismic anomaly continues underneath the off- and onshore Cameroon Volcanic Line (Celli et al., 2020). Thus a long, continuous channel of slow seismic velocities connects the Mid-Atlantic Ridge, the St. Helena Rise, and the Cameroon Volcanic Line (Celli et al., 2020). This observation is strikingly consistent with the observed isotopic similarity of the associated basalts (Figure 5a).

However, volcanism along the Cameroon Volcanic Line is episodic, but coeval at both off- and onshore locations over 100–1,000 km distances (e.g., Fitton and Dunlop, 1985; Lee et al., 1994; Marzoli et al., 1999; Njome and deWit, 2014). It is thus difficult to reconcile with simple age-progression of volcanism resulting from migration over a single focussed mantle upwelling (e.g., Adam, 2022; Lee et al., 1994; Marzoli et al., 2000; Njome and de Wit, 2014; Reusch et al., 2010; Steinberger, 2000). A number of studies therefore attribute volcanism along the Cameroon Volcanic Line to regional mantle upwelling caused by shear-driven upwelling, small scale or edge driven convection, or lithospheric instabilities (e.g., Adams, 2022; Adams et al., 2015; Ballmer et al., 2015; King and Ritsema, 2000; Meyers et al., 1998; Milelli et al., 2012; Reusch et al., 2010, 2011; for a recent review and references therein). Although not all of these mechanisms are equally compatible with all geophysical observations (see Adam, 2022 for a recent review), the continuous channel of slow seismic velocities from Cameroon to the Mid-Atlantic Ridge may be related to “...hot asthenosphere moving along the gradient of the [shallowing] oceanic lithosphere–asthenosphere boundary” (Celli et al., 2020).

A different mechanism of mantle upwelling is therefore generally invoked for volcanism on St. Helena Island and the associated seamounts of the St. Helena Rise, and the Cameroon Volcanic Line. But the result is a chain of isotopically similar lavas, which raises the question if volcanism along the Cameroon Volcanic Line, to St. Helena Island and along the St. Helena Rise ultimately relates to mantle with similar origin, and may actually have a similar geodynamic cause. It should be tested, however, if the isotopic similarity persists when more (Hf) isotope data become available for lavas from the off-shore Cameroon Volcanic Line and the seamounts of the St. Helena Rise.

#### 4.4.8. Isotopic “Point Sources”

The t-SNE cluster of Hawaiian lavas (cluster 10, Figures 5b, 6, 8, and 10) indicates that Hawaiian volcanism is fed by mantle that is isotopically distinct on a global scale. Many local features of volcanism and geochemical variations in the Hawaiian lavas remain poorly understood (e.g., Ballmer et al., 2013; Bianco et al., 2008, 2011; Harrison et al., 2017; Jones et al., 2017; Stracke, 2021b; Weis et al., 2020), but in a global context, Hawaiian volcanism occurs over a classic long-lived, deep “mantle plume” (Morgan, 1971). As such, it is also a “point source” of isotopically distinct, but heterogeneous mantle feeding volcanism along the Hawaiian-Emperor chain for >80 Ma (e.g., Clague and Dalrymple, 1989; Shaw et al., 1980). Hence prolonged influx into its deep-mantle root must have sustained the upwelling (Davaille and Vatteville, 2005) and has led to production of voluminous intra-plate magmas (e.g., Wessel, 2016).

The Caroline Islands are another point source of intra-plate volcanism in our database that produces isotopically distinct basalts on a global scale (t-SNE cluster 8, Figures 5b, 6, 8, and 10). Compared to Hawaii, however, the duration of volcanism appears to be relatively short (ca. 11 Ma, Keating, Matthey, Helsley et al., 1984; Keating, Matthey, Naughton & Helsley, 1984; Jackson et al., 2017) and thus the mantle upwelling that produced the Caroline Islands may be rather short-lived (e.g., Davaille and Vatteville, 2005).

Overall, the t-SNE clusters defined by the Hawaiian and Caroline Islands are the two cases in the investigated database where isotopically distinct intra-plate basalts from one location are connected to a single long or short-lived transient mantle upwelling, and thus point-sources of isotopically similar mantle. In most cases, however, isotopically similar basalts are much more dispersed geographically, and remarkably, in most cases occur in both ridge and intra-plate tectonic settings, an aspect that will be discussed in more detail in the following.

### 4.5. The Isotopic Affinity of MORB and OIB

#### 4.5.1. Temporarily Common Mantle Sources for MORB and OIB

MORB and OIB within any of the composite t-SNE clusters have the same isotopic affinity on a regional scale, but there is also extensive isotopic overlap between MORB and OIB on a global scale (Section 3.3; Figures 2, 3, and 10–12). As discussed in Section 4.4, the interplay between active mantle upwellings, large-scale mantle flow and lithosphere thickness (i.e., ridge axis locations and lithospheric structure of the continents) determines how actively upwelling mantle is dispersed, where it reaches shallow-enough depths to melt and hence, where surface volcanism occurs, and how it is distributed geographically (e.g., Celli et al., 2021; Dymnt et al., 2007; Ito et al., 2003; Jellinek et al., 2003; Morgan, 1978, 1981; Ribe, 1996; Schilling, 1992; Sleep, 1990, 1997; Small, 1995; Steinberger et al., 2019; Whittaker et al., 2015). Specifically, the capturing of mantle upwellings by nearby ridges, either at present, or during the prior evolution of the present ocean basins, and the Atlantic and Indian Ocean basins in particular (Sections 4.4.3 and 4.4.4), has led to intermittent replacement of pre-existing asthenospheric mantle under the ridge axes and thus melting of mantle from the same active mantle upwelling over a large area in ridge and intra-plate tectonic settings (Section 4.4).

Early geochemical models advocate that the actively upwelling mantle (“plume”) “mixes” with or “contaminates” the sub-ridge mantle (e.g., Morgan, 1978, Schilling, 1973, 1985, 1991, 1992). Recent geodynamic models show, however, that “... there is little or no mixing or stirring between the [upwelling] and ambient mantle. The [actively upwelling mantle] is predicted to spread along the axis and simply push the ambient material away so that only plume material is present in the melting zone over the whole distance of ridge influenced by the plume” (Ito et al., 1997, 2003 and references therein; Ito and Bianco, 2015; see also; Bredow et al., 2017; Celli et al., 2021; Feighner et al., 1995; Kincaid et al., 1995; Ribe, 1996; Steinberger et al., 2019). Hence, a simple, self-consistent explanation for the large extent of isotopic similarity between MORB and OIB on a regional and global scale is that, intermittently, the same mantle melts in ridge and intra-plate settings.

#### 4.5.2. Isotopic Differences Between MORB and OIB

Despite the extensive overlap and close isotopic affinity between MORB and OIB on a regional scale, however, OIBs have higher average Sr and Pb, and lower average Nd and Hf isotope ratios than MORB on a global scale (Figures 11 and 12; e.g., White, 2010, and references therein). The long-held view is that OIBs sample a different blend of isotopically discrete components than MORB. Alternatively, and perhaps easier to reconcile with the close isotopic affinity of MORB and OIB on a regional scale (Figures 5, 6, 8, 10, and 12) is that

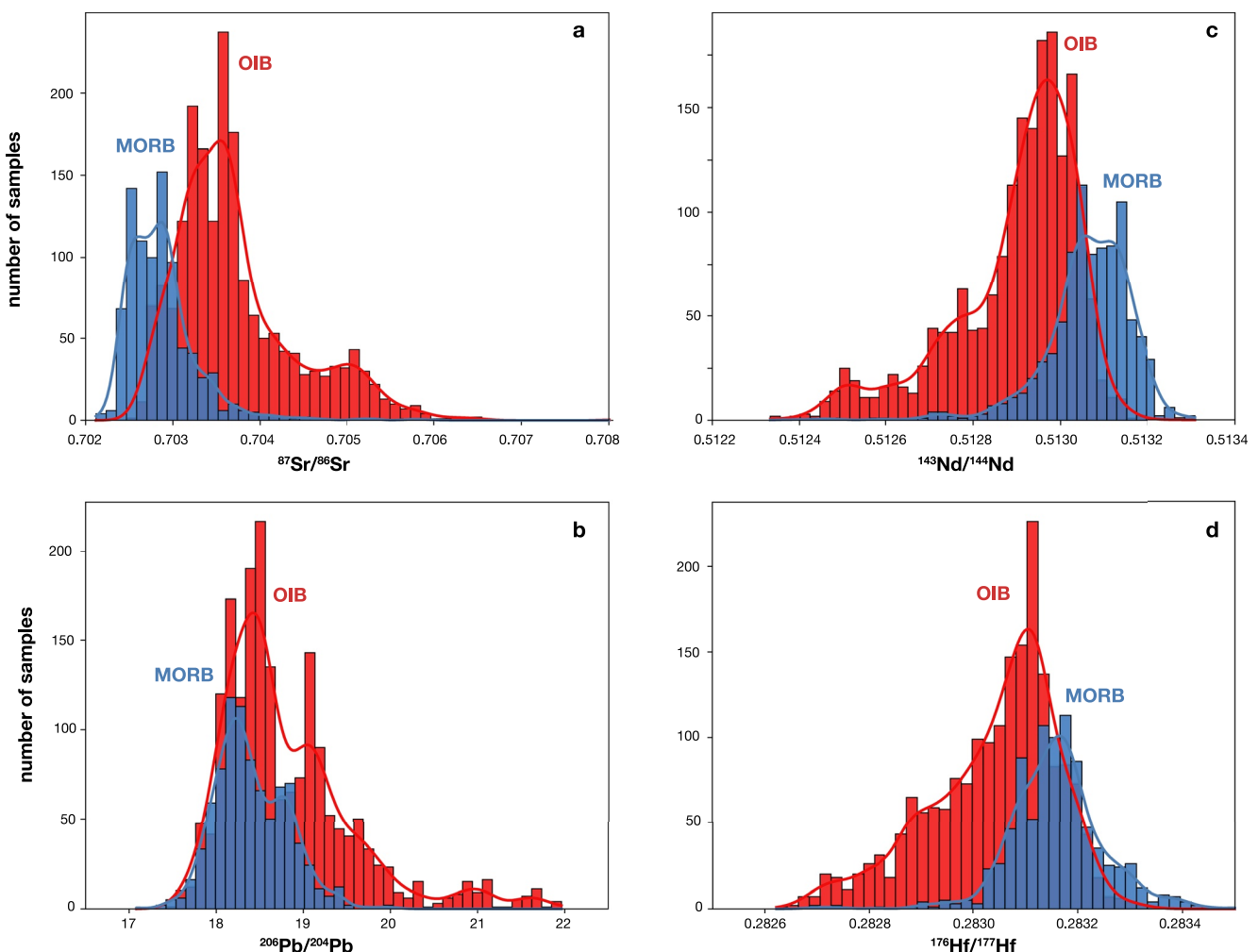


**Figure 11.** Histograms showing the distribution of mid ocean ridge and ocean island basalts  $^{87}\text{Sr}/^{86}\text{Sr}$  (a),  $^{206}\text{Pb}/^{204}\text{Pb}$  (b),  $^{143}\text{Nd}/^{144}\text{Nd}$  (c), and  $^{176}\text{Hf}/^{177}\text{Hf}$  (d) data compiled for this study (Figures 2 and 3, Table S1).

MORB and OIB sources contain similar ingredients, but partial melting under different P-T conditions and/or melt extraction through different drainage networks causes systematic differences in the aggregate melts erupted on the surface (e.g., Armienti and Gasperini, 2007; Ito and Mahoney, 2005; Helffrich and Wood, 2001; Kellogg et al., 2002, 2007; Kostitsyn, 2007; Meibom and Anderson, 2003; Morgan and Morgan, 1999; Rudge et al., 2013; Stracke, 2012, 2021a, 2021b; Stracke and Bourdon, 2009; Stracke et al., 1999, 2003a, 2005; Zindler et al., 1979). Whether source or sampling differences are more important has to be evaluated on a case-by-case basis, and there may not be a universally applicable answer to this issue. But at least in cases where active mantle upwellings have been captured by nearby ridges, the same mantle melts in on and off-ridge settings (Section 4.4). In these instances, isotopic differences between MORB and OIB must originate from sampling differences. Nevertheless, the systematic offsets in the average Sr-Nd-Hf-(Pb) isotope ratios between MORB and OIB are robust, even when including MORB produced close to active mantle upwellings in the comparison (Figures 11 and 12).

The prevailing explanation is that the sub-ridge mantle contains a higher proportion of incompatible element depleted source components than the mantle sources of OIB (e.g., Hofmann, 1997; White, 2010; Zindler and Hart, 1986). However, the excess buoyancy of the actively upwelling mantle under most OIB locations may, in part, derive from its residual nature (e.g., Matthews et al., 2016, 2021; Shorttle et al., 2014, 2020; Stracke et al., 2019), that is, the upwelling mantle contains a large proportion of mantle that has previously been melted and has thus become very incompatible element depleted, but also less dense (e.g., Afonso and Schutt, 2012; Schutt and Lesher, 2006). Such residual mantle can still produce considerable amounts of melts (e.g., Byerly and Lassiter, 2014; Sanfilippo et al., 2021), because incompatible elements are almost quantitatively extracted for

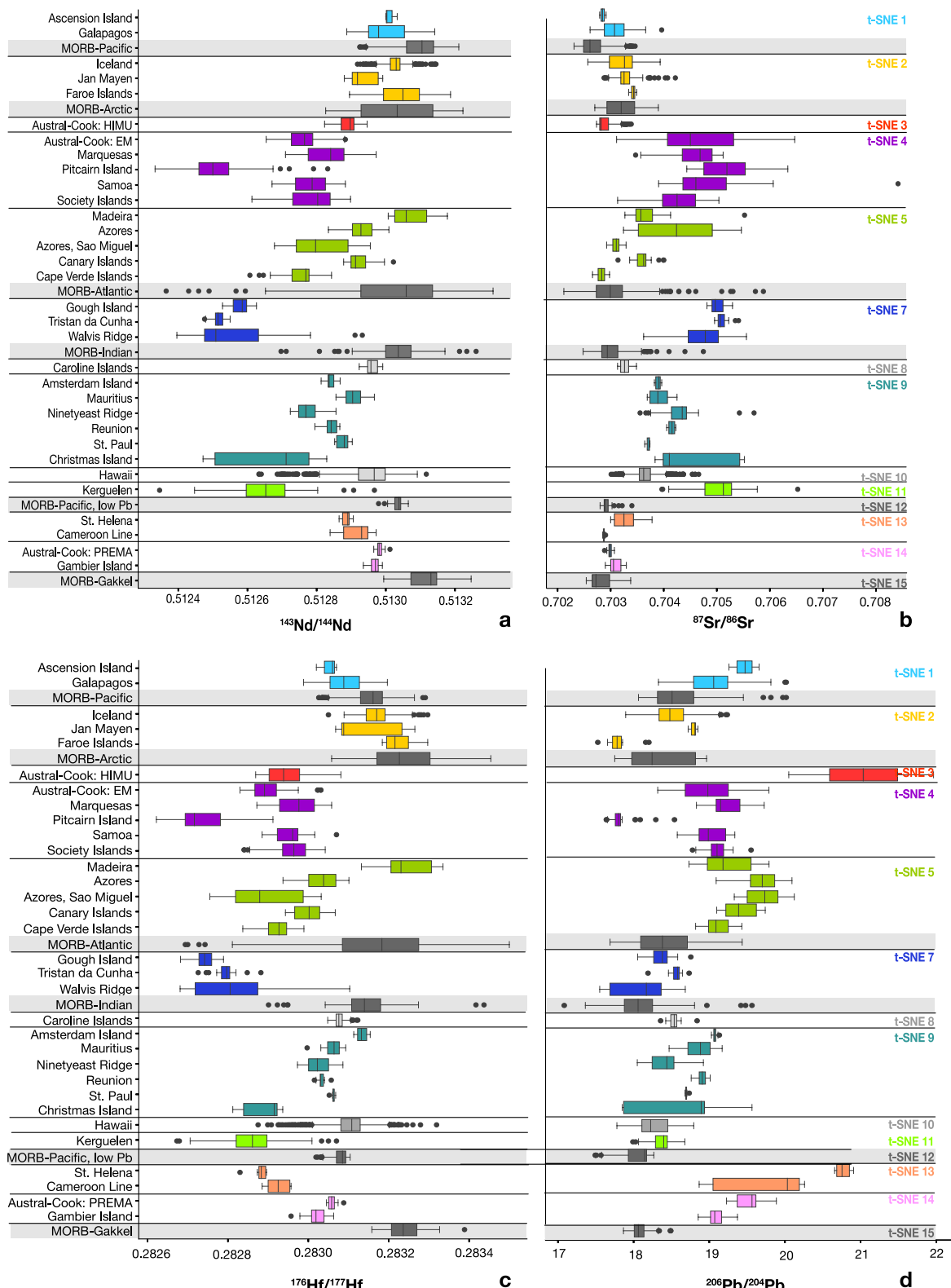


**Figure 12.** Box plots showing the range of  $^{87}\text{Sr}/^{86}\text{Sr}$ ,  $^{206}\text{Pb}/^{204}\text{Pb}$ ,  $^{143}\text{Nd}/^{144}\text{Nd}$ , and  $^{176}\text{Hf}/^{177}\text{Hf}$  variation in each sample group (Figures 2 and 3, Table S1). There is often nearly complete overlap between MORB and OIB (e.g.,  $^{143}\text{Nd}/^{144}\text{Nd}$ ), but the average mid ocean ridge and ocean island basalts Sr-Nd-Hf-Pb isotope ratios are statistically different. Color coding and grouping into 15 t-SNE clusters as in Figures 5b, 7, and 10.

small extents of melts extraction ( $\sim 1\text{--}5\%$ ), but it takes up to 20% of melt extraction to exhaust clinopyroxene, and thus considerably lower melt productivity (e.g., Asimow et al., 1997). Hence residual mantle contributes little to the incompatible element budget, and therefore to the Sr-Nd-Hf-Pb isotope ratios of the erupted melts, which are a weighted average of melts from all source constituents (e.g., Rudge et al., 2013; Stracke, 2021a, 2021b; Stracke and Bourdon, 2009; Stracke et al., 2011; Willig et al., 2020). In this case, the incompatible element budget of the erupted melts will be dominated by the incompatible element enriched, but volumetrically minor source components. Compared to MORBs, this effect is exacerbated by the greater mean depth and lower average extent of melting that is imposed by the thicker lithospheric lid at most OIB locations, particularly if the incompatible element enriched source components have a lower melting temperature than the residual mantle (e.g., Ballmer et al., 2013; Bianco et al., 2008, 2011; Hirschmann and Stolper, 1996; Ito and Mahoney, 2005; Kogiso et al., 2003; Lambart et al., 2016; Morgan and Morgan, 1999; Pertermann and Hirschmann, 2003; Shorttle et al., 2014; Stracke et al., 1999, 2003a, 2021a, 2021b).

Contrary the common notion, therefore, the actively upwelling mantle under most OIB locations may contain a greater proportion and/or more incompatible element depleted, residual mantle than the sub-ridge mantle (e.g., Stracke et al., 2019; Willbold and Stracke, 2006) in good agreement with the results of recent geodynamic models (Tucker et al., 2022), which also suggest that the lower mantle, that is, the ultimate root zone for many active mantle upwellings, is “enriched in highly processed material.”

## 5. Synthesis

Analysis of multi-variate isotope data with t-SNE is useful for identifying isotopic affinities of oceanic basalts. The t-SNE map (Figure 5a) confirms some of the isotopic resemblances previously gleaned from inspection of 2-3D isotope ratios diagrams (i.e., among several of the “EM”-type basalts; e.g., Zindler and Hart, 1986; Stracke, 2012; Willbold and Stracke, 2010), and also confirms the isotopic distinctiveness of “HIMU”-type basalts (e.g., Stracke et al., 2005; Zindler and Hart, 1986). But the t-SNE map also reveals isotopic affinities not previously recognized (discussed in detail in Sections 3 and 4), and shows that inspecting multi-variate isotope data in 2-3D isotope ratios diagrams can be misleading (e.g., Zindler et al., 1982). In particular, the apparent overlap of MORB-OIB data trends in 2-3D isotope space is not present in multi-dimensional isotope space (compare Figures 1–3, 4e, and 5). The inferred discrete “common component” to most MORB-OIB mantle sources (e.g., Farley et al., 1992; Hanan and Graham, 1996; Hart et al., 1992; Zindler and Hart, 1986; Zindler et al., 1982) is therefore a red herring (Section 4.1.2).

Figure 7 shows that the Sr-Nd-Hf-Pb isotope ratios of basalts from a given locality within each t-SNE cluster have variable ranges and overlap to different extents with one another and with basalts in other clusters. This observation suggests that oceanic basalts do not sample a small number of discrete, isotopically homogeneous components (e.g., equivalent to the number of t-SNE clusters), but rather suggest a stochastic distribution and sampling of small-scale isotopic heterogeneities (e.g., Stracke, 2021b and references therein). Moreover, the t-SNE clusters identify latitudinal domains of isotopically similar basalts (Figure 10), reminiscent of large-scale “isotopic anomalies” postulated previously, namely the so-called “DUPAL anomaly” in the Indo-Atlantic (Dupré and Allègre, 1983; Hart, 1984) or the “South Pacific Isotopic and Thermal Anomaly” (SOPITA; Staudigel et al., 1991). The latitudinal domains delineated by basalts in a given t-SNE cluster are not restricted to the SW Pacific and Indo-Atlantic, however, but are distributed globally (Figure 10 and Figure S8 in Supporting Information S2).

MORB in both polar regions (t-SNE clusters 6 and 15, Figure 10), for example, form distinct isotopic domains far from active upwellings (see additional discussion in Supporting Information S2). In the SW Pacific, on the other hand, the linear chains of intra-plate volcanoes with similar isotopic affinities are produced in a complicated geodynamic setting where the interplay of passive mantle upwelling driven by lithospheric forces and multiple active upper mantle upwellings, which probably have a common deep mantle root, results in the complex distribution of isotopically similar basalts (Section 4.4.5). In the Indian and Atlantic Oceans, isotopically similar basalts are observed in widely spaced intra-plate, but also near- or on-ridge locations (Sections 4.4.1–4.4.4). Most of the individual mantle upwellings in the Indian and Atlantic Oceans have, at present or during their prior evolution, intermittently supplied mantle to ambient ridges, which causes the regional-scale isotopic affinity of MORB and OIB in these ocean basins. Common to the Pacific and the Indo-Atlantic ocean basins is that the isotopic

similarity inferred for active mantle upwellings within a given isotopic domain often appears related to subsidiary upwellings in the upper mantle that rise from a common deep mantle root, leading to volcanism fed by similar mantle over large surface areas (e.g., Civiero et al., 2021; Davaille et al., 2005; Davaille and Romanowicz, 2020; Doucet et al., 2020; Flament et al., 2022; French and Romanowicz, 2015; Hassan et al., 2015; Tsekhnistrenko et al., 2021).

Overall, the results of the t-SNE analysis define a new basis for relating isotopic variations in oceanic basalts to mantle geodynamics. Nevertheless, it should be considered that the data analysis presented here, and thus the identified t-SNE clusters, will likely change to some extent with increasing number of data and isotope ratios included (e.g., Ce isotope ratio; Israel et al., 2020; Willig et al., 2020; compare the-SNE analysis of the 6D (Sr-Nd-Hf-Pb) data set, Figures 5–10 with that of the 5D (Sr-Nd-Pb) data set discussed in Supporting Information S2, Figures S3–S8 in Supporting Information S2). It should also be kept in mind that the isotopic variability of basalts does not correspond in a one-to-one fashion to mantle composition, due to variable mixing of melts from an unknown number of isotopically different mantle source components during extraction and evolution in the local melt drainage and storage networks. Hence any analysis of basalt data requires further forensic work to better constrain the nature and distribution of their mantle source ingredients, from a local to global scale (e.g., Stracke, 2021b and references therein).

## 6. Implications for “Chemical Geodynamics”

### 6.1. “Chemical Geodynamics” Since the 1980s

Allègre (1982) defined “chemical geodynamics, [as] an integrated study of the chemical and physical structure and evolution of the solid Earth” resulting in “a unified theory for terrestrial mass transfer phenomena.” Zindler and Hart (1986) stated that “the two approaches are [...] necessary and complementary to each other, and [...] will surely flourish in the years to come.” Indeed, both fields, geochemistry and geophysics, have progressed tremendously since the 1980s.

A vast amount and variety of geochemical data has become available (e.g., Table S1), allowing an increasingly detailed and precise chemical and isotopic characterization of the accessible Earth. The field of geophysics has seen several important breakthroughs. The invention of seismic tomography and the increasing extent and resolution of seismology have delivered increasingly detailed “images” of Earth’s density structure and thus current flow field. The latter show that the present Earth operates in a mode of whole-mantle convection, with continuous material exchange between the surface and the inner Earth. Laboratory studies and numerical models of mantle convection have substantially refined our understanding of mantle flow in the current “plate tectonic mode” of convection, where self-initiating active thermo-chemical upwellings (“plumes”) and downwellings (subduction) trigger passive response flows, and govern the distribution and stirring of materials with different physico-chemical properties (e.g., density and viscosity). Numerical geodynamic models, which were in their infancy during the 1980s, integrate data from seismology, experiments, and mineral physics, and track how tracers with given geochemical properties develop and distribute in the convective flow field. In theory, numerical geodynamic models therefore overcome the principal limitation that observational geophysics can only characterize the present state of the Earth (e.g., Zindler and Hart, 1986). Taken together, all of these major developments have fundamentally changed our perception of Earth’s inner workings and the geodynamic framework for interpreting the geochemical data.

But the field of geochemistry, largely, has struggled to keep pace with the progress in geophysics. This is due, in part, to often ignoring the cautionary advice not to transpose the 1980s categorization of basalt “phenotypes” to a small number of mantle components, let alone “reservoirs” (Section 4.1.1; White, 1985; Zindler and Hart, 1986). As a result, the community inherits an over-simplified, if not dubious view of mantle geochemical evolution, which has led to a particularly vexing stagnation in the field. Moreover, several simplistic concepts linger on that are firmly rooted in the 1980s view of a layered mantle with a “primitive,” or “undegassed” lower mantle and an incompatible element depleted upper mantle, with limited exchange between the two. There is, for example, the unwarranted notion that high  $^3\text{He}/^4\text{He}$  of many OIB require survival of some remaining fraction of “primitive” mantle in the lower mantle (e.g., Hilton and Porcelli, 2014). While alternative explanations (e.g., Bouhifd et al., 2020; Class and Goldstein, 2005; Gonnermann and Mukhopadhyay, 2009; Olson and Sharp, 2022; Parman, 2007; Tackley, 2015; Wang et al., 2022) are consistent with mantle geodynamics, the survival of some

fraction of primitive mantle remains a frequent requirement of geodynamic models (e.g., Jones et al., 2021 and references therein). In addition there is the “...widespread notion that the MORB-source mantle is isotopically nearly uniform, a myth that has persisted through many repetitions in the literature” (Hofmann, 2014), despite any obvious justification (Figure 2). One consequence has been that mantle geochemistry has disproportionately focused on investigating the origins of incompatible element enriched mantle components. Although this effort has resulted in the important insight that re-enrichment of Earth’s mantle in incompatible elements is largely due to recycling of oceanic and continental crust (e.g., Hofmann, 1997; Stracke, 2012; White, 2015; Zindler and Hart, 1986; and references in these studies), these recycled crustal components probably constitute only a small part (<10%, e.g., Lambart et al., 2016; Salters and Stracke, 2004; Sobolev et al., 2007; Stracke et al., 2003b) of Earth’s mantle.

Much less attention has been dedicated to investigating the other >90% of the mantle, which is largely the (peridotitic) residuum that is left behind by ocean crust formation (Section 4.5.2). Extraction of the oceanic crust depletes the residual mantle in incompatible trace elements, and makes it less dense. These density differences are significant (e.g., Afonso and Schutt, 2012; Schutt and Lesher, 2006), and coupled to variable incompatible element depletions that lead to enormous radiogenic isotope variations with time (e.g., Salters et al., 2011; Stracke, 2021a, 2021b; Stracke et al., 2011; Willig et al., 2020). This intrinsic coupling between radiogenic isotope variability, density, and thus seismic properties of the mantle, is a unique link between mantle geochemistry and geodynamics that has been little explored, but one that has enormous potential for advancing “chemical geodynamics” (e.g., Stracke, 2021b; Stracke et al., 2011, 2019).

## 6.2. “Chemical Geodynamics” in the 21st Century

Billions of years of generating and recycling oceanic and continental crust control the mantle’s chemical evolution. When recycled back into the mantle, the crust is stretched, disintegrated, redistributed, and stirred into the convective flow. But unless the length scale of the recycled crust is reduced to meters or centimeters, it does not re-homogenize by solid-state diffusion, or otherwise, with the residual mantle (e.g., Hofmann and Hart, 1978; Stracke, 2018, 2021a, 2021b; Tackley, 2015; and references in these studies). Earth’s mantle has therefore evolved into a lithologically and chemically heterogeneous agglomerate of variably incompatible element depleted residual mantle (peridotites) and incompatible element enriched recycled oceanic and continental crust ( $\pm$  the underlying lithosphere and other components).

The critical parameter for generating and destroying mantle heterogeneity therefore is how often mantle gets processed through melting regions in the shallow mantle, the so-called “mantle processing rate” (e.g., Huang and Davies, 2007; Stracke, 2018, 2021a, 2021b; Tackley, 2015; Tucker et al., 2022). The mantle processing rate also scales with the extent of incompatible element depletion of Earth’s residual mantle, which has generally been inferred from the radiogenic isotope ratios of MORB, or mass balances based on a simplistic account of crust-mantle complementarity, that is, effectively assuming that only the present mass of the continents has been produced. Both approaches essentially ignore the continental return flux into Earth’s mantle and therefore underestimate the average extent of incompatible element depletion of the residual mantle, and hence the mantle processing rate (see detailed discussion in Stracke, 2021b). Much higher Nd-Hf isotope ratios than in MORB are found in abyssal peridotites (Cipriani et al., 2004; Salters and Dick, 2002; Stracke et al., 2011; Warren et al., 2009) and melt inclusions (Stracke et al., 2019). These isotope signatures are a smoking gun that parts of Earth’s mantle have evolved with higher extents of incompatible element depletion than previously thought, for several  $10^8$ – $10^9$  years prior to sampling today. This implies that the rate of mantle processing (oceanic crust production), mantle-crust cycling, continent formation and destruction, and the vigor of mantle convection may be underestimated (e.g., Stracke, 2021a, 2021b; Stracke et al., 2011, 2019).

Notably, the chance for survival of some fraction of “primitive,” that is, previously unmelted mantle, decreases with increasing mantle processing rate. But trapped in the 1980s concept of a lower, mostly “primitive” (“undegassed”) mantle and the alluring prospect of discovering a sample of “bulk silicate Earth” (geochemistry’s “holy grail”), geochemists are hesitant to give up the hope that such “primitive” mantle exists. Presently available mantle samples, however, provide no chemical or isotopic evidence for any truly “primitive” mantle. Moreover, preventing mantle from being cycled through melting regions for 4.56 billion years is only feasible if it became considerably more dense and/or viscous than the remainder of the mantle (e.g., Becker et al., 1999; Davaille et al., 2003; Deschamps et al., 2011; Gurnis, 1986a, 1986b; Manga, 2010; McNamara and Zhong, 2004;

van Keken et al., 2014). Geochemical “box-models” or numerical geodynamic models set up to preserve some fraction or “primitive” mantle (e.g., Jones et al., 2021 and references therein) should therefore be viewed as end-members of a spectrum of models with more flexible boundary conditions. Widening the parameter space of geochemical “box-models” (e.g., Gonnerman and Mukhopadhyay, 2009; Kellogg et al., 2002, 2007; Kumari et al., 2016, 2019; Paul et al., 2002; Rosas and Korenaga, 2018; Rudge et al., 2005; Tucker et al., 2020) or numerical geodynamic models with integrated chemical tracers (e.g., Brandenburg et al., 2008; Christensen and Hofmann, 1994; Davies, 2002; Jones et al., 2019, 2021; Tucker et al., 2022; Xie and Tackley, 2004) to allow for faster mantle processing rates without the need to preserve some fraction of “primitive” mantle may therefore open up fundamentally new perspectives on the “chemical geodynamics” of the silicate Earth.

Deciphering the vigor and complexities of convective mantle flow is not only key for assessing if some “primitive” mantle has become stranded and thus preserved for billions of years. More generally, it allows assessing how the diverse materials with different origin, age and size spectra are dispersed and transported throughout the mantle. Among the principal driving forces of mantle flow are active thermo-chemical upwellings (“plumes”), transient mantle currents with complex shapes and sizes rising from a thermal boundary layer, most likely the core-mantle boundary (e.g., Ballmer et al., 2015; Davaille and Limare, 2015; Davaille and Vattemille, 2005; Davaille et al., 2003; Farnetani and Samuel, 2005; Jellinek and Manga, 2004; Koppers et al., 2021; Kumagai et al., 2008; Loper and Stacey, 1983; Olson and Singer, 1985; Ribe et al., 2007). Deep-rooted thermo-chemical upwellings, probably triggered by episodic aggregation and disaggregation of materials at the core-mantle boundary (Davaille and Romanowicz, 2020; Flament et al., 2022; Davaille et al., 2005; Jellinek and Manga, 2004; Li and Zhong, 2009; McNamara, 2019; Steinberger and Torsvik, 2012) may change their flow pattern and direction (e.g., Ballmer et al., 2013; Bredow et al., 2017; Celli et al., 2021; Davaille et al., 2002; Gassmöller et al., 2016; McNamara and Zhong, 2004; Steinberger, 2000; Tan et al., 2002), and get captured by ridges in the upper mantle (e.g., Celli et al., 2021; Dyment et al., 2007; Ito et al., 2003; Jellinek et al., 2003; Morgan, 1978, 1981; Ribe, 1996; Schilling, 1992; Sleep, 1990, 1997; Small, 1995; Steinberger et al., 2019), which in some instances produces large oceanic plateaus (e.g., Celli et al., 2021; Sager et al., 2019; Steinberger et al., 2019; Whittaker et al., 2015). Deep-rooted mantle thus melts and gets sampled by volcanism in both intra-plate and ridge settings. After locally overtaking the global stream of mantle flow on its way up, however, active upwellings reintegrate and get stirred back into the global mantle flow on their way down.

To what extent deep-rooted active upwellings therefore sample a different population of mantle materials than ambient lower mantle, and especially the passively upwelling upper mantle under MORBs, depends largely on viscosity-related differences in stirring efficiency between the upper and lower mantle. The lower mantle is probably 1 or 2 orders of magnitude more viscous than the upper mantle (e.g., Hager and Richards, 1989; Lithgow-Bertelloni and Richards, 1998; Mitrovica and Forte, 2004; van Keken et al., 2014), which causes less effective disaggregation, deformation and stirring of heterogeneous materials than in the upper mantle (e.g., Brandenburg and van Keken, 2007; Christensen and Hofmann, 1994; Davies, 2002; Farnetani and Samuel, 2003; Gurnis, 1986a, 1986b; Loper, 1985; Manga, 1996, 2010; Olson et al., 1984; Stegmann et al., 2002; Tackley, 2015; van Keken et al., 2014). Deep-rooted thermo-chemical upwellings may therefore transport a less efficiently stirred assemblage of similar materials, or an altogether different population of materials to the surface. Contrary to the long-held notion, however, such deep-mantle assemblages may contain a greater proportion and/or more depleted residual mantle than the sub-ridge mantle (e.g., Stracke et al., 2019; Tucker et al., 2022), which is consistent with the isotopic differences between average MORB and OIB (Section 4.5.2), their excess buoyancy (King and Adam, 2014; Sleep, 1990), and relatively moderate excess temperature (e.g., Green, 2015; Green and Falloon, 2015; Herzberg et al., 2007; Putirka, 2008), as well as recent geodynamic models (Tucker et al., 2022).

Much remains to be learned about the origin, residence time, distribution, and size spectrum of the different materials in the mantle. The latter is not only critical for assessing the mantle “provenance” of MORB and OIB sources, but also for how melting conveys mantle composition to the erupted melts. Generally, the composition of individual source components is suppressed by mixing with melts from other source components. Hence, melting blurs mantle heterogeneity and identifying the amount and composition of individual source components from the isotopic composition of the lavas presents a major challenge (e.g., Stracke, 2021b and references therein).

Overall, unraveling the chemical evolution of the solid Earth necessitates a sound understanding of the governing physical processes and their underlying driving mechanisms. But connecting geochemical information to the underlying geodynamics also requires accepting the inherent limitations of both disciplines. Geochemistry, for

example, “is inherently weak in terms of providing 3D information” (Zindler and Hart, 1986). That is, the averaging effect of melting makes it difficult, if not impossible, to relate the isotopic variability of basalts to the spatial distribution of individual materials in their mantle source in any simple fashion. Naive views, which postulate a one-to-one correspondence between isotope variations in lavas and the spatial distribution of materials in the underlying mantle source (or even beyond), should therefore not become constraints for geophysical models.

To some extent, these inherent limitations of the geochemical investigation of lavas can be avoided by studying actual mantle rocks, peridotites. The scarcity, small-scale, and multi-step evolution of peridotites –they have all melted to variable extents previously, reacted with traversing or trapped melts and seawater– makes deducing their pristine chemical and isotopic composition an intricate task (e.g., Bodinier and Godard, 2014; Brunelli et al., 2006; Dick, 1989; Hellebrand et al., 2002; Johnson et al., 1990; Seyler et al., 2007; Stracke et al., 2011; Warren, 2016). Nevertheless, isotopic data on abyssal peridotites offer complementary insights and perspectives on mantle evolution that are not available from the lavas, and are therefore key for further improving our understanding of the mantle’s geochemical evolution (e.g., Alard et al., 2005; Brandon et al., 2000; Brunelli et al., 2018; Cipriani et al., 2004; Day et al., 2017; Harvey et al., 2006; Lassiter et al., 2014; Liu et al., 2008; Paquet et al., 2022; Salters and Dick, 2002; Snow et al., 1994; Stracke et al., 2011; Warren, 2016).

The main limitation of geophysics is that “by its very nature, geophysics can only characterize the present state of the Earth” (Davaille and Vattewille, 2005; Zindler and Hart, 1986). This makes it exceedingly difficult to relate present geophysical observations to geochemical information about Earth’s mantle, which is all gathered on materials (peridotites and their melts, i.e., the ocean crust) that have been transported to the shallow mantle by past mantle flow. “Images” of the present seismic structure, and thus flow field of Earth’s mantle, for example, are only the final frame of a long, unseen convection “movie”. The prior tracks and ultimate “provenance” of the MORB and OIB sources in the shallow mantle are therefore notably disconnect from the present seismic “images” of the mantle (e.g., Davaille and Vattewille, 2005; Stracke, 2021b), which must be considered in attempts to relate geochemical and geophysical observations (Section 4.4). At least in theory, however, numerical models add a time dimension to geodynamics, can incorporate geochemical “tracers,” and they are thus a unique tool that bridges the gap between geochemistry and geophysics.

Ultimately, connecting geochemical observations to geodynamics requires a direct link between the parameters used in both fields. This link is the intrinsic coupling between increasing depletion in incompatible elements and iron of Earth’s residual mantle and the associated density decrease caused by multiple cycles of mantle melting (Sections 4.5.2 and 6.1, see also Stracke, 2018, 2021a, 2021b; Stracke et al., 2019). Better constraining the extent of chemical depletion of Earth’s residual mantle and how this affects first-order physical properties such as density, seismic wave speed, and perhaps also viscosity, is therefore key for better understanding the internal distribution of different materials (stirring) and convective vigor of Earth’s mantle. Eventually, the latter also controls the rate of mantle-crust interaction and continent formation. Better constraining how continuous melt extraction has affected the geochemical and geophysical properties of Earth’s residual mantle, which constitutes the vast majority of Earth’s mantle, may therefore change our perception of silicate Earth evolution, and may launch a 21st century era of “chemical geodynamics”.

## Data Availability Statement

All calculations were made with Python 3.9. A Jupyter notebook with the underlying data analysis is available from the authors upon request. Figures were made with Matplotlib (Hunter, 2007), available under the Matplotlib license at <https://matplotlib.org/>, or seaborn (Waskom, 2021). All compiled and newly reported MORB-OB data presented in this study are included in Excel format as supplementary tables (Tables S1 and S2) and available from the GEOROC Data Repository: Table S1: Stracke, Andreas; Willig, Michael; Genske, Felix; Béguelin, Paul; Todd, Erin, 2022, “Major and trace element concentrations and Sr, Nd, Hf, Pb isotope ratios of global mid ocean ridge and ocean island basalts,” <https://doi.org/10.25625/0SVW6S>, GRO.data, V1. Table S2: Stracke, Andreas; Willig, Michael; Genske, Felix; Béguelin, Paul; Todd, Erin, 2022, “Chemical and radiogenic isotope data of ocean island basalts from Tristan da Cunha, Gough, St. Helena, and the Cook-Austral Islands,” <https://doi.org/10.25625/BQENGN>, GRO.data, V1.

## Acknowledgments

A.S. thanks Erik Scherer for helpful discussions. This work was, in part, supported by the German Research Foundation (DFG) through Grant STR853/5-1. P.P. was, in part, supported by a Swiss National Science Foundation (SNF) Early Postdoc.Mobility Grant (P2SKP2\_187642) and a German Academic Exchange Service (DAAD) short-term research Grant (57552337). Oli Shorttle, Frances Jenner, and one anonymous reviewer are thanked for their thoughtful and constructive comments, which led to important clarifications. Paul Asimow is thanked for excellent editorial handling. Open Access funding enabled and organized by Projekt DEAL.

## References

- Adam, C., Madureira, P., Miranda, J. M., Lourenço, N., Yoshida, M., & Fitzenz, D. (2013). Mantle dynamics and characteristics of the Azores plateau. *Earth and Planetary Science Letters*, 362, 258–271. <https://doi.org/10.1016/j.epsl.2012.11.014>
- Adam, C., Yoshida, M., Isse, T., Suetsugu, D., Fukao, Y., & Barruol, G. (2010). South Pacific hotspot swells dynamically supported by mantle flows. *Geophysical Research Letters*, 37(8), L08302. <https://doi.org/10.1029/2010GL042534>
- Adam, C., Yoshida, M., Suetsugu, D., Fukao, Y., & Cadio, C. (2014). Geodynamic modeling of the South Pacific superswell. *Physics of the Earth and Planetary Interiors*, 229, 24–39. <https://doi.org/10.1016/j.pepi.2013.12.014>
- Adams, A. (2022). Insights into the source of magmatic hot-lines: Forty years of geophysical studies of the Cameroon volcanic line. *Frontiers of Earth Science*, 10, 838993. <https://doi.org/10.3389/feart.2022.838993>
- Adams, A. N., Wiens, D. A., Nyblade, A. A., Euler, G. G., Shore, P. J., & Tibi, R. (2015). Lithospheric instability and the source of the Cameroon volcanic line: Evidence from Rayleigh wave phase velocity tomography. *Journal of Geophysical Research: Solid Earth*, 120(3), 1708–1727. <https://doi.org/10.1002/2014jb011580>
- Afonso, J. C., & Schutt, D. L. (2012). The effects of polybaric partial melting on density and seismic velocities of mantle restites. *Lithos*, 134–135, 289–303. <https://doi.org/10.1016/j.lithos.2012.01.009>
- Alard, O., Luguet, A., Pearson, N. J., Griffin, W. L., Lorand, J.-P., Gannoun, A., et al. (2005). In situ Os isotopes in abyssal peridotites bridge the isotopic gap between MORBs and their source mantle. *Nature*, 436(7053), 1005–1008. <https://doi.org/10.1038/nature03902>
- Albarède, F. (1995). *Introduction to geochemical modeling*. Cambridge University Press.
- Allègre, C. J. (1982). Chemical geodynamics. *Tectonophysics*, 81(3–4), 109–132. [https://doi.org/10.1016/0040-1951\(82\)90125-1](https://doi.org/10.1016/0040-1951(82)90125-1)
- Allègre, C. J., Hamelin, B., Provost, A., & Dupré, B. (1987). Topology in isotopic multi-space and origin of the mantle chemical heterogeneities. *Earth and Planetary Science Letters*, 81(4), 319–337. [https://doi.org/10.1016/0012-821x\(87\)90120-8](https://doi.org/10.1016/0012-821x(87)90120-8)
- Armienti, P., & Gasperini, D. (2007). Do we really need mantle components to define mantle composition? *Journal of Petrology*, 48(4), 693–709. <https://doi.org/10.1093/petrology/egl078>
- Asimow, P. D., Hirschmann, M. M., & Stolper, E. M. (1997). An analysis of variations in isentropic melt productivity. *Philosophical Transactions of the Royal Society of London*, 355(1723), 255–281. <https://doi.org/10.1098/rsta.1997.0009>
- Balamurali, M., & Melkumyan, A. (2016). t-SNE based visualisation and clustering of geological domain. In A. Hirose, S. Ozawa, K. Doya, K. Ikeda, M. Lee, & D. Liu (Eds.), *Neural information processing. ICONIP 2016, Lecture notes in computer science* (Vol. 9950). Springer. [https://doi.org/10.1007/978-3-319-46681-1\\_67](https://doi.org/10.1007/978-3-319-46681-1_67)
- Ballmer, M. D., Ito, G., van Hunen, J., & Tackley, P. J. (2010). Small-scale sublithospheric convection reconciles geochemistry and geochronology of ‘Superplume’ volcanism in the western and south Pacific. *Earth and Planetary Science Letters*, 290(1–2), 224–232. <https://doi.org/10.1016/j.epsl.2009.12.025>
- Ballmer, M. D., Ito, G., Wolfe, C. J., & Solomon, S. C. (2013). Double layering of a thermochemical plume in the upper mantle beneath Hawaii. *Earth and Planetary Science Letters*, 376, 155–164. <https://doi.org/10.1016/j.epsl.2013.06.022>
- Ballmer, M. D., van Hunen, J., Ito, G., Bianco, T. A., & Tackley, P. J. (2009). Intra-plate volcanism with complex age-distance patterns: A case for small-scale sublithospheric convection. *Geochemistry, Geophysics, Geosystems*, 10(6), Q06015. <https://doi.org/10.1029/2009GC002386>
- Ballmer, M. D., van Keken, P. E., & Ito, G. (2015). 7.10—Hotspots, large igneous provinces, and melting anomalies. In G. Schubert (Ed.), *Treatise on geophysics* (2nd ed., pp. 393–459). Elsevier.
- Becker, T. W., Kellogg, J. B., & O’Connell, R. J. (1999). Thermal constraints on the survival of primitive bolbs in the lower mantle. *Earth and Planetary Science Letters*, 171(3), 351–365. [https://doi.org/10.1016/s0012-821x\(99\)00160-0](https://doi.org/10.1016/s0012-821x(99)00160-0)
- Belkina, A. C., Ciccolella, C. O., Anno, R., Halpert, R., Spidlen, J., & Snyder-Cappione, J. E. (2019). Automated optimized parameters for t-distributed stochastic neighbor embedding improve visualization and analysis of large datasets. *Nature Communications*, 10(1), 5415. <https://doi.org/10.1038/s41467-019-13055-y>
- Bianco, T. A., Conrad, C. P., & Smith, E. I. (2011). Time dependence of intraplate volcanism caused by shear-driven upwelling of low-viscosity regions within the asthenosphere. *Journal of Geophysical Research*, 116(B11), B11103. <https://doi.org/10.1029/2011JB008270>
- Bianco, T. A., Ito, G., van Hunen, J., Ballmer, M. D., & Mahoney, J. J. (2008). Geochemical variation at the Hawaiian hot spot caused by upper mantle dynamics and melting of a heterogeneous plume. *Geochemistry, Geophysics, Geosystems*, 9(11), Q11003. <https://doi.org/10.11029/2008GC002111>
- Blais, S., Guille, G. r., Guillou, H., Chauvel, C., Maury, R. C., Pernet, G., & Cotten, J. (2002). The island of Maupiti: The oldest emergent volcano in the society hot spot chain (French Polynesia). *Bulletin de la Société Géologique de France*, 173(1), 45–55. <https://doi.org/10.2113/173.1.45>
- Blichert-Toft, J., & White, W. M. (2001). Hf isotope chemistry of the Galapagos Islands. *Geochemistry, Geophysics, Geosystems*, 2(9), 2000GC000138. <https://doi.org/10.1029/2000gc000138>
- Bodinier, J. L., & Godard, M. (2014). 3.4—Orogenic, ophiolitic, and abyssal peridotites. In H. D. H. K. Turekian (Ed.), *Treatise on geochemistry* (2nd ed., pp. 103–167). Elsevier.
- Bonneville, A., Dosso, L., & Hildenbrand, A. (2006). Temporal evolution and geochemical variability of the South Pacific superplume activity. *Earth and Planetary Science Letters*, 244(1–2), 251–269. <https://doi.org/10.1016/j.epsl.2005.12.037>
- Bouhifd, M. A., Jephcoat, A. P., Porcelli, D., Kelley, S. P., & Marty, B. (2020). Potential of Earth’s core as a reservoir for noble gases: Case for helium and neon. *Geochemical Perspectives Letters*, 15, 15–18. <https://doi.org/10.7185/geochemlet.2028>
- Bourdon, B., Langmuir, C. H., & Zindler, A. (1996). Ridge-hotspot interaction along the Mid-Atlantic Ridge between 37°30' and 40°30'N: The U-Th disequilibrium evidence. *Earth and Planetary Science Letters*, 142(1–2), 175–189. [https://doi.org/10.1016/0012-821x\(96\)00092-1](https://doi.org/10.1016/0012-821x(96)00092-1)
- Brandenburg, J. P., Hauri, E. H., van Keken, P. E., & Ballentine, C. J. (2008). A multiple-system study of the geochemical evolution of the mantle with force-balanced plates and thermochemical effects. *Earth and Planetary Science Letters*, 276(1–2), 1–13. <https://doi.org/10.1016/j.epsl.2008.08.027>
- Brandenburg, J. P., & van Keken, P. E. (2007). Deep storage of oceanic crust in a vigorously convecting mantle. *Journal of Geophysical Research*, 112(B6), B06403. <https://doi.org/10.1029/2006JB004813>
- Brandon, A. D., Snow, J. E., Walker, R. J., Morgan, J. W., & Mock, T. D. (2000).  $^{190}\text{Pt}$ - $^{186}\text{Os}$  and  $^{187}\text{Re}$ - $^{187}\text{Os}$  systematics of abyssal peridotites. *Earth and Planetary Science Letters*, 177(3–4), 319–335. [https://doi.org/10.1016/s0012-821x\(00\)00044-3](https://doi.org/10.1016/s0012-821x(00)00044-3)
- Bredow, E., & Steinberger, B. (2018). Variable melt production rate of the Kerguelan HotSpot due to long-term plume-ridge interaction. *Geophysical Research Letters*, 45(1), 126–136. <https://doi.org/10.1029/2017gl075822>
- Bredow, E., Steinberger, B., Gassmöller, R., & Dannberg, J. (2017). How plume-ridge interaction shapes the crustal thickness pattern of the rRéunion hotspot track. *Geochemistry, Geophysics, Geosystems*, 18(8), 2930–2948. <https://doi.org/10.1029/2017GC006875>
- Brunelli, D., Cipriani, A., & Bonatti, E. (2018). Thermal effects of pyroxenites on mantle melting below mid-ocean ridges. *Nature Geoscience*, 11(7), 520–525. <https://doi.org/10.1038/s41561-018-0139-z>

- Brunelli, D., Seyler, M., Cipriani, A., Ottolini, L., & Bonatti, E. (2006). Discontinuous melt extraction and weak refertilization of mantle peridotites at the Vema lithospheric section (Mid-Atlantic Ridge). *Journal of Petrology*, 47(4), 745–771. <https://doi.org/10.1093/petrology/egi092>
- Bull, A. L., McNamara, A. K., Becker, T. W., & Ritsema, J. (2010). Global scale models of the mantle flow field predicted by synthetic tomography models. *Physics of the Earth and Planetary Interiors*, 182(3–4), 129–138. <https://doi.org/10.1016/j.pepi.2010.03.004>
- Bull, A. L., McNamara, A. K., & Ritsema, J. (2009). Synthetic tomography of plume cluster and thermochemical piles. *Earth and Planetary Science Letters*, 278(3–4), 152–162. <https://doi.org/10.1016/j.epsl.2008.11.018>
- Byerly, B. L., & Lassiter, J. C. (2014). Isotopically ultradepleted domains in the convecting upper mantle: Implications for MORB petrogenesis. *Geology*, 42(3), 203–206. <https://doi.org/10.1130/g34757.1>
- Cadio, C., Panet, I., Davaille, A., Diament, M., Métivier, L., & de Viron, O. (2011). Pacific geoid anomalies revisited in light of thermochemical oscillating domes in the lower mantle. *Earth and Planetary Science Letters*, 306(1–2), 123–135. <https://doi.org/10.1016/j.epsl.2011.03.040>
- Castillo, P. (1988). The Dupal anomaly as a trace of the upwelling lower mantle. *Nature*, 336(6200), 667–670. <https://doi.org/10.1038/336667a0>
- Celli, N. L., Lebedev, S., Schaeffer, A. J., & Gaina, C. (2021). The tilted Iceland Plume and its effect on the North Atlantic evolution and magmatism. *Earth and Planetary Science Letters*, 569, 117048. <https://doi.org/10.1016/j.epsl.2021.117048>
- Celli, N. L., Lebedev, S., Schaeffer, A. J., Ravenna, M., & Gaina, C. (2020). The upper mantle beneath the South Atlantic Ocean, South America and Africa from waveform tomography with massive datasets. *Geophysical Journal International*, 221(1), 178–204. <https://doi.org/10.1093/gji/gjz574>
- Cevik, I. S., Olivo, G. R., & Ortiz, J. M. (2021). A combined multivariate approach analyzing geochemical data for knowledge discovery: The Vazante–Paracatu Zinc District, Minas Gerais, Brazil. *Journal of Geochemical Exploration*, 221, 106696. <https://doi.org/10.1016/j.gexplo.2020.106696>
- Chaffey, D. J., Cliff, R. A., & Wilson, B. M. (1989). *Characterization of the St. Helena magma source*. In A. D. Saunders & M. J. Norry (Eds.) (pp. 257–276). Geological Society.
- Chauvel, C., Maury, R. C., Blais, S., Lewin, E., Guillou, H., Guille, G., et al. (2012). The size of plume heterogeneities constrained by Marquesas isotopic stripes. *Geochemistry, Geophysics, Geosystems*, 13(7), Q07005. <https://doi.org/10.1029/2012GC004123>
- Chauvel, C., McDonough, W., Guille, G., Maury, R., & Duncan, R. (1997). Contrasting old and young volcanism in Rurutu Island, Austral chain. *Chemical Geology*, 139(1–4), 125–143. [https://doi.org/10.1016/s0009-2541\(97\)00029-6](https://doi.org/10.1016/s0009-2541(97)00029-6)
- Christensen, U. R., & Hofmann, A. W. (1994). Segregation of subducted oceanic crust in the convecting mantle. *Journal of Geophysical Research*, 99(B10), 19867–19884. <https://doi.org/10.1029/93jb03403>
- Christie, D. M., Werner, R., Hauff, F., Hoernle, K., & Hanan, B. B. (2005). Morphological and geochemical variations along the eastern Galápagos spreading center. *Geochemistry, Geophysics, Geosystems*, 6(1), Q01006. <https://doi.org/10.1029/2004GC000714>
- Cipriani, A., Brueckner, H. K., Bonatti, E., & Brunelli, D. (2004). Oceanic crust generated by elusive parents: Sr and Nd isotopes in basalt-peridotite pairs from the mid-Atlantic Ridge. *Geology*, 32(8), 657–660. <https://doi.org/10.1130/g20560.1>
- Civiero, C., Custódio, S., Neres, M., Schlaphorst, D., Mata, J., & Silveira, G. (2021). The role of the seismically slow central-east Atlantic anomaly in the genesis of the Canary and Madeira volcanic provinces. *Geophysical Research Letters*, 48(13), e2021GL092874. <https://doi.org/10.1029/2021gl092874>
- Clague, D. A., & Dalrymple, G. B. (1989). Tectonics, geochronology and origin of the Hawaiian–Emperor volcanic chain. In E. L. Winterer, D. M. Hussong, & R. W. Decker (Eds.), *The geology of North America, volume N: The eastern Pacific Ocean and Hawaii* (pp. 188–217). Geological Society of America.
- Class, C., & Goldstein, S. L. (2005). Evolution of helium isotopes in the Earth's mantle. *Nature*, 436(7054), 1107–1112. <https://doi.org/10.1038/nature03930>
- Class, C., & le Roex, A. (2011). South Atlantic DUPAL anomaly—dynamic and compositional evidence against a recent shallow origin. *Earth and Planetary Science Letters*, 305(1–2), 92–102. <https://doi.org/10.1016/j.epsl.2011.02.036>
- Clouard, V., & Bonneville, A. (2005). Ages of Seamounts, islands, and plateaus on the Pacific plate. In G. Foulger, J. H. Natland, D. C. Presnall, & D. L. Anderson (Eds.), *Plumes, plates, and paradigms* (pp. 71–90). Special Paper 388.
- Clouard, V., & Gerbault, M. (2008). Break-up spots: Could the Pacific open as a consequence of plate kinematics? *Earth and Planetary Science Letters*, 265(1–2), 195–208. <https://doi.org/10.1016/j.epsl.2007.10.013>
- Coffin, M. F., Pringle, M. S., Duncan, R. A., Gladzenko, T. P., Storey, M., Müller, R. D., & Ghagan, L. A. (2002). Kerguelen hotspot magma output since 130 Ma. *Journal of Petrology*, 43(7), 1121–1137. <https://doi.org/10.1093/petrology/43.7.1121>
- Colli, L., Ghelichkhan, S., Bunge, H. P., & Oeser, J. (2018). Retrodictions of Mid Paleogene mantle flow and dynamic topography in the Atlantic region from compressible high resolution adjoint mantle convection models: Sensitivity to deep mantle viscosity and tomographic input model. *Gondwana Research*, 53, 252–272. <https://doi.org/10.1016/j.gr.2017.04.027>
- Conrad, C. P., Bianco, T. A., Smith, E. I., & Wessel, P. (2011). Patterns of intraplate volcanism controlled by asthenospheric shear. *Nature Geoscience*, 4(5), 317–321. <https://doi.org/10.1038/ngeo1111>
- Conrad, C. P., Wu, B., Smith, E. I., Bianco, T. A., & Tibbetts, A. (2010). Shear-driven upwelling induced by lateral viscosity variations and asthenospheric shear: A mechanism for intraplate volcanism. *Physics of the Earth and Planetary Interiors*, 178(3–4), 162–175. <https://doi.org/10.1016/j.pepi.2009.10.001>
- Cordier, C., Chauvel, C., & Hémond, C. (2016). High-precision lead isotopes and stripy plumes: Revisiting the Society chain in French Polynesia. *Geochimica et Cosmochimica Acta*, 189, 236–250. <https://doi.org/10.1016/j.gca.2016.06.010>
- Courtillot, V., Besse, J., Vandamme, D., Montigny, R., Jaeger, J.-J., & Cappetta, H. (1986). Deccan flood basalts at the Cretaceous/Tertiary boundary? *Earth and Planetary Science Letters*, 80(3–4), 361–374. [https://doi.org/10.1016/0012-821x\(86\)90118-4](https://doi.org/10.1016/0012-821x(86)90118-4)
- Davaille, A. (1999). Simultaneous generation of hotspots and superswells by convection in a heterogeneous planetary mantle. *Nature*, 402(6763), 756–760. <https://doi.org/10.1038/45461>
- Davaille, A., Girard, F., & Le Bars, M. (2002). How to anchor hotspots in a convecting mantle? *Earth and Planetary Science Letters*, 203(2), 621–634. [https://doi.org/10.1016/s0012-821x\(02\)00897-x](https://doi.org/10.1016/s0012-821x(02)00897-x)
- Davaille, A., Le Bars, M., & Carbone, C. (2003). Thermal convection in a heterogeneous mantle. *Comptes Rendus Geoscience*, 335(1), 141–156. [https://doi.org/10.1016/s1631-0713\(03\)00003-8](https://doi.org/10.1016/s1631-0713(03)00003-8)
- Davaille, A., & Limare, A. (2015). 7.03—laboratory studies of mantle convection. In G. Schubert (Ed.), *Treatise on geophysics* (2nd ed., pp. 73–144). Elsevier.
- Davaille, A., & Romanowicz, B. (2020). Deflating the LLSVPs: Bundles of mantle thermochemical plumes rather than thick stagnant “piles”. *Tectonics*, 39(10), e2020TC006265. <https://doi.org/10.1029/2020TC006265>
- Davaille, A., Stutzmann, E., Silveira, G., Besse, J., & Courtillot, V. (2005). Convective patterns under the Indo-Atlantic box. *Earth and Planetary Science Letters*, 239(3–4), 233–252. <https://doi.org/10.1016/j.epsl.2005.07.024>

- Davaille, A., & Vatteville, J. (2005). On the transient nature of mantle plumes. *Geophysical Research Letters*, 32(14), L14309. <https://doi.org/10.1029/2005GL023029>
- Davies, G. F. (2002). Stirring geochemistry in mantle convection models with stiff plates and slabs. *Geochimica et Cosmochimica Acta*, 66(17), 3125–3142. [https://doi.org/10.1016/s0016-7037\(02\)00915-8](https://doi.org/10.1016/s0016-7037(02)00915-8)
- Davies, G. R., Norry, M. J., Gerlach, D. C., & Cliff, R. A. (1989). *A combined chemical and Pb-Sr-Nd isotope study of the Azores and Cape Verde hot-spots: The geodynamic implications*. In A. D. Saunders & M. J. Norry (Eds.) (pp. 231–255). Geological Society of London.
- Day, J. M. D., Walker, R. J., & Warren, J. M. (2017).  $^{186}\text{Os}$ – $^{187}\text{Os}$  and highly siderophile element abundance systematics of the mantle revealed by abyssal peridotites and Os-rich alloys. *Geochimica et Cosmochimica Acta*, 200, 232–254. <https://doi.org/10.1016/j.gca.2016.12.013>
- Deschamps, F., Kaminski, E., & Tackley, P. J. (2011). A deep mantle origin for the primitive signature of ocean island basalt. *Nature Geoscience*, 4(12), 879–882. <https://doi.org/10.1038/ngeo1295>
- Detrick, R. S., Sinton, J. M., Ito, G., Canales, J. P., Behn, M., Blacic, T., et al. (2002). Correlated geophysical, geochemical, and volcanological manifestations of plume-ridge interaction along the Galápagos Spreading Center. *Geochemistry, Geophysics, Geosystems*, 3(10), 8501–8514. <https://doi.org/10.1029/2002GC000350>
- Dick, H. J. B. (1989). Abyssal peridotites, very slow spreading ridges and ocean ridge magmatism. In A. D. Saunders & M. J. Norry (Eds.), *Magmatism in the ocean basins* (pp. 71–105). Geological Society Special Publication.
- Doucet, L. S., Li, Z.-X., Gamal El Dien, H., Pourteau, A., Murphy, J. B., Collins, W. J., et al. (2020). Distinct formation history for deep-mantle domains reflected in geochemical differences. *Nature Geoscience*, 13(7), 511–515. <https://doi.org/10.1038/s41561-020-0599-9>
- Doucet, S., Weis, D., Scoates, J. S., V. D., & Giret, A. (2004). Geochemical and Hf-Pb-Sr-Nd isotope constraints on the origin of the Amsterdam-St. Paul (Indian Ocean) hotspot basalts. *Earth and Planetary Science Letters*, 218(1–2), 179–195. [https://doi.org/10.1016/s0012-821x\(03\)00636-8](https://doi.org/10.1016/s0012-821x(03)00636-8)
- Douglass, J., Schilling, J. G., & Fontignie, D. (1999). Plume-ridge interactions of the Discovery and Shona mantle plumes with the southern Mid-Atlantic Ridge (40°–55°S). *Journal of Geophysical Research*, 104(B2), 2941–2962. <https://doi.org/10.1029/98jb02642>
- Duncan, R. A. (1985). Radiometric ages from volcanic rocks along the new Hebrides-Samoa lineament. In T. M. Brocher (Ed.), *Investigations of the northern Melanesian Borderland, Circum-pacific council for energy and mineral resources* (Vol. 3, pp. 67–76).
- Duncan, R. A. (1991). Age distribution of volcanism along aseismic ridges in the eastern Indian Ocean. *Proceedings of the Ocean Drilling Program, Scientific Results*, 121, 507–517.
- Duncan, R. A., McCulloch, M. T., Barsczus, H. G., & Nelson, D. R. (1986). Plume versus lithospheric sources for melts at Ua Pou, Marquesas Islands. *Nature*, 322(6079), 534–538. <https://doi.org/10.1038/322534a0>
- Dupré, B., & Allègre, C. J. (1980). Pb-Sr-Nd isotopic correlation and the chemistry of the North Atlantic mantle. *Nature*, 286(5768), 17–22. <https://doi.org/10.1038/286017a0>
- Dupré, B., & Allègre, C. J. (1983). Pb-Sr isotope variation in Indian Ocean basalts and mixing phenomena. *Nature*, 303(5913), 142–146. <https://doi.org/10.1038/303142a0>
- Dupuy, C., Vidal, P., Barsczus, H. G., & Chauvel, C. (1987). Origin of basalts from the Marquesas Archipelago (south central Pacific Ocean); isotope and trace element constraints. *Earth and Planetary Science Letters*, 82(1–2), 145–152. [https://doi.org/10.1016/0012-821x\(87\)90114-2](https://doi.org/10.1016/0012-821x(87)90114-2)
- Dymnt, J., Lin, J., & Baker, E. T. (2007). Ridge-hotspot interactions: What mid-ocean ridges tell us about deep Earth processes. *Oceanography*, 20(1), 102–115. <https://doi.org/10.5670/oceanog.2007.84>
- Eisele, J., Sharma, M., Galer, J. G., Blight-Toff, J., Devey, C. W., & Hofmann, A. W. (2002). The role of sediment recycling in EMI inferred from Os, Pb, Hf, Nd, Sr isotope and trace element systematics in the Pitcairn hotspot. *Earth and Planetary Science Letters*, 196(3–4), 197–212. [https://doi.org/10.1016/s0012-821x\(01\)00601-x](https://doi.org/10.1016/s0012-821x(01)00601-x)
- Farley, K. A., Natland, J. H., & Craig, H. (1992). Binary mixing of enriched and undegassed (primitive?) mantle components (He, Sr, Nd, Pb) in Samoan lavas. *Earth and Planetary Science Letters*, 111(1), 183–199. [https://doi.org/10.1016/0012-821x\(92\)90178-x](https://doi.org/10.1016/0012-821x(92)90178-x)
- Farnetani, C. G., & Samuel, H. (2003). Lagrangian structures and stirring in the Earth's mantle. *Earth and Planetary Science Letters*, 206(3–4), 335–348. [https://doi.org/10.1016/s0012-821x\(02\)01085-3](https://doi.org/10.1016/s0012-821x(02)01085-3)
- Farnetani, C. G., & Samuel, H. (2005). Beyond the thermal plume paradigm. *Geophysical Research Letters*, 32(7), L07311. <https://doi.org/10.1029/2005GL022360>
- Feighner, M. A., Kellogg, L. H., & Travis, B. J. (1995). Numerical modeling of chemically buoyant mantle plumes at spreading ridges. *Geophysical Research Letters*, 22(6), 715–718. <https://doi.org/10.1029/95gl00311>
- Fitton, J. G., & Dunlop, H. M. (1985). The Cameroonian line, West Africa, and its bearing on the origin of oceanic and continental alkali basalt. *Earth and Planetary Science Letters*, 72(1), 23–38. [https://doi.org/10.1016/0012-821x\(85\)90114-1](https://doi.org/10.1016/0012-821x(85)90114-1)
- Flament, N., Bodur, Ö. F., Williams, S. E., & Merdith, A. S. (2022). Assembly of the basal mantle structure beneath Africa. *Nature*, 603(7903), 846–851. <https://doi.org/10.1038/s41586-022-04538-y>
- French, S. W., & Romanowicz, B. (2015). Broad plumes rooted at the base of the Earth's mantle beneath major hotspots. *Nature*, 525(7567), 95–99. <https://doi.org/10.1038/nature14876>
- Frey, F. A., & Weis, D. (1995). Temporal evolution of the Kerguelen plume: Geochemical evidence from 38 to 82 Ma lavas forming the Ninetyeast ridge. *Contributions to Mineralogy and Petrology*, 121(1), 12–28. <https://doi.org/10.1007/s004100050087>
- Frey, F. A., & Weis, D. (1996). Reply to the Class et al. discussion of “temporal evolution of the Kerguelen plume: Geochemical evidence from ~38 to 82 Ma lavas forming the Ninetyeast Ridge”. *Contributions to Mineralogy and Petrology*, 124(1), 104–110. <https://doi.org/10.1007/s004100050178>
- Füri, E., Hilton, D. R., Murton, B. J., Hémond, C., Dyment, J., & Day, J. M. D. (2011). Helium isotope variations between Réunion Island and the Central Indian Ridge (17°–21°S): New evidence for ridge–hot spot interaction. *Journal of Geophysical Research*, 116(B2), B02207. <https://doi.org/10.1029/2010JB007609>
- Gale, A., Dalton, C. A., Langmuir, C. H., Su, Y., & Schilling, J.-G. (2013). The mean composition of ocean ridge basalts. *Geochemistry, Geophysics, Geosystems*, 14(3), 489–518. <https://doi.org/10.1029/2012GC004334>
- Garapić, G., Jackson, M. G., Hauri, E. H., Hart, S. R., Farley, K. A., Blusztajn, J. S., & Woodhead, J. D. (2015). A radiogenic isotopic (He-Sr-Nd-Pb-Os) study of lavas from the Pitcairn hotspot: Implications for the origin of EM-1 (enriched mantle 1). *Lithos*, 228–229, 1–11. <https://doi.org/10.1016/j.lithos.2015.04.010>
- Gassmöller, R., Dannberg, J., Bredow, E., Steinberger, B., & Torsvik, T. H. (2016). Major influence of plume-ridge interaction, lithosphere thickness variations, and global mantle flow on hotspot volcanism—The example of Tristan. *Geochemistry, Geophysics, Geosystems*, 17(4), 1454–1479. <https://doi.org/10.1002/2015GC006177>
- Gast, P. W., Tilton, G. R., & Hedge, C. (1964). Isotopic composition of lead and strontium from Ascension and Gough Islands. *Science*, 145(3637), 1181–1185. <https://doi.org/10.1126/science.145.3637.1181>
- Geist, D. J., White, W. M., & McBirney, A. R. (1988). Plume–asthenosphere mixing beneath the Galapagos archipelago. *Nature*, 333(6174), 657–660. <https://doi.org/10.1038/333657a0>

- Gente, P., Dymit, J., Maia, M., & Goslin, J. (2003). Interaction between the Mid-Atlantic Ridge and the Azores hot spot during the last 85 Ma: Emplacement and rifting of the hot spot-derived plateaus. *Geochemistry, Geophysics, Geosystems*, 4(8S14), 000523. <https://doi.org/10.1029/2003GC000527>
- Gonnermann, H. M., & Mukhopadhyay, S. (2009). Preserving noble gases in a convecting mantle. *Nature*, 459(7246), 560–563. <https://doi.org/10.1038/nature08018>
- Goslin, J., & Party, T. S. (1999). Extent of Azores plume influence on the Mid-Atlantic Ridge north of the hotspot. *Geology*, 27(11), 991–994. [https://doi.org/10.1130/0091-7613\(1999\)027<0991:eoapio>2.3.co;2](https://doi.org/10.1130/0091-7613(1999)027<0991:eoapio>2.3.co;2)
- Graham, D., Johnson, K., Priebe, L., & Lupton, J. (1999). Hotspot-ridge interaction along the Southeast Indian ridge near Amsterdam and St. Paul Islands: Helium isotope evidence. *Earth and Planetary Science Letters*, 167(3–4), 297–310. [https://doi.org/10.1016/s0012-821x\(99\)00030-8](https://doi.org/10.1016/s0012-821x(99)00030-8)
- Grand, S. P. (2002). Mantle shear-wave tomography and the fate of subducted slabs. *Philosophical Transactions of the Royal Society of London*, 360(1800), 2475–2491. <https://doi.org/10.1098/rsta.2002.1077>
- Green, D. H. (2015). Experimental petrology of peridotites, including effects of water and carbon on melting in the Earth's upper mantle. *Physics and Chemistry of Minerals*, 42(2), 95–122. <https://doi.org/10.1007/s00269-014-0729-2>
- Green, D. H., & Falloon, T. J. (2015). Mantle-derived magmas: Intraplate, hot-spots and mid-ocean ridges. *Science Bulletin*, 60(22), 1873–1900. <https://doi.org/10.1007/s11434-015-0920-y>
- Guillou, H., Maury, R. C., Blais, S., Cotten, J., Legendre, C., Guille, G. r., & Caroff, M. (2005). Age progression along the Society hotspot chain (French Polynesia) based on new unspiked K-Ar ages. *Bulletin de la Société Géologique de France*, 176(2), 135–150. <https://doi.org/10.2113/176.2.135>
- Guillou, H., Maury, R. C., Guille, G., Chauvel, C., Rossi, P., Pallares, C., et al. (2014). Volcanic successions in Marquesas eruptive centers: A departure from the Hawaiian model. *Journal of Volcanology and Geothermal Research*, 276, 173–188. <https://doi.org/10.1016/j.jvolgeores.2013.12.003>
- Gurnis, M. (1986a). The effect of chemical density differences on convective mixing in the Earth's mantle. *Journal of Geophysical Research*, 91(B11), 11407–11419. <https://doi.org/10.1029/jb091i11p11407>
- Gurnis, M. (1986b). Stirring and mixing in the mantle by plate-scale flow: Large persistent blobs and long tendrils coexist. *Geophysical Research Letters*, 13, 1474–1477. <https://doi.org/10.1029/gl013i013p01474>
- Hager, B. H., & O'Connell, R. J. (1979). Kinematic models of large-scale mantle flow. *Journal of Geophysical Research*, 84(B3), 1031–1048. <https://doi.org/10.1029/jb084i03p01031>
- Hager, B. H., & O'Connell, R. J. (1981). A simple global model of plate dynamics and mantle convection. *Journal of Geophysical Research*, 86(B6), 4843–4867. <https://doi.org/10.1029/jb086i06p04843>
- Hager, B. H., & Richards, M. A. (1989). Long-wavelength variations in Earth's geoid: Physical models and dynamical implications. *Philosophical Transactions of the Royal Society of London, Series A*, 328, 309–327.
- Hanan, B. B., & Graham, D. W. (1996). Lead and helium isotope evidence from oceanic basalts for a common deep source of mantle plumes. *Science*, 272(5264), 991–995. <https://doi.org/10.1126/science.272.5264.991>
- Hanan, B. B., Kingsley, R. H., & Schilling, J. G. (1986). Pb isotope evidence in the South Atlantic for migrating ridge-hotspot interactions. *Nature*, 322(6075), 137–144. <https://doi.org/10.1038/322137a0>
- Hanyu, T., Dosso, L., Ishizuka, O., Tani, K., Hanan, B., Adam, C., et al. (2013). Geochemical diversity in submarine HIMU basalts from Austral Islands, French Polynesia. *Contributions to Mineralogy and Petrology*, 166(5), 1285–1304. <https://doi.org/10.1007/s00410-013-0926-x>
- Hanyu, T., Kawabata, H., Tatsumi, Y., Kimura, J.-I., Hyodo, H., Sato, K., et al. (2014). Isotope evolution in the HIMU reservoir beneath St. Helena: Implications for the mantle recycling of U and Th. *Geochimica et Cosmochimica Acta*, 143, 232–252. <https://doi.org/10.1016/j.gca.2014.03.016>
- Hanyu, T., Tatsumi, Y., Senda, R., Miyazaki, T., Chang, Q., Hirahara, Y., et al. (2011). Geochemical characteristics and origin of the HIMU reservoir: A possible mantle plume source in the lower mantle. *Geochemistry, Geophysics, Geosystems*, 12(2), Q0AC09. <https://doi.org/10.1029/2010gc003252>
- Harpp, K. S., & White, W. M. (2001). Tracing a mantle plume: Isotopic and trace element variations of Galapagos seamounts. *Geochemistry, Geophysics, Geosystems*, 2(6), 2000GC000137. <https://doi.org/10.1029/2000gc000137>
- Harpp, K. S., Wirth, K. R., & Korich, D. J. (2002). Northern Galápagos province: Hotspot-induced, near-ridge volcanism at Genovesa Island. *Geology*, 30(5), 399–402. [https://doi.org/10.1130/0091-7613\(2002\)030<0399:ngpphi>2.0.co;2](https://doi.org/10.1130/0091-7613(2002)030<0399:ngpphi>2.0.co;2)
- Harrison, L. N., Weis, D., & Garcia, M. O. (2017). The link between Hawaiian mantle plume composition, magmatic flux, and deep mantle geodynamics. *Earth and Planetary Science Letters*, 463, 298–309. <https://doi.org/10.1016/j.epsl.2017.01.027>
- Hart, S. R. (1984). A large-scale isotope anomaly in the southern-hemisphere mantle. *Nature*, 309(5971), 753–757. <https://doi.org/10.1038/309753a0>
- Hart, S. R., Coetzee, M., Workman, R. K., Blusztajn, J., Johnson, K. T. M., Sinton, J. M., et al. (2004). Genesis of Western Samoa seamount province: Age, geochemical fingerprint and tectonics. *Earth and Planetary Science Letters*, 227(1–2), 37–56. <https://doi.org/10.1016/j.epsl.2004.08.005>
- Hart, S. R., Hauri, E. H., Oschmann, L. A., & Whitehead, J. A. (1992). Mantle plumes and entrainment—isotopic evidence. *Science*, 256(5056), 517–520. <https://doi.org/10.1126/science.256.5056.517>
- Hart, S. R., Schilling, J. G., & Powell, J. L. (1973). Basalts from Iceland and along the Reykjanes ridge: Sr isotope geochemistry. *Nature*, 246(555), 104–107. <https://doi.org/10.1038/physci246104a0>
- Harvey, J., Gannoun, A., Burton, K. W., Rogers, N. W., Alard, O., & Parkinson, I. J. (2006). Ancient melt extraction from the oceanic upper mantle revealed by Re-Os isotopes in abyssal peridotites from the Mid-Atlantic Ridge. *Earth and Planetary Science Letters*, 244(3–4), 606–621. <https://doi.org/10.1016/j.epsl.2006.02.031>
- Hassan, R., Flament, N., Gurnis, M., Bower, D. J., & Müller, D. (2015). Provenance of plumes in global convection models. *Geochemistry, Geophysics, Geosystems*, 16(5), 1465–1489. <https://doi.org/10.1002/2015GC005751>
- Hauri, E. H., & Hart, S. R. (1993). Re-Os isotope systematics of HIMU and EMII oceanic island basalts from the South-Pacific Ocean. *Earth and Planetary Science Letters*, 114(2–3), 353–371. [https://doi.org/10.1016/0012-821x\(93\)90036-9](https://doi.org/10.1016/0012-821x(93)90036-9)
- Helffrich, G. R., & Wood, B. J. (2001). The Earth's mantle. *Nature*, 412(6846), 501–507. <https://doi.org/10.1038/35087500>
- Hellebrand, E., Snow, J. E., Hoppe, P., & Hofmann, A. W. (2002). Garnet-field melting and late-stage refertilization in "residual" abyssal peridotites from the Central Indian Ridge. *Journal of Petrology*, 43(12), 2305–2338. <https://doi.org/10.1093/petrology/43.12.2305>
- Hémond, C., Devey, C. W., & Chauvel, C. (1994). Source compositions and melting processes in the society and Austral plumes (South-Pacific Ocean)—element and isotope (Sr, Nd, Pb, Th) geochemistry. *Chemical Geology*, 115(1–2), 7–45. [https://doi.org/10.1016/0009-2541\(94\)90143-0](https://doi.org/10.1016/0009-2541(94)90143-0)
- Herzberg, C., Asimow, P. D., Arndt, N., Niu, Y., Lesher, C. M., Fitton, J. G., et al. (2007). Temperatures in ambient mantle and plumes: Constraints from basalts, picrites, and komatiites. *Geochemistry, Geophysics, Geosystems*, 8(2), Q02006. <https://doi.org/10.1029/2006GC001390>

- Hilton, D. R., & Porcelli, D. (2014). 3.7—Noble gases as mantle tracers. In H. D. Holland & K. K. Turekian (Eds.), *Treatise on geochemistry* (2nd ed., pp. 293–325). Elsevier.
- Hirschmann, M. M., & Stolper, E. M. (1996). A possible role for garnet pyroxenite in the origin of the "garnet signature" in MORB. *Contributions to Mineralogy and Petrology*, 124(2), 185–208. <https://doi.org/10.1007/s004100050184>
- Hoernle, K., Rohde, J., Hauff, F., Garbe-Schönberg, D., Homrighausen, S., Werner, R., & Morgan, J. P. (2015). How and when plume zonation appeared during the 132 Ma evolution of the Tristan Hotspot. *Nature Communications*, 6(1), 7799. <https://doi.org/10.1038/ncomms8799>
- Hoernle, K., Schwindrofska, A., Werner, R., van den Bogaard, P., Hauff, F., Uenzelmann-Neben, G., & Garbe-Schönberg, D. (2016). Tectonic dissection and displacement of parts of Shona hotspot volcano 3500 km along the Agulhas-Falkland Fracture Zone. *Geology*, 44(4), 263–266. <https://doi.org/10.1130/g37582.1>
- Hofmann, A. W. (1997). Mantle Geochemistry: The message from oceanic volcanism. *Nature*, 385(6613), 219–229. <https://doi.org/10.1038/385219a0>
- Hofmann, A. W. (2014). 3.3—Sampling mantle heterogeneity through oceanic basalts: Isotopes and trace elements. In H. D. H. K. Turekian (Ed.), *Treatise on geochemistry* (2nd ed., pp. 67–101). Elsevier.
- Hofmann, A. W., & Hart, S. R. (1978). An assessment of local and regional isotopic equilibrium in the mantle. *Earth and Planetary Science Letters*, 38(1), 44–62. [https://doi.org/10.1016/0012-821x\(78\)90125-5](https://doi.org/10.1016/0012-821x(78)90125-5)
- Hofmann, C., Féraud, G., & Courtillot, V. (2000).  $^{40}\text{Ar}/^{39}\text{Ar}$  dating of mineral separates and whole rocks from the Western ghats lava pile: Further constraints on duration and age of the Deccan traps. *Earth and Planetary Science Letters*, 180(1–2), 13–27. [https://doi.org/10.1016/s0012-821x\(00\)00159-x](https://doi.org/10.1016/s0012-821x(00)00159-x)
- Hooft, E. E. E., Toomey, D. R., & Solomon, S. C. (2003). Anomalously thin transition zone beneath the Galápagos hotspot. *Earth and Planetary Science Letters*, 216(1–2), 55–64. [https://doi.org/10.1016/s0012-821x\(03\)00517-x](https://doi.org/10.1016/s0012-821x(03)00517-x)
- Horrocks, T., Holden, E.-J., Wedge, D., Wijns, C., & Fiorentini, M. (2019). Geochemical characterisation of rock hydration processes using t-SNE. *Computers & Geosciences*, 124, 46–57. <https://doi.org/10.1016/j.cageo.2018.12.005>
- Huang, J., & Davies, G. F. (2007). Stirring in three-dimensional mantle convection models and implications for geochemistry: 2. Heavy tracers. *Geochemistry, Geophysics, Geosystems*, 8(7), Q07004. <https://doi.org/10.1029/2007GC001621>
- Hunter, J. D. (2007). Matplotlib: A 2D graphics environment. *Computing in Science & Engineering*, 9(3), 90–95. <https://doi.org/10.1109/MCSE.2007.55>
- Igual, L., & Segui, S. (2017). *Introduction to data science. A Python approach to concepts, techniques and applications*. Springer International Publishing.
- Israel, C., Boyet, M., Doucelance, R., Bonnand, P., Frossard, P., Auclair, D., & Bouvier, A. (2020). Formation of the Ce-Nd mantle array: Crustal extraction vs. recycling by subduction. *Earth and Planetary Science Letters*, 530, 115941. <https://doi.org/10.1016/j.epsl.2019.115941>
- Ito, G., & Bianco, T. (2015). Patterns in Galápagos magmatism arising from the upper mantle dynamics of plume–ridge interaction. In K. S. Harpp, E. N. Mittelstaedt-Ozouville, & D. W. Graham (Eds.), *The Galápagos: A natural laboratory for the Earth sciences*, *Geophysical Monograph* 204. AGU.
- Ito, G., Lin, J., & Gable, C. (1997). Interaction of mantle plumes and migrating mid-ocean ridges: Implications for the Galápagos plume–ridge system. *Journal of Geophysical Research*, 102(B7), 15403–15418. <https://doi.org/10.1029/97jb01049>
- Ito, G., Lin, J., & Graham, D. (2003). Observational and theoretical studies of the dynamics of mantle plume–mid-ocean ridge interaction. *Review of Geophysics*, 41(4), 1017. <https://doi.org/10.1029/2002rg000117>
- Ito, G., & Mahoney, J. J. (2005). Flow and melting of a heterogeneous mantle: 2. Implications for a chemically nonlayered mantle. *Earth and Planetary Science Letters*, 230(1–2), 47–63. <https://doi.org/10.1016/j.epsl.2004.10.034>
- Ito, G., Shen, Y., Hirth, G., & Wolfe, C. J. (1999). Mantle flow, melting, and dehydration of the Iceland mantle plume. *Earth and Planetary Science Letters*, 165(1), 81–96. [https://doi.org/10.1016/s0012-821x\(98\)00216-7](https://doi.org/10.1016/s0012-821x(98)00216-7)
- Iwamori, H., & Albarède, F. (2008). Decoupled isotopic record of ridge and subduction zone processes in oceanic basalts by independent component analysis. *Geochemistry, Geophysics, Geosystems*, 9(4), Q04033. <https://doi.org/10.1029/2007gc001753>
- Iwamori, H., Yoshida, K., Nakamura, H., Kuwatani, T., Hamada, M., Haraguchi, S., & Ueki, K. (2017). Classification of geochemical data based on multivariate statistical analyses: Complementary roles of cluster, principal component, and independent component analyses. *Geochemistry, Geophysics, Geosystems*, 18(3), 994–1012. <https://doi.org/10.1002/2016GC006663>
- Jackson, M. G., Becker, T. W., & Konter, J. G. (2018). Evidence for a deep mantle source for EM and HIMU domains from integrated geochemical and geophysical constraints. *Earth and Planetary Science Letters*, 484, 154–167. <https://doi.org/10.1016/j.epsl.2017.11.052>
- Jackson, M. G., Hart, S. R., Konter, J. G., Koppers, A. A. P., Staudigel, H., Kurz, M. D., et al. (2010). Samoan hot spot track on a "hot spot highway": Implications for mantle plumes and a deep Samoan mantle source. *Geochemistry, Geophysics, Geosystems*, 11(12), Q12009. <https://doi.org/10.1029/2010GC003232>
- Jackson, M. G., Hart, S. R., Koppers, A. A. P., Staudigel, H., Konter, J., Blusztajn, J., et al. (2007). The return of subducted continental crust in Samoan lavas. *Nature*, 448(7154), 684–687. <https://doi.org/10.1038/nature06048>
- Jackson, M. G., Koga, K. T., Price, A., Konter, J. G., Koppers, A. A. P., Finlayson, V. A., et al. (2015). Deeply dredged submarine HIMU glasses from the Tuvalu Islands, Polynesia: Implications for volatile budgets of recycled oceanic crust. *Geochemistry, Geophysics, Geosystems*, 16(9), 3210–3234. <https://doi.org/10.1002/2015GC005966>
- Jackson, M. G., Price, A. A., Blichert-Toft, J., Kurz, M. D., & Reinhard, A. A. (2017). Geochemistry of lavas from the Caroline hotspot, Micronesia: Evidence for primitive and recycled components in the mantle sources of lavas with moderately elevated  $^3\text{He}/^4\text{He}$ . *Chemical Geology*, 455, 385–400. <https://doi.org/10.1016/j.chemgeo.2016.10.038>
- Janin, M., Hémond, C., Guillou, H., Maia, M., Johnson, K. T. M., Bollinger, C., et al. (2011). Hot spot activity and tectonic settings near Amsterdam–St. Paul Plateau (Indian Ocean). *Journal of Geophysical Research*, 116(B5), B05206. <https://doi.org/10.1029/2010JB007800>
- Jellinek, A. M., Gonnermann, H. M., & Richards, M. A. (2003). Plume capture by divergent plate motions: Implications for the distribution of hotspots, geochemistry of mid-ocean ridge basalts, and estimates of the heat flux at the core–mantle boundary. *Earth and Planetary Science Letters*, 205(3–4), 361–378. [https://doi.org/10.1016/s0012-821x\(02\)01070-1](https://doi.org/10.1016/s0012-821x(02)01070-1)
- Jellinek, A. M., & Manga, M. (2004). Links between long-lived hot spots, mantle plumes, D", and plate tectonics. *Review of Geophysics*, 42(3), RG3002. <https://doi.org/10.1029/2003RG000144>
- Jiang, Q., Jourdan, F., Olieroor, H. K. H., Merle, R. E., & Whittaker, J. M. (2020). Longest continuously erupting large igneous province driven by plume–ridge interaction. *Geology*, 49(2), 206–210. <https://doi.org/10.1130/g47850.1>
- Johnson, K. T. M., Dick, H. J. B., & Shimizu, N. (1990). Melting in the oceanic upper mantle—An Ion microprobe study of diopsides in abyssal peridotites. *Journal of Geophysical Research*, 95(B3), 2661–2678. <https://doi.org/10.1029/jb095ib03p02661>

- Johnson, K. T. M., Graham, D. W., Rubin, K. H., Nicolaysen, K., Scheirer, D. S., Forsyth, D. W., et al. (2000). Boomerang Seamount: The active expression of the Amsterdam-St. Paul hotspot, Southeast Indian ridge. *Earth and Planetary Science Letters*, 183(1–2), 245–259. [https://doi.org/10.1016/s0012-821x\(00\)00279-x](https://doi.org/10.1016/s0012-821x(00)00279-x)
- Jones, R. E., van Keeken, P. E., Hauri, E. H., Tucker, J. M., Vervoort, J., & Ballentine, C. J. (2019). Origins of the terrestrial Hf-Nd mantle array: Evidence from a combined geodynamical-geochemical approach. *Earth and Planetary Science Letters*, 518, 26–39. <https://doi.org/10.1016/j.epsl.2019.04.015>
- Jones, T. D., Davies, D. R., Campbell, I. H., Iaffaldano, G., Yaxley, G., Kramer, S. C., & Wilson, C. R. (2017). The concurrent emergence and causes of double volcanic hotspot tracks on the Pacific plate. *Nature*, 545(7655), 472–476. <https://doi.org/10.1038/nature22054>
- Jones, T. D., Sime, N., & van Keeken, P. E. (2021). Burying Earth's primitive mantle in the slab Graveyard. *Geochemistry, Geophysics, Geosystems*, 22(3), e2020GC009396. <https://doi.org/10.1029/2020GC009396>
- Jordahl, K. A., McNutt, M. K., & Caress, D. W. (2004). Multiple episodes of volcanism in the Southern Austral Islands: Flexural constraints from bathymetry, seismic reflection, and gravity data. *Journal of Geophysical Research*, 109(B6), B06103. <https://doi.org/10.1029/2003JB002885>
- Kawabata, H., Hanyu, T., Chang, Q., Kimura, J.-I., Nichols, A. R. L., & Tatsumi, Y. (2011). The petrology and geochemistry of St. Helena alkali basalts: Evaluation of the oceanic crust-recycling model for HIMU OIB. *Journal of Petrology*, 52(4), 791–838. <https://doi.org/10.1093/petrology/egr003>
- Keating, B. H., Mattey, D. P., Helsley, C. E., Naughton, J. J., Epp, D., Lazarewicz, A., & Schwank, D. (1984). Evidence for a hotspot origin of the Caroline Islands. *Journal of Geophysical Research*, 89(B12), 9937–9948. <https://doi.org/10.1029/jb089ib12p09937>
- Keating, B. H., Mattey, D. P., Naughton, J. J., & Helsley, C. E. (1984). Age and origin of Truk Atoll, eastern Caroline Islands: Geochemical, radiometric-age, and paleomagnetic evidence. *The Geological Society of America Bulletin*, 95(3), 350–356. [https://doi.org/10.1130/0016-7606\(1984\)95<350:aaoot>2.0.co;2](https://doi.org/10.1130/0016-7606(1984)95<350:aaoot>2.0.co;2)
- Kellogg, J. B., Jacobsen, S. B., & O'Connell, R. J. (2002). Modeling the distribution of isotopic ratios in geochemical reservoirs. *Earth and Planetary Science Letters*, 204(1–2), 183–202. [https://doi.org/10.1016/s0012-821x\(02\)00981-0](https://doi.org/10.1016/s0012-821x(02)00981-0)
- Kellogg, J. B., Jacobsen, S. B., & O'Connell, R. J. (2007). Modeling lead isotopic heterogeneity in mid-ocean ridge basalts. *Earth and Planetary Science Letters*, 262(3–4), 328–342. <https://doi.org/10.1016/j.epsl.2007.06.018>
- Kelly, A., & Bercovici, D. (1997). The clustering of rising diapirs and plume heads. *Geophysical Research Letters*, 24(2), 201–204. <https://doi.org/10.1029/96gl03904>
- Kineaid, C., Ito, G., & Gable, C. (1995). Laboratory investigation of the interaction of off-axis mantle plumes and spreading centres. *Nature*, 376(6543), 758–761. <https://doi.org/10.1038/376758a0>
- King, S. D., & Adam, C. (2014). Hotspot swells revisited. *Physics of the Earth and Planetary Interiors*, 235, 66–83. <https://doi.org/10.1016/j.pepi.2014.07.006>
- King, S. D., & Ritsema, J. (2000). African hot spot volcanism: Small-scale convection in the upper mantle beneath cratons. *Science*, 290(5494), 1137–1140. <https://doi.org/10.1126/science.290.5494.1137>
- Klein, E. M., & Langmuir, C. H. (1989). Local versus global variations in ocean ridge basalt composition—A reply. *Journal of Geophysical Research*, 94(B4), 4241–4252. <https://doi.org/10.1029/jb094ib04p04241>
- Kobak, D., & Berens, P. (2019). The art of using t-SNE for single-cell transcriptomics. *Nature Communications*, 10(1), 5416. <https://doi.org/10.1038/s41467-019-13056-x>
- Kogiso, T., Hirschmann, M. M., & Frost, D. J. (2003). High-pressure partial melting of garnet pyroxenite: Possible mafic lithologies in the source of ocean island basalts. *Earth and Planetary Science Letters*, 216(4), 603–617. [https://doi.org/10.1016/s0012-821x\(03\)00538-7](https://doi.org/10.1016/s0012-821x(03)00538-7)
- Kogiso, T., Tatsumi, Y., Shimoda, G., & Barsczus, H. G. (1997). High  $\mu$  (HIMU) ocean island basalts in southern Polynesia: New evidence for whole mantle scale recycling of subducted oceanic crust. *Journal of Geophysical Research*, 102(B4), 8085–8103. <https://doi.org/10.1029/96jb03892>
- Konter, J., Hanan, B., Blichert-Toft, J., Koppers, A., Plank, T., & Staudigel, H. (2008). One hundred million years of mantle geochemical history suggest the retiring of mantle plumes is premature. *Earth and Planetary Science Letters*, 275(3–4), 285–295. <https://doi.org/10.1016/j.epsl.2008.08.023>
- Konter, J. G., & Jackson, M. G. (2012). Large volumes of rejuvenated volcanism in Samoa: Evidence supporting a tectonic influence on late-stage volcanism. *Geochemistry, Geophysics, Geosystems*, 13(6), Q0AM04. <https://doi.org/10.1029/2011GC003974>
- Koppers, A. A. P., Becker, T. W., Jackson, M. G., Konrad, K., Müller, R. D., Romanowicz, B., et al. (2021). Mantle plumes and their role in Earth processes. *Nature Reviews Earth & Environment*, 2(6), 382–401. <https://doi.org/10.1038/s43017-021-00168-6>
- Koppers, A. A. P., Staudigel, H., Pringle, M. S., & Wijbrans, J. R. (2003). Short-lived and discontinuous intraplate volcanism in the South Pacific: Hot spots or extensional volcanism? *Geochemistry, Geophysics, Geosystems*, 4(10), 1089. <https://doi.org/10.1029/2003GC000533>
- Koppers, A. P., Russel, J. A., Jackson, M. G., Konter, J. G., Staudigel, H., & Hart, S. R. (2008). Samoa reinstated as a primary hotspot trail. *Geology*, 36(6), 435–438. <https://doi.org/10.1130/G24630A.1>
- Kostitsyn, Y. A. (2007). Relationships between the chemical and isotopic (Sr, Nd, Hf, and Pb) heterogeneity of the mantle. *Geochemistry International*, 45(12), 1173–1196. <https://doi.org/10.1134/s0016702907120014>
- Kumagai, I., Davaille, A., Kurita, K., & Stutzmann, E. (2008). Mantle plumes: Thin, fat, successful, or failing? Constraints to explain hot spot volcanism through time and space. *Geophysical Research Letters*, 35(16), L16301. <https://doi.org/10.1029/2008GL035079>
- Kumari, S., Paul, D., & Stracke, A. (2016). Open system models of isotopic evolution in Earth's silicate reservoirs: Implications for crustal growth and mantle heterogeneity. *Geochimica et Cosmochimica Acta*, 195, 142–157. <https://doi.org/10.1016/j.gca.2016.09.011>
- Kumari, S., Paul, D., & Stracke, A. (2019). Constraints on Archean crust formation from open system models of Earth evolution. *Chemical Geology*, 530, 119307. <https://doi.org/10.1016/j.chemgeo.2019.119307>
- Lambart, S., Baker, M. B., & Stolper, E. M. (2016). The role of pyroxenites in basalt Genesis: Melt-PX, a melting parameterization for mantle pyroxenites between 0.9 and 5 GPa. *Journal of Geophysical Research: Solid Earth*, 121(8), 5708–5735. <https://doi.org/10.1002/2015JB012762>
- Lassiter, J. C., Blichert-Toft, J., Hauri, E. H., & Barsczus, H. G. (2003). Isotope and trace element variations in lavas from Raivavae and Rapa, Cook-Austral islands: Constraints on the nature of HIMU- and EM-mantle and the origin of mid-plate volcanism in French Polynesia. *Chemical Geology*, 250(1–2), 115–138. <https://doi.org/10.1016/j.chemgeo.2003.08.002>
- Lassiter, J. C., Byerly, B. L., Snow, J. E., & Hellebrand, E. (2014). Constraints from Os-isotope variations on the origin of Lena Trough abyssal peridotites and implications for the composition and evolution of the depleted upper mantle. *Earth and Planetary Science Letters*, 403, 178–187. <https://doi.org/10.1016/j.epsl.2014.05.033>
- Le Dez, A., Maury, R. C., Vidal, P., Bellon, H., Cotten, J., & Brousse, R. (1996). Geology and geochemistry of Nuku Hiva, Marquesas: Temporal trends in a large Polynesian shield volcano. *Bulletin de la Société Géologique de France*, 167, 197–209.
- Lee, D.-C., Halliday, A. N., Fittor, J. G., & Poli, G. (1994). Isotopic variations with distance and time in the volcanic Islands of the Cameroon line: Evidence for a mantle plume origin. *Earth and Planetary Science Letters*, 123(1–3), 119–138. [https://doi.org/10.1016/0012-821x\(94\)90262-3](https://doi.org/10.1016/0012-821x(94)90262-3)

- Legendre, C., Maury, R. C., Caroff, M., Guillou, H., Cotten, J., Chauvel, C., et al. (2005). Origin of exceptionally abundant Phonolites on Ua Pou Island (Marquesas, French Polynesia): Partial melting of Basanites followed by crustal contamination. *Journal of Petrology*, 46(9), 1925–1962. <https://doi.org/10.1093/petrology/egi043>
- Li, Z.-X., & Zhong, S. (2009). Supercontinent–superplume coupling, true polar wander and plume mobility: Plate dominance in whole-mantle tectonics. *Physics of the Earth and Planetary Interiors*, 176(3–4), 143–156. <https://doi.org/10.1016/j.pepi.2009.05.004>
- Linderman, G. C., & Steinerberger, S. (2019). Clustering with t-SNE, Provably. *SIAM Journal on Mathematics of Data Science*, 12(2), 313–332. <https://doi.org/10.1137/18m1216134>
- Lithgow-Bertelli, C., & Richards, M. A. (1998). The dynamics of cenozoic and mesozoic plate motions. *Review of Geophysics*, 36(1), 27–78. <https://doi.org/10.1029/97rg02282>
- Liu, C. Z., Snow, J. E., Hellebrand, E., Brügmann, G., von der Handt, A., Büchl, A., & Hofmann, A. W. (2008). Ancient, highly depleted heterogeneous mantle beneath Gakkel Ridge, Arctic Ocean. *Nature*, 452(7185), 311–316. <https://doi.org/10.1038/nature06688>
- Loper, D. E. (1985). A simple-model of whole-mantle convection. *Journal of Geophysical Research Atmospheres*, 90(B2), 1809–1836. <https://doi.org/10.1029/jb090ib02p1809>
- Loper, D. E., & Stacey, F. D. (1983). The dynamical and thermal structure of deep mantle plumes. *Physics of the Earth and Planetary Interiors*, 33(4), 304–317. [https://doi.org/10.1016/0031-9201\(83\)90047-x](https://doi.org/10.1016/0031-9201(83)90047-x)
- Maggi, A., Debayle, E., Priestley, K., & Barruol, G. (2006). Multimode surface waveform tomography of the Pacific Ocean: A closer look at the lithospheric cooling signature. *Geophysical Journal International*, 166(3), 1384–1397. <https://doi.org/10.1111/j.1365-246x.2006.03037.x>
- Maher, S. M., Wessel, P., Müller, R. D., Williams, S. E., & Harada, Y. (2015). Absolute plate motion of Africa around Hawaii–Emperor bend time. *Geophysical Journal International*, 201(3), 1743–1764. <https://doi.org/10.1093/gji/gjv104>
- Mahoney, J. J., Macdougall, J. D., Lugmair, G. W., & Gopalan, K. (1983). Kerguelen hotspot source for Rajmahal traps and Ninetyeast Ridge? *Nature*, 303(5916), 385–389. <https://doi.org/10.1038/303385a0>
- Mahoney, J. J., Natland, J. H., White, W. M., Poreda, R., Bloomer, S. H., Fisher, R. L., & Baxter, A. N. (1989). Isotopic and geochemical provinces of the Western Indian ocean spreading centers. *Journal of Geophysical Research*, 94(B4), 4033–4052. <https://doi.org/10.1029/jb094ib04p04033>
- Maia, M., Pessanha, I., Courrèges, E., Patriat, M., Gente, P., Hémond, C., et al. (2011). Building of the Amsterdam–Saint Paul Plateau: A 10 Ma history of a ridge-hot spot interaction and variations in the strength of the hot spot source. *Journal of Geophysical Research*, 116(B9), B09104. <https://doi.org/10.1029/2010JB007768>
- Maimon, O., & Rokach, L. (2006). “Clustering methods”. *Data mining and knowledge discovery handbook* (pp. 321–352). Springer.
- Manga, M. (1996). Mixing of heterogeneities in the mantle: Effect of viscosity differences. *Geophysical Research Letters*, 23(4), 403–406. <https://doi.org/10.1029/96gl00242>
- Manga, M. (2010). Low-viscosity mantle blobs are sampled preferentially at regions of surface divergence and stirred rapidly into the mantle. *Physics of the Earth and Planetary Interiors*, 180(1–2), 104–107. <https://doi.org/10.1016/j.pepi.2010.02.013>
- Marzoli, A., Piccirillo, E. M., Renne, P. R., Bellieni, G., Iacumin, M., Nyobe, J. B., & Tongwa, A. T. (2000). The Cameroon volcanic line revisited: Petrogenesis of continental basaltic magmas from lithospheric and asthenospheric mantle sources. *Journal of Petrology*, 41(1), 87–109. <https://doi.org/10.1093/petrology/41.1.87>
- Marzoli, A., Renne, P. R., Piccirillo, E. M., Francesca, C., Bellieni, G., Melfi, A. J., et al. (1999). Silicic magmas from the continental Cameroon volcanic line (Oku, Bamouto and Ngaoundere):  $^{40}\text{Ar}$ - $^{39}\text{Ar}$  Dates, petrology, Sr-Nd-O isotopes and their Petrogenetic significance. *Contributions to Mineralogy and Petrology*, 135(2–3), 133–150. <https://doi.org/10.1007/s004100050502>
- Masters, T. G., Laske, G., Bolton, H., & Dziewonski, A. (2000). The relative behavior of velocity, bulk sound speed and compressional velocity in the mantle: Implications for chemical and thermal structure. In S.-I. Karato, A. Forte, R. Liebermann, G. Masters, & L. stixrude (Eds.). In *Earth's deep interior. Mineral physics and tomography from the to the global scale. AGU geophysical Monograph* (Vol. 117, p. 63).
- Matthews, S., Shorttle, O., & MacLennan, J. (2016). The temperature of the Icelandic mantle from olivine-spinel aluminum exchange thermometry. *Geochemistry, Geophysics, Geosystems*, 17(11), 4725–4752. <https://doi.org/10.1002/2016GC006497>
- Matthews, S., Wong, K., Shorttle, O., Edmonds, M., & MacLennan, J. (2021). Do olivine crystallization temperatures faithfully record mantle temperature variability? *Geochemistry, Geophysics, Geosystems*, 22(4), e2020GC009157. <https://doi.org/10.1029/2020gc009157>
- McKenzie, D., & O’Nions, R. K. (1998). Melt production beneath oceanic islands. *Physics of the Earth and Planetary Interiors*, 107(1–3), 143–182. [https://doi.org/10.1016/s0031-9201\(97\)00132-5](https://doi.org/10.1016/s0031-9201(97)00132-5)
- McNamara, A. K. (2019). A review of large low shear velocity provinces and ultra low velocity zones. *Tectonophysics*, 760, 199–220. <https://doi.org/10.1016/j.tecto.2018.04.015>
- McNamara, A. K., & Zhong, S. (2004). Thermochemical structures within a spherical mantle: Superplumes or piles? *Journal of Geophysical Research*, 109(B7), B07402. <https://doi.org/10.1029/2003JB002847>
- McNutt, M., & Bonneville, A. (2000). A shallow, chemical origin for the Marquesas Swell. *Geochemistry, Geophysics, Geosystems*, 1(6), 1014. <https://doi.org/10.1029/1999GC000028>
- McNutt, M. K., Caress, D. W., Reynolds, J., Jordahl, K. A., & Duncan, R. A. (1997). Failure of plume theory to explain midplate volcanism in the southern Austral islands. *Nature*, 389(6650), 479–482. <https://doi.org/10.1038/39013>
- McNutt, M. K., & Fischer, K. M. (1987). The South Pacific superswell. In A. Keating (Ed.), *Seamounts, Islands* (pp. 25–34). AGU.
- Megnin, C., & Romanowicz, B. (2000). The three-dimensional shear velocity structure of the mantle from the inversion of body, surface and higher-mode waveforms. *Geophysical Journal International*, 143(3), 709–728. <https://doi.org/10.1046/j.1365-246x.2000.00298.x>
- Meibom, A., & Anderson, D. L. (2003). The statistical upper mantle assemblage. *Earth and Planetary Science Letters*, 217(1–2), 123–139. [https://doi.org/10.1016/s0012-821x\(03\)00573-9](https://doi.org/10.1016/s0012-821x(03)00573-9)
- Meyers, J. B., Rosendahl, B. R., Harrison, C. G. A., & Ding, Z.-D. (1998). Deep imaging seismic and gravity results from the offshore Cameroon volcanic line, and speculation of African Hotlines. *Tectonophysics*, 284(1–2), 31–63. [https://doi.org/10.1016/s0040-1951\(97\)00173-x](https://doi.org/10.1016/s0040-1951(97)00173-x)
- Milelli, L., Fourel, L., & Jaupart, C. (2012). A lithospheric instability origin for the Cameroon volcanic line. *Earth and Planetary Science Letters*, 335–336, 80–87. <https://doi.org/10.1016/j.epsl.2012.04.028>
- Mitrovica, J. X., & Forte, A. (2004). A new inference of mantle viscosity upon joint inversion of convection and glacial isostatic adjustment data. *Earth and Planetary Science Letters*, 225(1–2), 177–189. <https://doi.org/10.1016/j.epsl.2004.06.005>
- Mittelstaedt, E., Soule, S., Harpp, K., Fornari, D., McKee, C., Tivey, M., et al. (2012). Multiple expressions of plume–ridge interaction in the Galápagos: Volcanic lineaments and ridge jumps. *Geochemistry, Geophysics, Geosystems*, 13, Q05018. <https://doi.org/10.1029/2012GC004093>
- Montelli, R., Nolet, G., Dahlen, F. A., & Mastres, G. (2006). A catalogue of deep mantle plumes: New results from finite-frequency tomography. *Geochemistry, Geophysics, Geosystems*, 7(11), Q11007. <https://doi.org/10.11029/12006GC001248>
- Montelli, R., Nolet, G., Dahlen, F. A., Mastres, G., Engdahl, E. R., & Hung, S. H. (2004). Finite-frequency tomography reveals a variety of plumes in the mantle. *Science*, 303(5656), 338–343. <https://doi.org/10.1126/science.1092485>

- Morgan, J. P., & Morgan, W. J. (1999). Two-stage melting and the geochemical evolution of the mantle: A recipe for mantle plum-pudding. *Earth and Planetary Science Letters*, 170(3), 215–239. [https://doi.org/10.1016/s0012-821x\(99\)00114-4](https://doi.org/10.1016/s0012-821x(99)00114-4)
- Morgan, J. P., Taramón, J. M., Araujo, M., Hasenclever, J., & Perez-Gussinye, M. (2020). Causes and consequences of asymmetric lateral plume flow during South Atlantic rifting. *Proceedings of the National Academy of Sciences*, 117(45), 27877–27883. <https://doi.org/10.1073/pnas.2012246117>
- Morgan, W. J. (1971). Convection plumes in the lower mantle. *Nature*, 230(5288), 42–43. <https://doi.org/10.1038/230042a0>
- Morgan, W. J. (1978). Rodriguez, Darwin, Amsterdam, ...: A second type of hotspot Island. *Journal of Geophysical Research*, 83(B11), 5355–5360. <https://doi.org/10.1029/jb083ib11p05355>
- Morgan, W. J. (1981). Hotspot tracks and the opening of the Atlantic and Indian oceans. In C. Emiliani (Ed.), *The sea. 7. The oceanic lithosphere* (pp. 443–487). Wiley.
- Mougel, B., Agranić, A., Hemond, C., & Gente, P. (2014). A highly unradiogenic lead isotopic signature revealed by volcanic rocks from the East Pacific Rise. *Nature Communications*, 5(1), 4474. <https://doi.org/10.1038/ncomms5474>
- Müller, R. D., Seton, M., Zahirovic, S., Williams, S. E., Matthews, K. J., Wright, N. M., et al. (2016). Ocean basin evolution and global-scale plate reorganization events since Pangea Breakup. *Annual Review of Earth and Planetary Sciences*, 44(1), 107–138. <https://doi.org/10.1146/annurev-earth-060115-012211>
- Mutter, J. C., & Cande, S. C. (1983). The early opening between Broken Ridge and Kerguelen Plateau. *Earth and Planetary Science Letters*, 65(2), 369–376. [https://doi.org/10.1016/0012-821x\(83\)90174-7](https://doi.org/10.1016/0012-821x(83)90174-7)
- Nakamura, Y., & Tatsumoto, M. (1988). Pb, Nd, and Sr isotopic evidence for a multicomponent source for rocks of Cook-Austral Islands and heterogeneities of mantle plumes. *Geochimica et Cosmochimica Acta*, 52(12), 2909–2924. [https://doi.org/10.1016/0016-7037\(88\)90157-3](https://doi.org/10.1016/0016-7037(88)90157-3)
- Nauret, F., Abouchami, W., Galer, S. J. G., Hofmann, A. W., Hemond, C., Chauvel, C., & Dymnt, J. (2006). Correlated trace element-Pb isotope enrichments in Indian MORB along 18–20°S, Central Indian Ridge. *Earth and Planetary Science Letters*, 245(1–2), 137–152. <https://doi.org/10.1016/j.epsl.2006.03.015>
- Nebel, O., Arculus, R. J., van Westrenen, W., Woodhead, J. D., Jenner, F. E., Nebel-Jacobsen, Y. J., et al. (2013). Coupled Hf–Nd–Pb isotope co-variations of HIMU oceanic island basalts from Mangaia, Cook-Austral islands, suggest an Archean source component in the mantle transition zone. *Geochimica et Cosmochimica Acta*, 112, 87–101. <https://doi.org/10.1016/j.gca.2013.03.005>
- Nicolaysen, K. P., Frey, F. A., Mahoney, J. J., Johnson, K. T. M., & Graham, D. (2007). Influence of the Amsterdam/St. Paul hot spot along the Southeast Indian Ridge between 77 and 88 E: Correlations of Sr, Nd, Pb, and He isotopic variations with ridge segmentation.
- Nielsen, F. (2016). “8. Hierarchical clustering”. In *Introduction to HPC with MPI for data science* (pp. 195–211). Springer.
- Njome, M. S., & de Wit, M. J. (2014). The Cameroon line: Analysis of an intraplate magmatic province Transecting both oceanic and continental lithospheres: Constraints, controversies and models. *Earth-Science Reviews*, 139, 168–194. <https://doi.org/10.1016/j.earscirev.2014.09.003>
- Nobre Silva, I. G., Weis, D., Scoates, J. S., & Barling, J. (2013). The Ninetyeast Ridge and its relation to the Kerguelen, Amsterdam and St. Paul hotspots in the Indian Ocean. *Journal of Petrology*, 54(6), 1177–1210. <https://doi.org/10.1093/petrology/egt009>
- O’Connor, J., Jokat, W., Wijbrans, J., & Colli, L. (2018). Hotspot tracks in the South Atlantic located above bands of fast flowing asthenosphere driven by waning pulsations from the African LLSVP. *Gondwana Research*, 53, 197–208. <https://doi.org/10.1016/j.gr.2017.05.014>
- O’Connor, J. M., & Jokat, W. (2015). Tracking the Tristan-Gough mantle plume using discrete chains of intraplate volcanic centers buried in the Walvis Ridge. *Geology*, 43(8), 715–718. <https://doi.org/10.1130/g36767.1>
- O’Connor, J. M., Jokat, W., le Roex, A. P., Class, C., Wijbrans, J. R., Keßling, S., et al. (2012). Hotspot trails in the South Atlantic controlled by plume and plate tectonic processes. *Nature Geoscience*, 5(10), 735–738. <https://doi.org/10.1038/ngeo1583>
- O’Connor, J. M., & LeRoex, A. P. (1992). South Atlantic hot spot-plume systems: I. Distribution of volcanism in time and space. *Earth and Planetary Science Letters*, 113(3), 343–364. [https://doi.org/10.1016/0012-821x\(92\)90138-1](https://doi.org/10.1016/0012-821x(92)90138-1)
- O’Connor, J. M., Stoffers, P., van den Bogaard, P., & McWilliams, M. (1999). First seamount age evidence for significantly slower African Plate motion since 19 to 30 Ma. *Earth and Planetary Science Letters*, 171(4), 575–589. [https://doi.org/10.1016/s0012-821x\(99\)00183-1](https://doi.org/10.1016/s0012-821x(99)00183-1)
- O’Neill, C., & Sigloch, K. (2018). Crust and mantle structure beneath the Azores hotspot—evidence from geophysics. In U. Kueppers & C. Beier (Eds.), *Volcanoes of the Azores: Revealing the geological secrets of the central Northern Atlantic Islands* (pp. 71–87). Springer Berlin Heidelberg.
- Obayashi, M., Yoshimitsu, J., Sugioka, H., Ito, A., Isse, T., Shiobara, H., et al. (2016). Mantle plumes beneath the South Pacific superswell revealed by finite frequency P tomography using regional seafloor and island data. *Geophysical Research Letters*, 43(22), 11628–11634. <https://doi.org/10.1002/2016GL070793>
- Olson, P., & Singer, H. (1985). Creeping plumes. *Journal of Fluid Mechanics*, 158, 511–531. <https://doi.org/10.1017/S0022112085002749>
- Olson, P., Yuen, D. A., & Balsiger, D. (1984). Convective mixing and the fine structure of mantle heterogeneity. *Physics of the Earth and Planetary Interiors*, 36(3–4), 291–304. [https://doi.org/10.1016/0031-9201\(84\)90053-0](https://doi.org/10.1016/0031-9201(84)90053-0)
- Olson, P. L., & Sharp, Z. D. (2022). Primordial helium-3 exchange between Earth’s core and mantle. *Geochemistry, Geophysics, Geosystems*, 23(3), e2021GC009985.5. <https://doi.org/10.1029/2021GC009985>
- Palacz, Z. A., & Saunders, A. D. (1986). Coupled trace element and isotope enrichment in the Cook-Austral-Samoa islands, southwest Pacific. *Earth and Planetary Science Letters*, 79(3–4), 270–280. [https://doi.org/10.1016/0012-821x\(86\)90185-8](https://doi.org/10.1016/0012-821x(86)90185-8)
- Paquet, M., Day, J. M. D., Brown, D. B., & Waters, C. L. (2022). Effective global mixing of the highly siderophile elements into Earth’s mantle inferred from oceanic abyssal peridotites. *Geochimica et Cosmochimica Acta*, 316, 347–362. <https://doi.org/10.1016/j.gca.2021.09.033>
- Parman, S. W. (2007). Helium isotopic evidence for episodic mantle melting and crustal growth. *Nature*, 446(7138), 900–903. <https://doi.org/10.1038/nature05691>
- Paul, D., White, W. M., & Turcotte, D. L. (2002). Modelling the isotopic evolution of the Earth. *Philosophical Transactions of the Royal Society*, 360(1800), 2433–2474. <https://doi.org/10.1098/rsta.2002.1076>
- Pedregosa, F., Varoquaux, G., Gramfort, A., Michel, V., Thirion, B., Grisel, O., et al. (2011). Scikit-learn: Machine learning in Python. *Journal of Machine Learning Research*, 12, 2825–2830.
- Pertermann, M., & Hirschmann, M. M. (2003). Partial melting experiments on a MORB-like pyroxenite between 2 and 3GPa: Constraints on the presence of pyroxenite in basalt source regions from solidus location and melting rate. *Journal of Geophysical Research*, 108(B2), 215. <https://doi.org/10.1029/2000JB000118>
- Putirka, K. (2008). Excess temperatures at ocean islands: Implications for mantle layering and convection. *Geology*, 36(4), 283–286. <https://doi.org/10.1130/g24615a.1>
- Reusch, A. M., Nyblade, A. A., Ateba, B., Wiens, D. A., Shore, P. J., Tabod, C. T., & Nnange, J. M. (2010). Upper mantle structure beneath Cameroon from body wave tomography and the origin of the Cameroon volcanic line. *Geochemistry, Geophysics, Geosystems*, 11(10), Q10W07. <https://doi.org/10.1029/2010GC003200>

- Reusch, A. M., Nyblade, A. A., Tibi, R., Wiens, D. A., Shore, P. J., Bekoa, A., et al. (2011). Mantle transition zone thickness beneath Cameroon: Evidence for an upper mantle origin for the Cameroon volcanic line. *Geophysical Journal International*, 187(3), 1146–1150. <https://doi.org/10.1111/j.1365-246x.2011.05239.x>
- Ribe, N., Davaille, A., & Christensen, U. (2007). Fluid dynamics of mantle plumes. In J. R. R. Ritter & U. R. Christensen (Eds.), *Mantle plumes*. Springer. [https://doi.org/10.1007/978-3-540-68046-8\\_1](https://doi.org/10.1007/978-3-540-68046-8_1)
- Ribe, N. M. (1996). The dynamics of plume ridge interaction, 2: Off-ridge plumes. *Journal of Geophysical Research*, 101(B7), 16195–116204. <https://doi.org/10.1029/96jb01187>
- Ritsema, J., Deuss, A., van Heijst, H. J., & Woodhouse, J. H. (2011). S4ORTS: A degree-40 shear-velocity model for the mantle from new Rayleigh wave dispersion, teleseismic traveltimes and normal-mode splitting function measurements. *Geophysical Journal International*, 184(3), 1223–1236. <https://doi.org/10.1111/j.1365-246x.2010.04884.x>
- Rohde, J., Hoernle, K., Hauff, F., Werner, R., O'Connor, J., Class, C., et al. (2013). 70 Ma chemical zonation of the Tristan-Gough hotspot track. *Geology*, 41(3), 335–338. <https://doi.org/10.1130/g33790.1>
- Rosas, J. C., & Korenaga, J. (2018). Rapid crustal growth and efficient crustal recycling in the early Earth: Implications for Hadean and Archean geodynamics. *Earth and Planetary Science Letters*, 494, 42–49. <https://doi.org/10.1016/j.epsl.2018.04.051>
- Rudge, J., McKenzie, D., & Haynes, P. H. (2005). A theoretical approach to understanding the isotopic heterogeneity of mid-ocean ridge basalt. *Geochimica et Cosmochimica Acta*, 69(15), 3873–3887. <https://doi.org/10.1016/j.gca.2005.03.004>
- Rudge, J. F., MacLennan, J., & Stracke, A. (2013). The geochemical consequences of mixing melts from a heterogeneous mantle. *Geochimica et Cosmochimica Acta*, 114, 112–143. <https://doi.org/10.1016/j.gca.2013.03.042>
- Sager, W. W., Huang, Y., Tominaga, M., Greene, J. A., Nakaniishi, M., & Zhang, J. (2019). Oceanic plateau formation by seafloor spreading implied by Tamu Massif magnetic anomalies. *Nature Geoscience*, 12(8), 661–666. <https://doi.org/10.1038/s41561-019-0390-y>
- Saki, M., Thomas, C., Nippes, S. E. J., & Lessing, S. (2015). Topography of upper mantle seismic discontinuities beneath the North Atlantic: The Azores, Canary and Cape Verde plumes. *Earth and Planetary Science Letters*, 409, 193–202. <https://doi.org/10.1016/j.epsl.2014.10.052>
- Salters, V. J. M., & Dick, H. J. B. (2002). Mineralogy of the mid-ocean-ridge basalt source from neodymium isotopic composition of abyssal peridotites. *Nature*, 418(6893), 68–72. <https://doi.org/10.1038/nature00798>
- Salters, V. J. M., Mallick, S., Hart, S. R., Langmuir, C. H., & Stracke, A. (2011). Domains of depleted mantle; new evidence from hafnium and neodymium isotopes. *Geochimica et Cosmochimica Acta*, 75(18), 5001–5017. <https://doi.org/10.1016/j.gca.2011.03.004>
- Salters, V. J. M., & Stracke, A. (2004). Composition of the depleted mantle. *Geochemistry, Geophysics, Geosystems*, 5, Q05B07. <https://doi.org/10.1029/2003GC000597>
- Sanfilippo, A., Salters, V. J. M., Sokolov, S. Y., Peyve, A. A., & Stracke, A. (2021). Ancient refractory asthenosphere revealed by mantle re-melting at the Arctic Mid-Atlantic Ridge. *Earth and Planetary Science Letters*, 566, 116981. <https://doi.org/10.1016/j.epsl.2021.116981>
- Saunders, A. D., Storey, M., Gibson, I. L., Leat, P., Hergt, J. M., & Thompson, R. N. (1991). Chemical and isotopic constraints of the origin of basalts from Ninetyeast Ridge, Indian Ocean: Results from DSDP Leg 22 and 26 and ODP Leg 121. In J. Weissel, J. Pearce, & E. Taylor (Eds.), *Proceedings of the Ocean Drilling program, scientific results* (pp. 559–590). Ocean Drilling Program.
- Scheirer, D. S., Forsyth, D. W., Conder, J. A., Eberle, M. A., Hung, S. H., Johnson, K. T. M., & Graham, D. W. (2000). Anomalous seafloor spreading of the Southeast Indian Ridge near the Amsterdam-St. Paul Plateau. *Journal of Geophysical Research*, 105(B4), 8243–8262. <https://doi.org/10.1029/1999jb900407>
- Schiano, P., Burton, K. W., Dupre, B., Birck, J. L., Guille, G., & Allègre, C. J. (2001). Correlated Os-Pb-Nd-Sr isotopes in the Austral-Cook chain basalts: The nature of mantle components in plume sources. *Earth and Planetary Science Letters*, 186(3–4), 527–537. [https://doi.org/10.1016/s0012-821x\(01\)00265-5](https://doi.org/10.1016/s0012-821x(01)00265-5)
- Schilling, J. G. (1973). Iceland mantle plume: Geochemical study of Reykjanes Ridge. *Nature*, 242(5400), 565–571. <https://doi.org/10.1038/242565a0>
- Schilling, J. G. (1985). Upper mantle heterogeneities and dynamics. *Nature*, 314(6006), 62–67. <https://doi.org/10.1038/314062a0>
- Schilling, J. G. (1991). Fluxes and excess temperatures of mantle plumes inferred from their interaction with migrating mid-ocean ridges. *Nature*, 352(6334), 397–403. <https://doi.org/10.1038/352397a0>
- Schilling, J. G. (1992). Oceanic domains and the mantle. In J. L. Duthou (Ed.), *Société Française de Minéralogie et de Crystallographie* (pp. 1–34).
- Schilling, J. G., Fontignie, D., Blöcher-Toft, J., Kingsley, R. H., & Tomiza, U. (2003). Pb-Hf-Nd-Sr isotope variations along the Galapagos Spreading Center (101°–83°W): Constraints on the dispersal of the Galapagos mantle plume. *Geochimica et Cosmochimica Acta*, 67(10), 8512. <https://doi.org/10.1029/2002GC000495>
- Schilling, J.-G., Kingsley, R., & Devine, J. (1982). Galapagos hot spot-spreading center system: 1. Spatial petrological and geochemical variations (83°W–101°W). *Journal of Geophysical Research*, 87(B7), 5593–5610. <https://doi.org/10.1029/jb087ib07p05593>
- Schilling, J. G., Zajac, M., Evans, R., Johnston, T., White, W., Devine, J. D., & Kingsley, R. (1983). Petrologic and geochemical variations along the Mid-Atlantic Ridge from 29°N to 73°N. *American Journal of Science*, 283(6), 510–586. <https://doi.org/10.2475/ajs.283.6.510>
- Schoene, B., Samperton, K. M., Eddy, M. P., Keller, G., Adatte, T., Bowring, S. A., et al. (2015). U-Pb geochronology of the Deccan Traps and relation to the end-Cretaceous mass extinction. *Science*, 347(6218), 182–184. <https://doi.org/10.1126/science.aaa0118>
- Schubert, G., Masters, G., Olson, P., & Tackley, P. (2004). Superplumes or plume clusters? *Physics of the Earth and Planetary Interiors*, 146(1–2), 147–162. <https://doi.org/10.1016/j.pepi.2003.09.025>
- Schutt, D. L., & Lesser, C. E. (2006). Effects of melt depletion on the density and seismic velocity of garnet and spinel lherzolite. *Journal of Geophysical Research*, 111(B5), B05401. <https://doi.org/10.1029/2000JB002950>
- Schwindrofska, A., Hoernle, K., Hauff, F., van den Bogaard, P., Werner, R., & Garbe-Schönberg, D. (2016). Origin of enriched components in the south Atlantic: Evidence from 40 Ma geochemical zonation of the discovery Seamounts. *Earth and Planetary Science Letters*, 441, 167–177. <https://doi.org/10.1016/j.epsl.2016.02.041>
- Seyler, M., Lorand, J.-P., Dick, H. J. B., & Drouin, M. (2007). Pervasive melt percolation reactions in ultra-depleted refractory harzburgites at the Mid-Atlantic Ridge, 15°20'N: ODP Hole 1274A. *Contributions to Mineralogy and Petrology*, 153(3), 303–319. <https://doi.org/10.1007/s00410-006-0148-6>
- Shaw, H. R., Jackson, E. D., & Bargar, K. E. (1980). Volcanic periodicity along the Hawaiian-Emperor chain. *American Journal of Science*, 280-A, 667–798.
- Shorttle, O., MacLennan, J., & Lambart, S. (2014). Quantifying lithological variability in the mantle. *Earth and Planetary Science Letters*, 395, 24–40. <https://doi.org/10.1016/j.epsl.2014.03.040>
- Shorttle, O., Matthews, S., & MacLennan, J. (2020). Finding harzburgite in the mantle. A comment on Brown et al. (2020): “Markov chain Monte Carlo inversion of mantle temperature and source composition, with application to Reykjanes Peninsula, Iceland” [earth Planet. Sci. Lett. 532 (2020) 116007]. *Earth and Planetary Science Letters*, 548, 116503. <https://doi.org/10.1016/j.epsl.2020.116503>

- Sleep, N. H. (1990). Hotspots and mantle plumes - some phenomenology. *Journal of Geophysical Research*, 95(B5), 6715–6736. <https://doi.org/10.1029/jb095ib05p06715>
- Sleep, N. H. (1997). Lateral flow and ponding of starting plume material. *Journal of Geophysical Research*, 102(B5), 10001–10012. <https://doi.org/10.1029/97jb00551>
- Sleep, N. H. (2002). Ridge-crossing mantle plumes and gaps in tracks. *Geochemistry, Geophysics, Geosystems*, 3(12), 8505–8533. <https://doi.org/10.1029/2001GC000290>
- Small, C. (1995). Observations of ridge-hotspot interactions in the Southern Ocean. *Journal of Geophysical Research*, 100(B9), 17931–17946. <https://doi.org/10.1029/95jb01377>
- Snow, J. E., Hart, S. R., & Dick, H. J. B. (1994). Nd and Sr isotope evidence linking mid-ocean-ridge basalts and abyssal peridotites. *Nature*, 371(6492), 57–60. <https://doi.org/10.1038/371057a0>
- Sobolev, A. V., Hofmann, A. W., Kuzmin, D. V., Yaxley, G. M., Arndt, N. T., Chung, S.-L., et al. (2007). The amount of recycled crust in sources of mantle-derived melts. *Science*, 316(5823), 412–417. <https://doi.org/10.1126/science.1138113>
- Staudigel, H., Park, K. H., Pringle, M., Rubenstone, J. L., Smith, W. H. F., & Zindler, A. (1991). The longevity of the South-Pacific isotopic and thermal anomaly. *Earth and Planetary Science Letters*, 102(1), 24–44. [https://doi.org/10.1016/0012-821x\(91\)90015-a](https://doi.org/10.1016/0012-821x(91)90015-a)
- Stegman, D. R., Richards, M. A., & Baumgardner, J. R. (2002). Effects of depth-dependnet viscosity and plate motions on maintaining a relatively uniform mid-ocean ridge basalts reservoir in whole mantle flow. *Journal of Geophysical Research*, 107(B6), 2116. <https://doi.org/10.1029/2001JB000192>
- Steinberger, B. (2000). Plumes in a convecting mantle: Models and observations for individual hotspots. *Journal of Geophysical Research*, 105(B5), 11127–11152. <https://doi.org/10.1029/1999jb900398>
- Steinberger, B., Bredow, E., Lebedev, S., Schaeffer, A., & Torsvik, T. H. (2019). Widespread volcanism in the Greenland–North Atlantic region explained by the Iceland plume. *Nature Geoscience*, 12(1), 61–68. <https://doi.org/10.1038/s41561-018-0251-0>
- Steinberger, B., & O'Connell, R. J. (1998). Advection of plumes in mantle flow: Implications for hotspot motion, mantle viscosity and plume distribution. *Geophysical Journal International*, 132(2), 412–434. <https://doi.org/10.1046/j.1365-246x.1998.00447.x>
- Steinberger, B., & Torsvik, T. H. (2012). A geodynamic model of plumes from the margins of large low shear velocity provinces. *Geochemistry, Geophysics, Geosystems*, 13(1), Q01W09. <https://doi.org/10.1029/2011GC003808>
- Stracke, A. (2012). Earth's heterogeneous mantle: A product of convection-driven interaction between crust and mantle. *Chemical Geology*, 330–331, 274–299. <https://doi.org/10.1016/j.chemgeo.2012.08.007>
- Stracke, A. (2018). Mantle geochemistry. In W. M. White (Ed.), *Encyclopedia of geochemistry: A comprehensive reference source on the chemistry of the Earth*. Springer International Publishing.
- Stracke, A. (2021a). Composition of Earth's mantle. In D. Alderton & S. A. Elias (Eds.), *Encyclopedia of geology* (2nd ed., pp. 164–177). Academic Press.
- Stracke, A. (2021b). A process-oriented approach to mantle geochemistry. *Chemical Geology*, 579, 120350. <https://doi.org/10.1016/j.chemgeo.2021.120350>
- Stracke, A., Bizimis, M., & Salters, V. J. M. (2003b). Recycling of oceanic crust: Quantitative constraints. *Geochemistry, Geophysics, Geosystems*, 4(3), 8003. <https://doi.org/10.1029/2001GC000223>
- Stracke, A., & Bourdon, B. (2009). The importance of melt extraction for tracing mantle heterogeneity. *Geochimica et Cosmochimica Acta*, 73(1), 218–238. <https://doi.org/10.1016/j.gca.2008.10.015>
- Stracke, A., Genske, F., Berndt, J., & Koornneef, J. M. (2019). Ubiquitous ultra-depleted domains in Earth's mantle. *Nature Geoscience*, 12(10), 851–855. <https://doi.org/10.1038/s41561-019-0446-z>
- Stracke, A., Hofmann, A. W., & Hart, S. R. (2005). FOZO, HIMU and the rest of the mantle zoo. *Geochemistry, Geophysics, Geosystems*, 6(5), Q05007. <https://doi.org/10.1029/2004GC000824>
- Stracke, A., Salters, V. J. M., & Sims, K. W. W. (1999). Assessing the presence of garnet-pyroxenite in the mantle sources of basalts through combined hafnium-neodymium-thorium isotope systematics. *Geochemistry, Geophysics, Geosystems*, 1(12), 1006. <https://doi.org/10.1029/1999GC000013>
- Stracke, A., Snow, J. E., Hellebrand, E., von der Handt, A., Bourdon, B., Birbaum, K., & Günther, D. (2011). Abyssal peridotite Hf isotopes identify extreme mantle depletion. *Earth and Planetary Science Letters*, 308(3–4), 359–368. <https://doi.org/10.1016/j.epsl.2011.06.012>
- Stracke, A., Zindler, A., Salters, V. J. M., McKenzie, D., Blöcher-Toft, J., Albarède, F., & Grönvold, K. (2003a). Theistareykir revisited. *Geochemistry, Geophysics, Geosystems*, 4(2), 8507. <https://doi.org/10.1029/2001GC000201>
- Suetsugu, D., & Hanyu, T. (2013). Origin of hotspots in the South Pacific: Recent advances in seismological and geochemical models. *Geochemical Journal*, 47(2), 259–284. <https://doi.org/10.2343/geochemj.2.0229>
- Suetsugu, D., Isse, T., Tanaka, S., Obayashi, M., Shiobara, H., Sugioka, H., et al. (2009). South Pacific mantle plumes imaged by seismic observation on islands and seafloor. *Geochemistry, Geophysics, Geosystems*, 10(11), Q11014. <https://doi.org/10.1029/2009GC002533>
- Tackley, P. J. (2015). 7.12—Mantle geochemical geodynamics. In G. Schubert (Ed.), *Treatise on geophysics* (pp. 521–585). Elsevier.
- Tan, E., Gurnis, M., & Han, L. (2002). Slabs in the lower mantle and their modulation of plume formation. *Geochemistry, Geophysics, Geosystems*, 3(11), 1067–1124. <https://doi.org/10.1029/2001GC000238>
- Tanaka, S., Obayashi, M., Suetsugu, D., Shiobara, H., Sugioka, H., Yoshimitsu, J., et al. (2009). P-wave tomography of the mantle beneath the South Pacific Superswell revealed by joint ocean floor and islands broadband seismic experiments. *Physics of the Earth and Planetary Interiors*, 172(3–4), 268–277. <https://doi.org/10.1016/j.pepi.2008.10.016>
- Tatsumoto, M. (1966). Genetic relations of oceanic basalts as indicated by lead isotopes. *Science*, 153(3740), 1094–1101. <https://doi.org/10.1126/science.153.3740.1094>
- Tatsumoto, M., Hedge, C. E., & Engel, A. E. J. (1965). Potassium, rubidium, strontium, thorium, uranium, and the ratio of strontium-87 to strontium-86 in Oceanic Tholeiitic basalt. *Science*, 150(3698), 886–888. <https://doi.org/10.1126/science.150.3698.886>
- Tsekhnistrenko, M., Sigloch, K., Hosseini, K., & Barruol, G. (2021). A tree of Indo-African mantle plumes imaged by seismic tomography. *Nature Geoscience*, 14(8), 612–619. <https://doi.org/10.1038/s41561-021-00762-9>
- Tucker, J. M., van Keken, P. E., & Ballentine, C. J. (2022). Earth's missing argon paradox resolved by recycling of oceanic crust. *Nature Geoscience*, 15(1), 85–90. <https://doi.org/10.1038/s41561-021-00870-6>
- Tucker, J. M., van Keken, P. E., Jones, R. E., & Ballentine, C. J. (2020). A role for subducted oceanic crust in generating the depleted mid-ocean ridge basalts mantle. *Geochemistry, Geophysics, Geosystems*, 21(8), e2020GC009148. <https://doi.org/10.1029/2020GC009148>
- Turner, D. L., & Jarrad, R. D. (1982). K-Ar dating of the Cook-Austral island chain: A test of the hot-spot hypothesis. *Journal of Volcanology and Geothermal Research*, 12(3–4), 187–220. [https://doi.org/10.1016/0377-0273\(82\)90027-0](https://doi.org/10.1016/0377-0273(82)90027-0)
- Uto, K., Yamamoto, Y., Sudo, M., Uchiumi, S., Ishizuka, O., Kogiso, T., & Tsunakawa, H. (2007). New K-Ar ages of the Society Islands, French Polynesia, and implications for the society hotspot feature. *Earth Planets and Space*, 59(7), 879–885. <https://doi.org/10.1186/bf03352750>

- van der Maaten, L. (2014). Accelerating t-SNE using tree-based algorithms. *Journal of Machine Learning Research*, 15, 3221–3245.
- van der Maaten, L., & Hinton, G. (2008). Visualizing data using t-SNE. *Journal of Machine Learning Research*, 9, 2579–2605.
- van Keken, P. E., Ballantine, C. J., & Hauri, E. H. (2014). 3.14—Convective mixing in the Earth's mantle. In H. D. H. K. Turekian (Ed.), *Treatise on geochemistry* (2nd ed., pp. 509–525). Elsevier.
- Vidal, P., Chauvel, C., & Brousse, R. (1984). Large mantle heterogeneity beneath French Polynesia. *Nature*, 307(5951), 536–538. <https://doi.org/10.1038/307536a0>
- Villagómez, D. R., Toomey, D. R., Hooft, E. E. E., & Solomon, S. C. (2007). Upper mantle structure beneath the Galápagos Archipelago from surface wave tomography. *Journal of Geophysical Research*, 112(B7), B07303. <https://doi.org/10.1029/2006JB004672>
- Vogt, P. R. (1974). The Iceland phenomenon; imprints of a hot spot on the ocean crust, and implications for flow below the plates. In L. Kristjanson (Ed.), *Geodynamics of Iceland and the North Atlantic area* (pp. 105–126). Kluwer Academic, University of Iceland.
- Vogt, P. R., & Jung, W.-Y. (2018). The “Azores Geosyndrome” and plate tectonics: Research history, synthesis, and unsolved puzzles. In U. Kueppers & C. Beier (Eds.), *Volcanoes of the Azores: Revealing the geological secrets of the central Northern Atlantic Islands* (pp. 27–56). Springer Berlin Heidelberg.
- Wamba, M. D., Montagner, J.-P., Romanowicz, B., & Barruol, G. (2021). Multi-mode waveform tomography of the Indian Ocean upper and mid mantle around the Réunion hotspot. *Journal of Geophysical Research: Solid Earth*, 126(8), e2020JB021490. <https://doi.org/10.1029/2020JB021490>
- Wang, K., Lu, X., Liu, X., Zhou, M., & Yin, K. (2022). Partitioning of noble gases (He, Ne, Ar, Kr, Xe) during Earth's core segregation: A possible core reservoir for primordial noble gases. *Geochimica et Cosmochimica Acta*, 321, 329–342. <https://doi.org/10.1016/j.gca.2022.01.009>
- Warren, J. M. (2016). Global variations in abyssal peridotite compositions. *Lithos*, 248–251, 193–219. <https://doi.org/10.1016/j.lithos.2015.12.023>
- Warren, J. M., Shimizu, N., Sakaguchi, C., Dick, H. J. B., & Nakamura, E. (2009). An assessment of upper mantle heterogeneity based on abyssal peridotite isotopic compositions. *Journal of Geophysical Research*, 114(B12), B12203. <https://doi.org/10.11029/12008JB006186>
- Waskom, M. L. (2021). Seaborn: Statistical data visualization. *Journal of Open Source Software*, 6(60), 3021. <https://doi.org/10.21105/joss.03021>
- Wattenberg, M., Viégas, F., & Johnson, I. (2016). How to use t-SNE effectively. <https://doi.org/10.23915/distill.00002>
- Weis, D., & Frey, F. A. (1991). Isotope geochemistry of Ninetyeast Ridge basement basalts: Sr, Nd, and Pb evidence for involvement of the Kerguelen hot spot. In J. Weissel, J. Peirce, E. Taylor, & J. C. Alt (Eds.), *Proceedings of the Ocean Drilling Program, Scientific Results* (Vol. 121, pp. 591–610). Ocean Drilling Program.
- Weis, D., Harrison, L. N., McMillan, R., & Williamson, N. M. B. (2020). Finescale structure of Earth's deep mantle resolved through statistical analysis of Hawaiian Basalt Geochemistry. *Geochemistry, Geophysics, Geosystems*, 21(11), e2020GC009292. <https://doi.org/10.1029/2020GC009292>
- Weis, D., White, W. M., Frey, F. A., Duncan, R. A., Fisk, M. R., Dehn, J., et al. (1992). *The influence of mantle plumes in generation of Indian oceanic crust, synthesis of results from scientific drilling in the Indian ocean* (pp. 57–89). American Geophysical Union.
- Wessel, P. (2016). Regional-residual separation of bathymetry and revised estimates of Hawaii plume flux. *Geophysical Journal International*, 204(2), 932–947. <https://doi.org/10.1093/gji/ggv472>
- White, W. M. (1985). Sources of oceanic basalts - Radiogenic isotopic evidence. *Geology*, 13(2), 115–118. [https://doi.org/10.1130/0091-7613\(1985\)13<115:soobri>2.0.co;2](https://doi.org/10.1130/0091-7613(1985)13<115:soobri>2.0.co;2)
- White, W. M. (2010). Oceanic island basalts and mantle plumes: The geochemical perspective. *Annual Review of Earth and Planetary Sciences*, 38(1), 133–160. <https://doi.org/10.1146/annurev-earth-040809-152450>
- White, W. M. (2015). Isotopes, DUPAL, LLSPVs, and Anekantavada. *Chemical Geology*, 419, 10–28. <https://doi.org/10.1016/j.chemgeo.2015.09.026>
- White, W. M., & Duncan, R. A. (1996). Geochemistry and geochronology of the Society Islands: New evidence for deep mantle recycling. In S. R. Hart & A. Basu (Eds.), *Isotope studies of crust mantle evolution* (pp. 183–206). American Geophysical Union.
- White, W. M., McBirney, A. R., & Duncan, R. A. (1993). Petrology and geochemistry of the Galapagos-Islands—portrait of a pathological mantle plume. *Journal of Geophysical Research*, 98(B11), 19533–19563. <https://doi.org/10.1029/93jb02018>
- White, W. M., & Schilling, J. G. (1978). Nature and origin of geochemical variation in Mid-Atlantic Ridge basalts from central North-Atlantic. *Geochimica et Cosmochimica Acta*, 42(10), 1501–1516. [https://doi.org/10.1016/0016-7037\(78\)90021-2](https://doi.org/10.1016/0016-7037(78)90021-2)
- Whittaker, J. M., Afonso, J. C., Masterton, S., Müller, R. D., Wessel, P., Williams, S. E., & Seton, M. (2015). Long-term interaction between mid-ocean ridges and mantle plumes. *Nature Geoscience*, 8(6), 479–483. <https://doi.org/10.1038/ngeo2437>
- Whittaker, J. M., Williams, S. E., & Müller, R. D. (2013). Revised tectonic evolution of the eastern Indian Ocean. *Geochemistry, Geophysics, Geosystems*, 14(6), 1891–1909. <https://doi.org/10.1002/ggge.20120>
- Willbold, M., & Stracke, A. (2006). Trace element composition of mantle end-members: Implications for recycling of oceanic and upper and lower continental crust. *Geochemistry, Geophysics, Geosystems*, 7(4), Q04004. <https://doi.org/10.1029/02005GC001005>
- Willbold, M., & Stracke, A. (2010). Formation of enriched mantle components by recycling of upper and lower continental crust. *Chemical Geology*, 276(3–4), 188–197. <https://doi.org/10.1016/j.chemgeo.2010.06.005>
- Willig, M., Stracke, A., Beier, C., & Salters, V. J. M. (2020). Constraints on mantle evolution from Ce-Nd-Hf isotope systematics. *Geochimica et Cosmochimica Acta*, 272, 36–53. <https://doi.org/10.1016/j.gca.2019.12.029>
- Woodhead, J. D. (1996). Extreme HIMU in an oceanic setting: The geochemistry of Mangaia island (Polynesia), and temporal evolution of the Cook-Austral hot spot. *Journal of Volcanology and Geothermal Research*, 72(1–2), 1–19. [https://doi.org/10.1016/0377-0273\(96\)00002-9](https://doi.org/10.1016/0377-0273(96)00002-9)
- Wright, E., & White, W. M. (1987). The origin of Samoa—New evidence from Sr, Nd, and Pb isotopes. *Earth and Planetary Science Letters*, 81(2–3), 151–162. [https://doi.org/10.1016/0012-821x\(87\)90152-x](https://doi.org/10.1016/0012-821x(87)90152-x)
- Xie, S., & Tackley, P. J. (2004). Evolution of U-Pb and Sm-Nd systems in numerical models of mantle convection and plate tectonics. *Journal of Geophysical Research*, 109(B11), B11204. <https://doi.org/10.11029/12004JB003176>
- Yale, M. M., & Morgan, J. P. (1998). Asthenosphere flow model of hotspot-ridge interactions: A comparison of Iceland and Kerguelen. *Earth and Planetary Science Letters*, 161(1–4), 45–56. [https://doi.org/10.1016/s0012-821x\(98\)00136-8](https://doi.org/10.1016/s0012-821x(98)00136-8)
- Yang, T., Shen, Y., van der Lee, S., Solomon, S. C., & Hung, S.-H. (2006). Upper mantle structure beneath the Azores hotspot from finite-frequency seismic tomography. *Earth and Planetary Science Letters*, 250(1–2), 11–26. <https://doi.org/10.1016/j.epsl.2006.07.031>
- Zhao, D. (2004). Global tomographic images of mantle plumes and subducting slabs: Insight into deep Earth dynamics. *Physics of the Earth and Planetary Interiors*, 146(1–2), 3–34. <https://doi.org/10.1016/j.pepi.2003.07.032>
- Zindler, A., & Hart, S. (1986). Chemical geodynamics. *Annual Review of Earth and Planetary Sciences*, 14(1), 493–571. <https://doi.org/10.1146/annurev.ea.14.050186.002425>
- Zindler, A., Hart, S. R., Frey, F. A., & Jakobsson, S. P. (1979). Nd and Sr isotope ratios and rare-Earth element abundances in Reykjanes Peninsula basalts—Evidence for mantle heterogeneity beneath Iceland. *Earth and Planetary Science Letters*, 45(2), 249–262. [https://doi.org/10.1016/0012-821x\(79\)90127-4](https://doi.org/10.1016/0012-821x(79)90127-4)

Zindler, A., Jagoutz, E., & Goldstein, S. (1982). Nd, Sr and Pb isotopic systematics in a three-component mantle—A new perspective. *Nature*, 298(5874), 519–523. <https://doi.org/10.1038/298519a0>

### References From the Supporting Information

Hamelin, C., Dosso, L., Hanan, B. B., Moreira, M., Kositsky, A. P., & Thomas, M. Y. (2011). Geochemical portray of the Pacific Ridge: New isotopic data and statistical techniques. *Earth and Planetary Science Letters*, 302(1–2), 154–162. <https://doi.org/10.1016/j.epsl.2010.12.007>